

**FINAL PROGRESS REPORT OF THE WORK DONE ON THE MAJOR
RESEARCH PROJECT**

(1-04-2013 to 31-03-2017)

Title of the Project

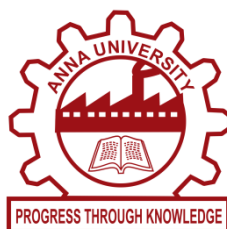
**Development of polymer- CdTe-TiO₂ based nanocomposites
for low cost solar cells**

(F.No.: 42-855/2013 (SR) Dated: 22-03-2013)



Submitted to

**UNIVERSITY GRANTS COMMISSION
NEWDELHI – 110 002**



By

PROF. S. MOORTHY BABU

Principal Investigator

Crystal Growth Centre

Anna University

Chennai- 600025

AUGUST 2018

Final Progress Report:

“ Development of polymer- CdTe-TiO₂ based nanocomposites for low cost solar cells”

Group II –VI semiconductors have attracted much attention due to their size tunable optical properties and absorption of light in visible region and so forth. The light absorption and emission properties of semiconductor quantum dots can be tuned through wide spectral range by varying their size and shape of the nanoparticles. Such as this tunability in the optical properties makes semiconductor quantum dots as a potential candidate for the application such as emitters, light harvest and biological labels. As in the biological labels, the semiconductor quantum dots are functionalized with molecules that are attached with specific target molecules. When this functional molecules are mixed with unknown samples and irradiated with light of the energy above the band gap of quantum dot, the strong photoluminescence from the quantum dot will indicate the presence of the target material. The linear optical properties of semiconductor quantum dot possess large nonlinearities, makes them efficient nonlinear absorption of light. The present work were concentrated on the synthesis of Cadmium based chalcogenides (CdS, CdSe and CdTe). Among these cadmium based chalcogenides- CdSe nanoparticles have attracted prominence due to the high quantum yield and tunable emission spectrum wavelength. Most of the synthesis routes are based on organometallics with high temperature process and it is toxic. Therefore, the alternative choice for the synthesis of cadmium based nanoparticles was depending on the aqueous –based process and this method was highlighted with the non-toxic nature. The major hinderance of aqueous medium was that the particles does not dissolve in organic solvent. Hence, there is another way to enhance the aqueous synthesis process, that was “phase transfer chemistry” by this way, one can transfer or replace the ligand on the surface of nanoparticles thereby to make green solar cells. The preliminary work starts from the synthesis of CdSe in aqueous medium with air stable selenium source namely sodium selenide and thioglycolic acid as stabilizer. Herein, 1-dodecanethiol was used as a phase transferring reagent, it exchanges the nanoparticles from hydrophilic to hydrophobic nature. The transformation of the solvent were visualized in naked eye, the image were insert below in Fig.1.

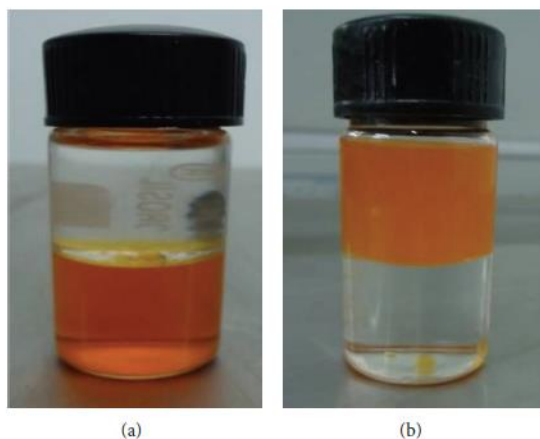


Fig 1: CdSe (a) in water (b) in dodecanethiol

HRTEM images were taken for this synthesized sample to study the particle size distribution and phase transferred nature of the material. The phase transferred sample shows good size distribution compared with samples without phase transformation and the particle size in the range of 5 nm for the phase transferred samples. But, the particle synthesized in aqueous medium was agglomerated. Here, it is summarized that the phase transferred particles act as a good electron acceptor (active layer) in organic polymer solar cells or hybrid solar cells.

In another work, CdSe nanoparticles were synthesized in aqueous medium using mercaptopropanic acid as a stabilizer at 100° C as shown in Fig.2. The synthesized CdSe nanoparticles were used in co-sensitized TiO₂ nanotube with N3 dye. Electrochemical anodization technique was employed to prepare TiO₂ nanotubes in the presence of hydro fluoride (HF) as a electrolyte. The prepared TiO₂ was used to fabricate solar cell. In the device, co-sensitized TiO₂ with N3 dye/ CdSe was used as an anode, platinum coated FTO as cathode and polysulphide (S²⁻/S^{2-x-}) mixture were used as an electrolyte. However, the semiconductor nanoparticles are considered superior absorber than the organic dyes due to their higher photochemical stability, efficient transfer of electron to conduction band of the TiO₂ and multiple exciton generation. Whereas, the CdSe quantum dot nanoparticles in N3 dye was used to enhance the absorption property of the material. Herein, the TiO₂ nanotubes were used to reduce the recombination rate of the solar cells. After that, the ruthenium based N3 dye sensitizes with TiO₂ as considerable as effective sensitizer to produce the power conversion efficiency in this solar cell. Therefore, the polysulfide electrolyte was used instead of iodide to avoid the corrosion of the cathode. The fabricated solar cells were analyzed through Keithley source meter under the illumination of halogen lamp.

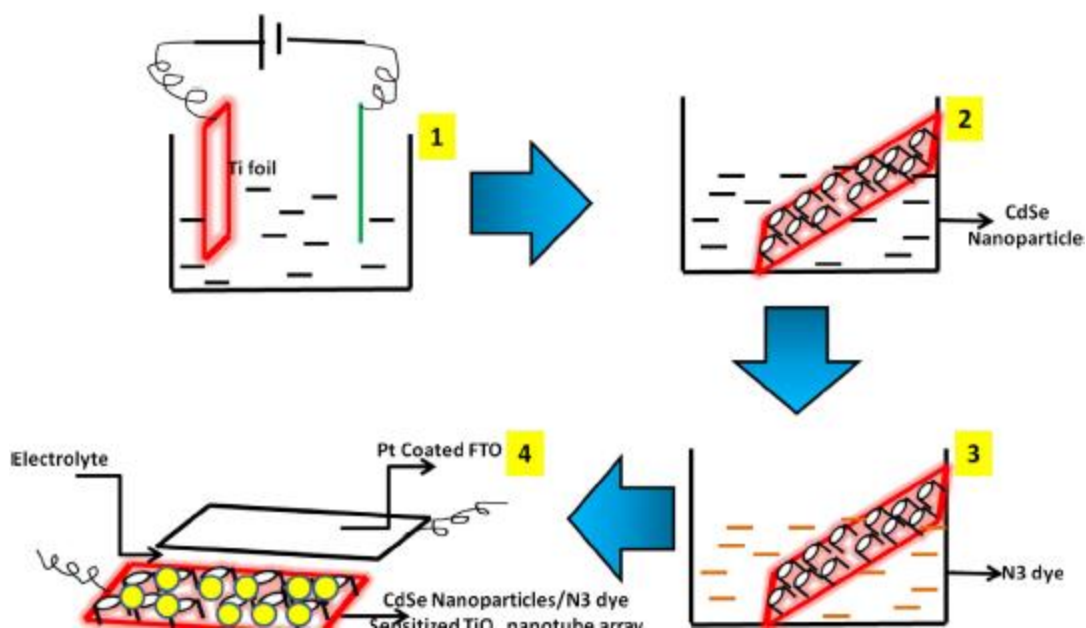


Fig.2. Schematic representation of (a) anodization process of Ti foil, (b) sensitization of TiO₂ nanotubes by CdSe nanoparticles, (c) sensitization of CdSe nanoparticles sensitized TiO₂ NTs by N3 dye and (d) final structure of the fabricated solar cell device.

Further, the work was extended to form a hybrid solar cell from this cadmium chalcogenide. To form hybrid solar cell, the synthesized nanoparticles were blend with polymer to form a composite. Here, thioglycic acid capped CdSe nanoparticles were successfully synthesized using aqueous medium through wet chemical method. After the synthesis, particles were transferred into the organic medium using 1-dodecanethiol via partial ligand exchange strategy. The phase transferred particles were blend with polymer Poly-3-hexyl thiophene (P3HT) in chloroform are shown in Fig.3. The various volume of polymer blended in the nanoparticles shows the effective coupling and charge transfer process in blend. The charge transfer properties were utilized in the solar cell application.

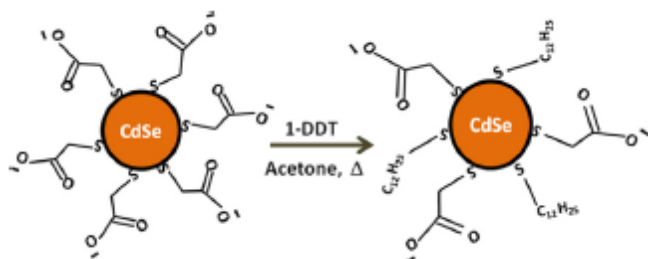


Fig.3. Phase transfer process of CdSe nanoparticles

Moreover, the morphological changes due to the influence of different selenium source were analyzed using this experiment. In this typical synthesis process, cadmium selenide (CdSe) were synthesized using colloidal aqueous medium method with two different

conditions of shown in Fig.4. Here, intermediated nanorod was synthesized by reduction in the presence of sodium borohydrate in water with selenium source, and sodium selenide as a selenium source. The nanorod shows trigonal phase while nanoparticles posses cubic zinc blend structure. The formation of nanorod depend upon the ratio of selenium and water. The reaction conditions prove the growth of the nanoparticles. The reaction conditions facilitate the growth from one dimension to zero dimension nanoparticles.

Now, the work concentrates on the synthesis of Cadmium Telluride (CdTe) nanoparticles for the solar cell application using aqueous medium method. In the typical synthesis process, 3- mercaptopropionic acid (MPA) acts as a capping agent to cap CdTe nanoparticles. The synthesis of CdTe NPs show power dependent up conversion photoluminescence (UCPL) nature. This up conversion luminescence emitted photons has large energy than the input photons. This UCPL effect is due to the presence of two- photon absorption in synthesized particles. In another work the CdTe were synthesized in aqueous medium and phase transfer method were applied to form organic stable ink. This ink blended with poly P3HT nanofibers to form an organic/inorganic composite as shown in Fig.5. The blending of inorganic nanoparticles in organic polymer were widely used in the solar cells to improve the charge transport property and percolation path than organic acceptor molecules in hybrid solar cells.

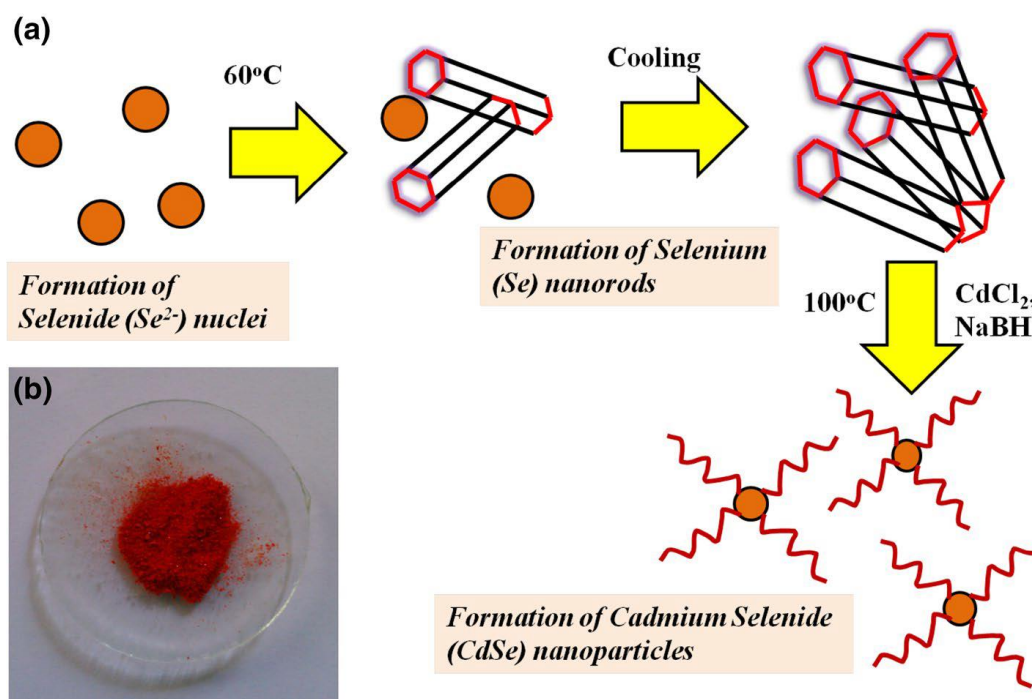


Fig.4. schematic diagram for the preparation of CdSe nanoparticles and nanorod

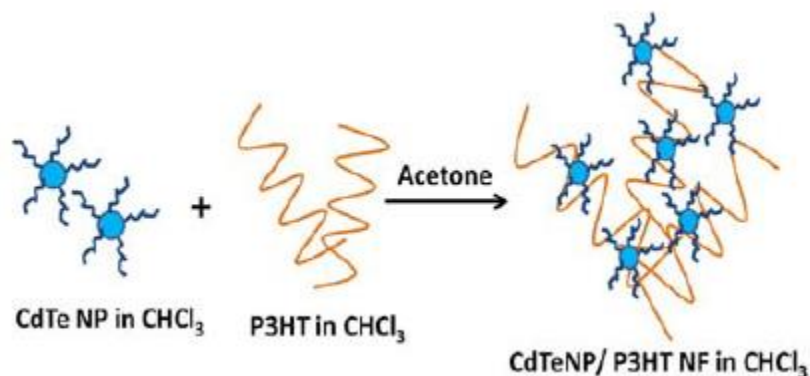


Fig.5. Formation procedure of CdTe nanoparticles/P3HT nanofiber blend

Furthermore, the work was also concentrated on the formation of ternary and quaternary semiconductor copper based chalcogenide for thin film solar cells and dye sensitized solar cells application. In these solar cells, the nanostructure and crystal structure play an important role to improve the power conversion efficiency of the device. The Copper indium diselenide (CuInSe_2) ternary chalcogenide were synthesized using hydrothermal synthesis method with two different capping agent. The role of the capping agent to form a rod like and cube like morphology was used in thin film solar cell application. Whereas, the quaternary copper zinc tin chalcogenide were synthesized using hot injection method as shown in Fig.6. Here the morphology of the nanoparticles was tuned by the influence of different organic solvent, while thiols play an important role in the formation of different crystallographic phase (kesterite and wurtzite). The CZTS has three crystal structures such as kesterite, stannite and wurtzite. The Kesterite is most stable tetragonal structure, whereas Wurtzite is Metastable Meta disordered with hexagonal structure. However, both ternary and quaternary belongs to p-type direct band gap with high absorption co-efficient. The CZTSSe as a thin film solar cell already reaches the efficiency above 12.6% and it has been reported by wang et al as hydrazine slurry based method. However, the hydrazine is highly toxic and need extreme caution before handling. So the research was focus on other methods like hydrothermal, solvothermal process and hot injection method. In the colloidal hot injection it exceeds the efficiency above 9%. The CZTS was also been proven as a effective counter electrode material to replace expensive platinum (Pt) in dye sensitized solar cells (DSSC). The world recorded efficiency of DSSC were 13% with conventional Pt counter electrode. The performance of CZTS in DSSC was recorded as 7.37%, whereas the Pt was 7.04% which highlights this material in DSSC application. In the thin film solar cells, kesterite structure has much attention as an absorber layer. In DSSC the wurtzite overtakes the performance compared with kesterite because of their high conductivity. These make this material as an interesting for research application.



Fig. 6. Synthesis process of CZTS nanoparticles in hot injection method

To prepare a counter electrode the synthesized of CZTS nanoparticles was dispersed in organic solvent to form a stable “nanoink”. Further the ink was spin coated on FTO to form a photocatode for DSSC application. Now the work was extended to fabricate DSSC solar cells using these quaternary nanoparticles as a counter electrode.



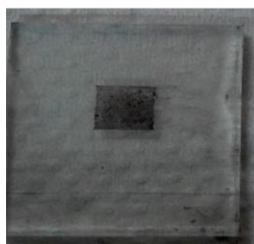
TiO₂ immersed
Dye Front view



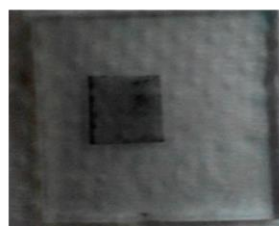
TiO₂ immersed
Dye black view



TiO₂ immersed
Dye Sensitizer



Wurtzite CZTS



Kesterite CZTS



Influence of different sulfur sources on the phase formation of $\text{Cu}_2\text{ZnSnS}_4$ (CZTS) nanoparticles (NPs)

C. Imla Mary¹ · M. Senthilkumar¹ · S. Moorthy Babu¹

Received: 11 December 2017 / Accepted: 29 March 2018 / Published online: 2 April 2018
© Springer Science+Business Media, LLC, part of Springer Nature 2018

Abstract

Wurtzite (Wz) and kesterite (Ks) phases of $\text{Cu}_2\text{ZnSnS}_4$ (CZTS) nanoparticles (NPs) have been selectively synthesized via hot injection method using 1-octadecene (1-ODE) as solvent. The solvents, 1-dodecanethiol (1-DDT) and *tert*-dodecanethiol (*t*-DDT) were utilized to control the reactivity of metal precursors and to tune the desirable crystallographic phases. The phase purity of the as synthesized CZTS NPs was confirmed using X-ray diffraction results. TEM images indicate that the developed nanoparticles consist of a mixture of triangular shaped (height 20 ± 3 nm, width 17 ± 2 nm) and sphere shaped NPs (13.4 ± 0.4 nm). These nanoparticles were formed due to the influence of thiols without any additional capping ligands. The band gap of as-synthesized CZTS NPs were calculated as 1.41 eV for wurtzite phase (Wz—1-DDT) and 1.47 eV for kesterite phase (Ks—*t*-DDT) from UV–Visible absorption results. CZTS thin films were prepared via spin coating and the electrical properties were analysed using Hall Effect measurements. Both the phases of CZTS films exhibit p-type conductivity. Wurtzite phase of CZTS has higher mobility ($23.6 \text{ cm}^{-2} \text{ V}^{-1} \text{ s}^{-1}$) and carrier concentration ($2.64 \times 10^{17} \text{ cm}^{-3}$) compared to kesterite phase of CZTS films.

1 Introduction

Thin-film solar cells based on CdSe, CdTe, $\text{CuIn}_x\text{Ga}_{1-x}(\text{Se})_2$ (CIGSe) were considered as promising materials with higher power conversion efficiency ($> 20\%$) and good stability [1, 2]. However, CdSe, CdTe, and CIGSe thin-film solar cells were not suitable for large scale applications because of the scarcity of indium (In) and toxicity (Cd, Te) of the constituents. Hence, an appropriate replacement for In and Ga was achieved through copper zinc tin chalcogenides which are inexpensive, less toxic and has earth abundant constituents. CZTS has high absorption coefficient and tunable band gap [3, 4]. Several methods were reported to produce CZTS NPs, but the solution based techniques were highlighted, due to the low cost preparation and ease of the chemical composition control [5]. The most popular solution methods to prepare CZTS NPs were hot injection method, high temperature assisted precipitation, hydrothermal and microwave synthesis [6–9]. Todorov co-workers reported, the fabrication of CZTSSe thin-film solar cell with

an efficiency of 12.6% using hydrazine slurry method via spin coating [10]. In the hydrazine slurry method, hydrazine is highly toxic and need extreme caution before handling [5]. Agrawal co-workers reported the alternative way for the fabrication of CZTSSe solar cell, prepared with thin layers of CZTS NPs with colloidal dispersion method through spin coating and the selenization process was carried out to form CZTSSe polycrystalline films which resulted in 7.2% efficiency [11]. Recently, several researchers have reported the synthesis of CZTS NPs using long chain alkyl ligands having high boiling point [12]. The CZTS NPs with kesterite phase have been synthesized using elemental sulfur with oleylamine by hot injection method were widely reported [13]. On the other hand there are reports on the synthesis of wurtzite CZTS NPs via hot injection method with alkyl thiols [14]. This work paves the novel way to synthesis of kesterite CZTS NPs without the elemental sulfur. In the present work, 1-DDT and *t*-DDT were used as the sulfur precursor to regulate the reaction with other three metal cation precursors to tune the crystalline phase of the CZTS NPs. Synthesized CZTS nanoparticles were characterized and the results are discussed.

✉ S. Moorthy Babu
babusm@yahoo.com; babu@annauniv.edu

¹ Crystal Growth Centre, Anna University, Chennai 600 025, India

2 Synthesis of wurtzite and kesterite phase CZTS NPs

The precursors, $\text{CuCl}_2 \cdot 2\text{H}_2\text{O}$, $\text{Zn}(\text{CH}_3\text{COO}) \cdot 2\text{H}_2\text{O}$ and $\text{SnCl}_2 \cdot 2\text{H}_2\text{O}$ from Fisher scientific, 1-octadecene, 1-dodecanethiol (*n*-DDT or 1-DDT) and *tert*-dodecanethiol (*t*-DDT) (mixture of isomers 95.8%) from Sigma-Aldrich, isopropanol and ethanol from SRL were used for the synthesis. All the chemicals were used without further purification. In the typical synthesis; 0.1 mM of copper chloride, 0.5 mM of zinc acetate, and 0.5 mM of tin chloride and 25 ml of 1-octadecene were added into the 100 ml three neck flask. The metal cation mixture was heated up to 140 °C under N_2 atm for 30 min. Then, the temperature of the mixture was raised to 240 °C and 5 ml of thiols (1-DDT, *t*-DDT) as sulfur source was rapidly injected into the mixture. Then, the reagent was heated up to 260 °C and maintained for 6 h to complete the reaction. These NPs were cooled naturally to room temperature and precipitated out by isopropanol followed by centrifugation. The supernatant was decanted and the precipitation was redispersed in ethanol thrice to remove residual precursors and ligands. Additionally, CZTS nanoparticles with kesterite phase were synthesized using elemental sulfur and *tert*-dodecanethiol with the following procedure: 2 mM of elemental sulfur was dissolved in ODE and mixed with metal cation at 140 °C. The rest of the synthesis process was similar to that of the synthesis of wurtzite phase of CZTS NPs.

2.1 Ink preparation and film deposition

The CZTS NPs were synthesized with different sulfur sources and dispersed in organic solvent to form a nano ink. Here, *n*-hexane was used to disperse the CZTS NPs with high concentration (10 mg ml^{-1}) [15]. The plain glass substrates were cut to 10 mm × 10 mm, cleaned by DI water and ethanol via sonication and allowed to dry. Then the prepared inks were coated on the plain glass substrate via spin coating with 4000 rpm for 10 s. After that, the films were dried at 150 °C for 10 min.

The crystalline structure of CZTS NPs was examined by XRD (Bruker D8 advance system). The surface morphology and elemental composition were determined by SEM (Carl Zeiss MA15/EVO 18) combined with energy dispersive X-ray spectroscopy (EDS). TEM images were collected using JEOL/JEM 2100. FTIR measurements were carried out using JASCO FTIR 6300 (ATR method). Optical measurements were analysed with JASCO UV-650 spectrophotometer. The electrical properties of CZTS films were carried out using ECOPIA Hall mobility measurement system.

3 Results and discussion

3.1 Structural analysis of kesterite and wurtzite phase of CZTS NPs

Kesterite and Wurtzite phase of CZTS NPs were synthesized using *t*-DDT and 1-DDT as sulfur sources. The *tert*-dodecanethiol (*t*-DDT) interacts with metal complexes via bond breaking process which leads to the formation of kesterite phase. The thermal decomposition of *t*-DDT was lower compared to 1-DDT with similar chemical bonding $\text{C}_{12}\text{H}_{26}\text{S}$ [16]. The preparation of kesterite phase CZTS NPs using the elemental sulfur is tedious and focused attention are needed to inject the sulfur anion into the metal cation to produce CZTS NPs. Other than elemental sulfur, using thiols is easier and it acts as sulfur source as well as capping ligand [17]. The Wurtzite phase was obtained by the slower phase evolution process. Sulfur is covalently bonded to carbon and hydrogen atoms, more stable than H_2S . After the injection of DDT into the metal complex, it gradually turns into black and these reactions undergo thiolate formation stage [18, 19]. The XRD pattern of as-synthesized CZTS NPs with kesterite and wurtzite phase are as shown in Fig. 1. The XRD pattern of CZTS NPs prepared using *t*-DDT as sulfur source shows the Ks-phase and matches well with JCPDS No-260575. The peaks observed at $2\theta = 28.5^\circ$, 32° , 47.4° , and 56.2° corresponding to (112), (200), (220), (312) planes confirm the kesterite phase. The diffraction peaks appear at $2\theta = 27^\circ$, 28.5° , 30.3° , 39.3° , 47.5° , 51.3° , and 56.3° correspond to (100), (002), (101), (102), (110), (103), and (112) planes of wurtzite phase, which matches well with the previous reports [20, 21]. CZTS NPs with kesterite and wurtzite structure exhibits, different composition (i.e.) Cu rich and Cu poor phases of CZTS. This may be due to the

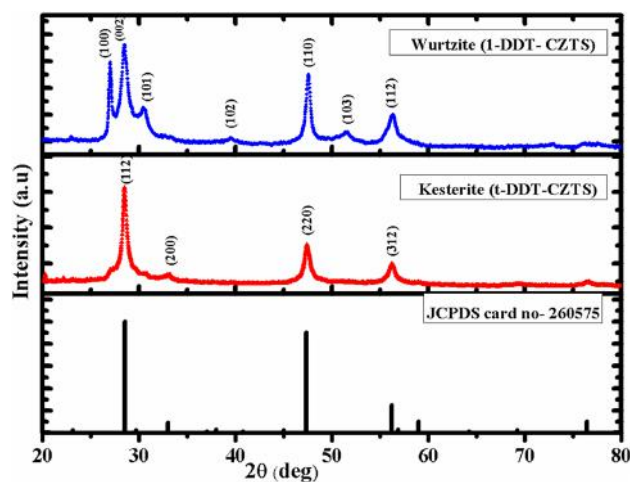


Fig. 1 XRD pattern of as-synthesized CZTS NPs

reactivity of metal precursors with different sulfur sources (1-DDT, *t*-DDT) [22].

3.2 Surface morphology and compositional analysis of CZTS NPs

Morphological properties of CZTS NPs synthesized using different sulfur sources such as 1-DDT, *t*-DDT were examined using SEM. Surface micrographs of CZTS NPs are shown in Fig. 2.

CZTS NPs of both the phases prepared with different sulfur sources have irregular nanosphere structure with agglomeration; it may be due to anisotropic growth of materials which result from the selective binding nature of the ligands. In addition to that, thiols plays the dual role (sulfur source and capping ligands) during the synthesis process. Whereas, 1-octadecene (ODE) was used as a non-coordinating solvent to make necessary balance between the nucleation and growth of the materials, it has no role on the particle morphology [5]. The morphology of the

resulting nanoparticles could be affected by the nature of various alkylthiols involved in the reaction. EDX confirm the presence of all elements in the synthesized $\text{Cu}_2\text{ZnSnS}_4$ NPs with different sulfur sources [18, 20]. The 1-dodecanethiol and *tert*-dodecanethiol ligands in the presence of non-coordinating solvent (ODE) control the morphology of CZTS NPs. Kesterite and wurtzite phase of CZTS NPs with different morphology were obtained using different thiols without any additional capping agents (as shown in Fig. 3). CZTS NPs employ 1-DDT as self capping ligand, exhibit mixture of triangular shape (height 20 ± 3 nm, width 17 ± 2 nm) and sphere shape (12.5 ± 1.5 nm) nanoparticles. The lattice fringes in image 3 (b) shows the interplanar spacing of 0.31 nm which corresponds to the (100) plane of wurtzite structure [14]. On the other hand, CZTS NPs obtained by *t*-DDT shows nanosphere with average diameter of 13.4 ± 0.4 nm. The fringes pattern (Fig. 3e) reveals the lattice spacing of 0.31 nm, for sample (2) which correspond to (112) plane of kesterite structured CZTS nanoparticles [18].

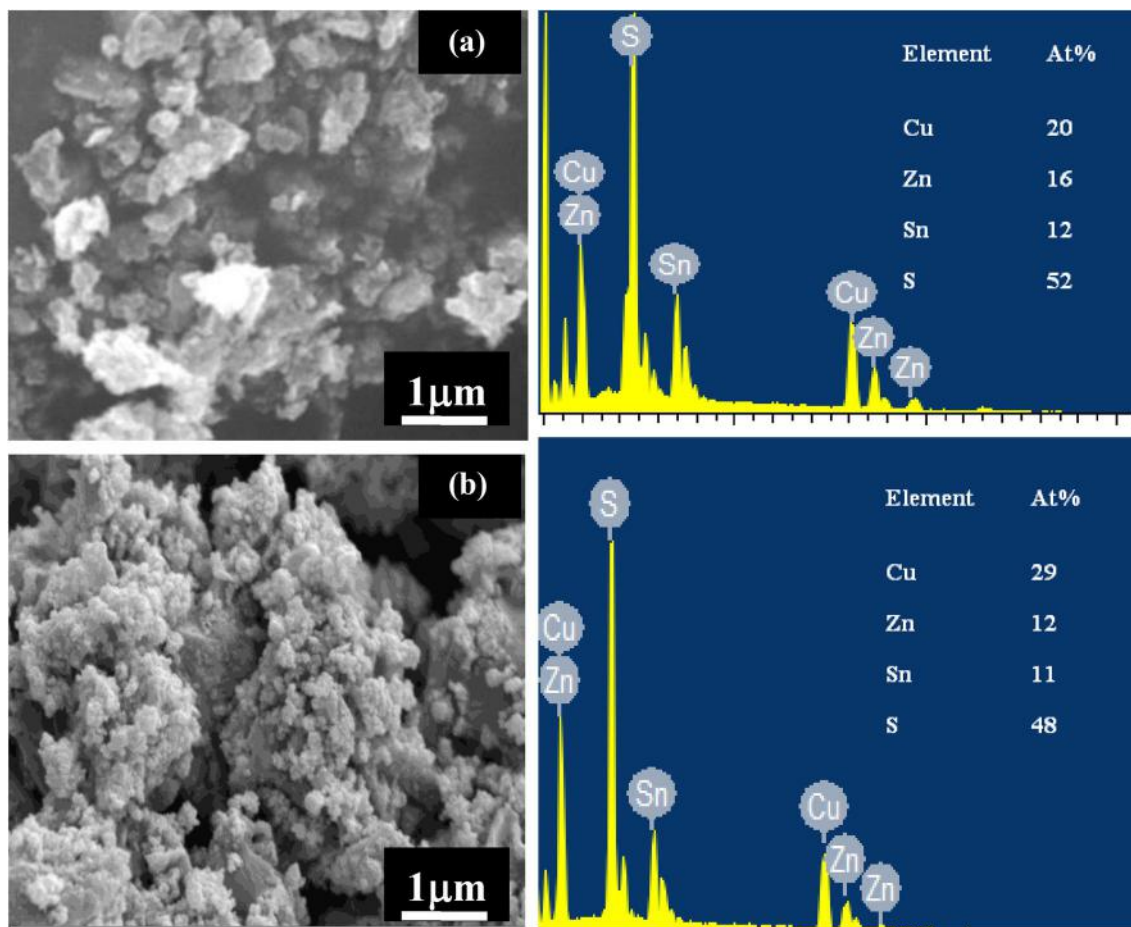


Fig. 2 SEM images **a** 1-DDT; **b** *t*-DDT synthesized CZTS NPs

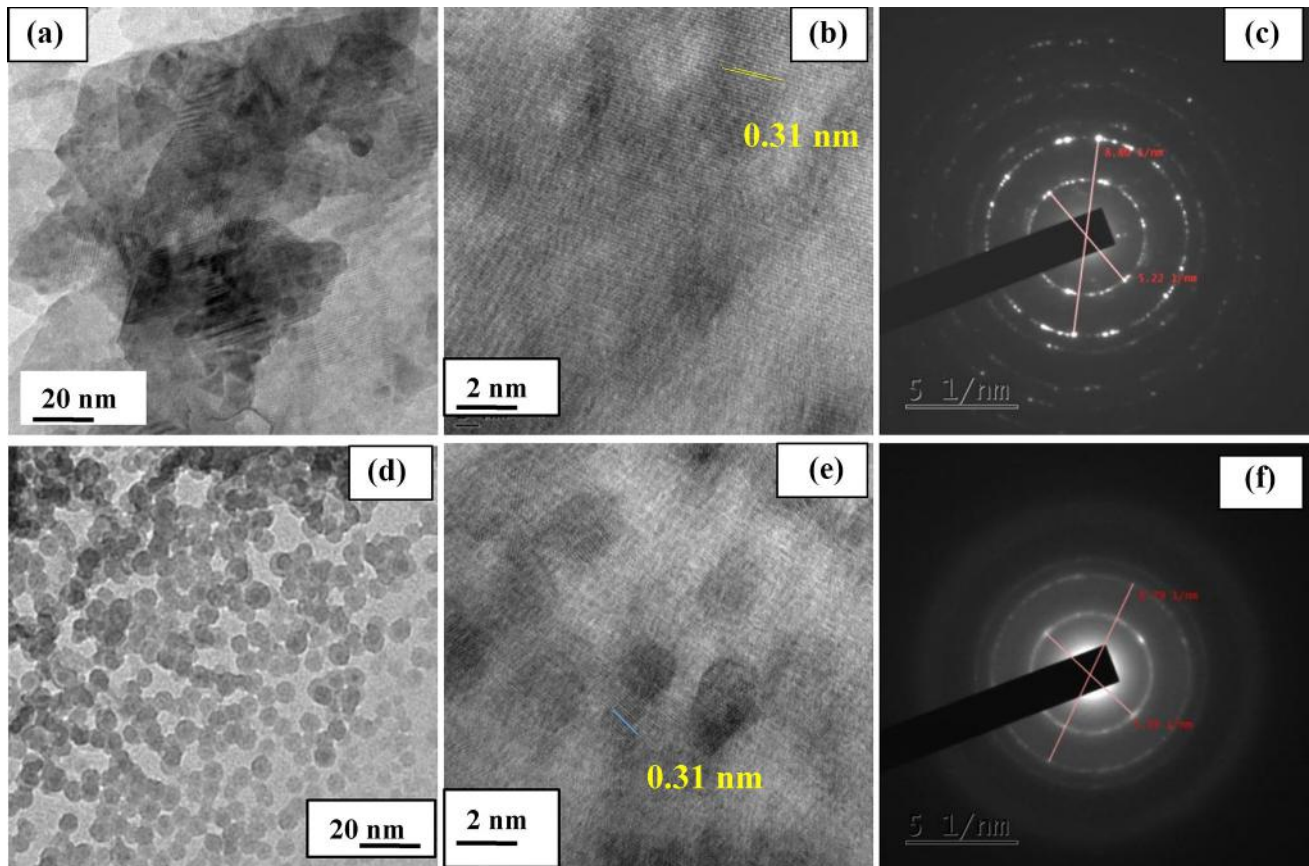


Fig. 3 a–c HR-TEM image of as-synthesized CZTS NPs with 1-DDT and d–f CZTS NPs with *t*-DDT

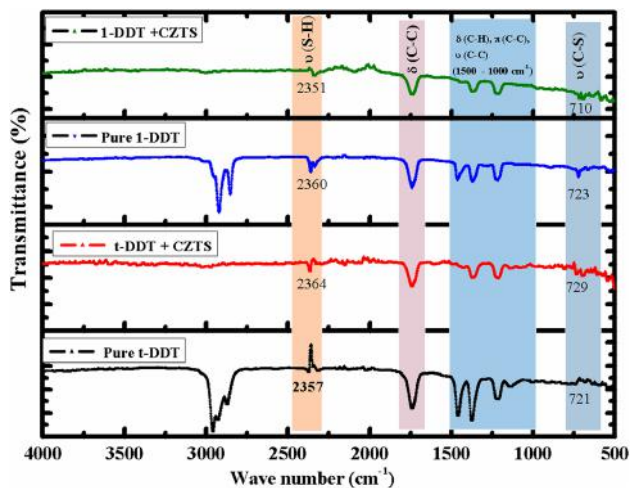


Fig. 4 ATR-FTIR spectra of as-synthesized CZTS NPs

3.3 FTIR analysis of CZTS NPs

ATR-FTIR spectra of as-synthesized NPs are shown in Fig. 4. The asymmetric and symmetric methylene stretching of pure *t*-DDT, 1-DDT and CZTS NPs appear in the

range 2957 to 2848 cm^{-1} . The S–H stretching modes were observed in the range of 2500–2300 cm^{-1} . The characteristic peaks in the range 1500–1000 cm^{-1} were attributed to C–H bending, wagging and C–C stretching. The vibrational modes present at 730–710 and 670–630 cm^{-1} were assigned to C–S ligand bonded with the as-synthesized CZTS NPs and carbonyl sulfide might serve as a sulfur-transfer reagent [23–25].

3.4 Optical studies of CZTS NPs

The UV–Visible absorption spectra of as-synthesized CZTS NPs are shown in Fig. 5a. The optical absorption also provide the information about the energy gap of the material. The Tauc plot was drawn from the absorption spectra to calculate the optical band gap of as-synthesized CZTS NPs. The band gap was obtained by extrapolating the linear portion of $(\alpha h\nu)$ versus $(h\nu)$ as shown in the insert of Fig. 5b. The band gap (e.g.) values of kesterite (*t*-DDT) and wurtzite (1-DDT) structure were estimated as 1.47 and 1.41 eV and these values match well with the previous reports [26]. The difference of absorption and shift in the band gap may be due to different structures/stoichiometry of the as-synthesized nanoparticles

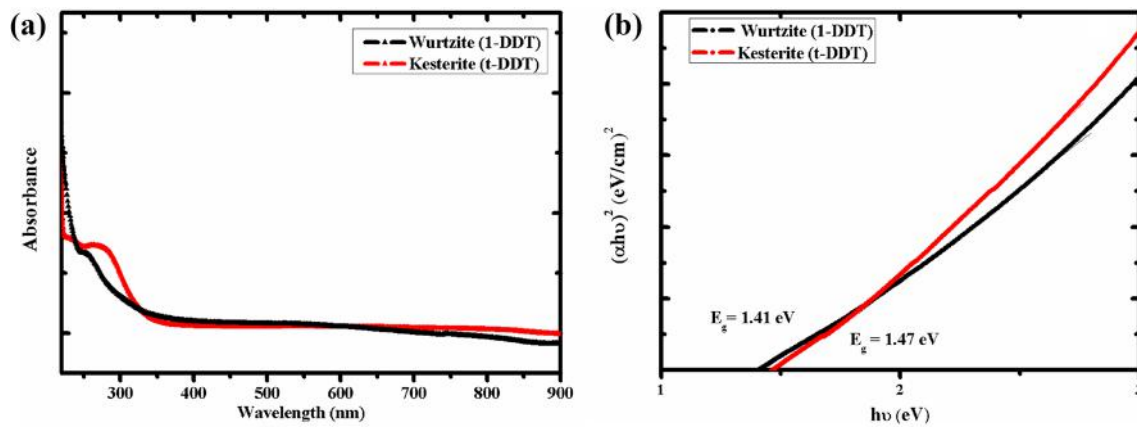


Fig. 5 **a** UV–Vis absorption spectra of as-synthesized CZTS NPs and **b** band gap of CZTS NPs. (Color figure online)

Table 1 represents the electrical properties of CZTS thin films with different crystalline phases

Sample (CZTS films)	Carrier concentration (cm ² Vs ⁻¹)	Hall mobility (cm ⁻³)	Resistivity (Ωcm)	Conductivity
Kesterite <i>t</i> -DDT	4.90×10^{17}	12.7	101	p-type
Wurtzite 1-DDT	2.64×10^{17}	23.6	100	p-type

owing to various sulfur sources as precursors. The resultant absorption spectra exhibit that the synthesized NPs has a broad absorption in the visible region [27–29].

3.5 Electrical properties of as-prepared CZTS films

The electrical properties of as-synthesized CZTS films were analysed using four probe—Hall Effect measurements at room temperature. Table 1. summarizes the carrier concentration, resistivity and hall mobility for the CZTS films prepared with alkyl thiols such as *tert*-dodecanethiol (*t*-DDT) and 1-dodecanethiol (1-DDT). The lower carrier concentration and higher mobility indicates the formation of larger grain boundaries [30]. The larger grain growth reduces the grain boundaries and the defect state in the CZTS films [30]. All the films exhibit p-type conductivity. In the kesterite phase CZTS films, the carrier concentration increases and the mobility decreases, it may be due to the presence of trace of different phases in the sample [31, 32].

4 Conclusion

Kesterite and wurtzite phase of CZTS NPs were successfully synthesized by hot injection method. The thiols with ODE were used to control the metal reactivity and result in the formation of different crystallographic phases. XRD results confirm the formation of kesterite and wurtzite phase, which depends on the reactivity of sulfur anion. Moreover, the change in band gap was established due to the nature of

sulfur precursors. TEM micrograph indicates that the thiols play an important role to form different morphology such as nanospheres and mixed morphology of nano triangular and spherical nanoparticles. The electrical properties were analyzed and all the films exhibit the p-type conductivity. Finally, the colloidal nanoparticles dispersed ink was prepared for the application in photovoltaic devices. Cu rich CZTS nanoparticles with kesterite structure will be beneficial for high efficiency photovoltaic devices.

Acknowledgements The authors sincerely thank Department of Science and Technology (DST-TM/SERI /FR/90 (G)) and University Grants Commission (F.No.42-855/2013) for funding the research work.

References

1. M.A. Green, K. Emery, Y. Hishikawa, W. Warta, Prog. Photovolt. Res. Appl. **19**, 84–92 (2011)
2. P. Jackson, D. Hariskos, E. Lotter, S. Paetel, R. Wuerz, R. Menner, W. Wischman, M. Powalla, Prog. Photovolt. Res. Appl. **19**, 894–897 (2011)
3. M.-H. Jao, H.-C. Liao, M.-C. Wu, W.-F. Su, Jpn. J. Appl. Phys. **51**, 10NC30 (2012)
4. S.W. Shin, J.H. Han, Y.C. Park, G. Agawane, C.H. Jeong, J.H. Yun, A.V. Moholkar, J.Y. Lee, J.H. Kim, J. Mater. Chem. **22**, 21727 (2012)
5. U. Ghorpade, M. Suryawanshi, S.W. Shin, K. Gurav, P. Patil, S. Pawar, C.W. Hang, J.H. Kim, S. Kolekar, Chem. Commun. **50**, 11258–11273 (2014)
6. D. Xia, P. Lei, Y. Zheng, B. Zhou, J. Mater. Sci.: Mater. Electron. **26**, 5426–5432 (2015)

7. V.A. Madiraju, K. Taneja, M. Kumar, R. Seelaboyina, *J. Mater. Sci.: Mater. Electron.* **27**, 3152–3157 (2016)
8. S.W. Shin, J.H. Han, Y.C. Park, G.L. Agawane, C.H. Jeong, J.H. Yun, A.V. Moholkar, J.Y. Lee, J.H. Kim, *J. Mater. Chem.* **22**, 21727–21732 (2012)
9. S.A. Vanalakar, G.L. Agwane, M.G. Gang, P.S. Patil, J.H. Kim, J.Y. Kim, *Phys. Status. Solidi C* **12**, 500–503 (2015)
10. W. Wang, M.T. Winkler, O. Gunawan, T. Gokmen, T.K. Todorov, Y. Zhu, D.B. Mitzi, *Adv. Energy. Mater.* **4**, 1301465 (2014)
11. Q. Guo, G.M. Ford, W.C. Yang, B.C. Walker, E.A. Stach, H.W. Hillhouse, R. Agrawal, *J. Am. Chem. Soc.* **132**, 17384–17386 (2010)
12. D. Aldakov, A. Lefrancois, P. Reiss, *J. Mater. Chem. C* **1**, 3756 (2013)
13. Q. Guo, H.W. Hillhouse, R. Agrawal, *J. Am. Chem.* **131**, 11672 (2009)
14. X. Lu, Z. Zhuang, Q. Peng, Y. Li, *Chem. Commun.* **47**, 3141–3143 (2011)
15. J. Kong, Z.-J. Zhou, M. Li, W.-H. Zhou, S.-J. Yuan, R.-Y. Yao, Y. Zhao, S.-X. Wu, *Nanoscale Res. Lett.* **8**, 464 (2013)
16. M. Kruszynska, H. Borchert, J. Parisi, J.K. Olesika, *J. Am. Chem. Soc.* **132**, 15976–15986 (2010)
17. S. Ananthakumar, J. Ramkumar, Y. Hayakawa, S. Moorthy Babu, *Jpn. J. Appl. Phys.* **54**, 08KA10 (2015)
18. Z. Li, A.L.K. Lui, K.H. Lam, L. Xi, Y.M. Lam, *Inorg. Chem.* **53**, 10874–10880 (2014)
19. M.D. Regulacio, C. Ye, S.H. Lim, M. Bosman, E. Ye, *Chem. Eur. J.* **18**, 3127–3131 (2014)
20. M. Li, W.-H. Zhou, J. Guo, Y.-L. Zhou, Z.-L. Hou, J. Jiao, Z.-J. Zhou, Z.-L. Du, S.-X. Wu, *J. Phys. Chem. C* **116**, 26507–26516 (2012)
21. Z. Hao, Z. Zhang, S. Liu, Y. Cui, *Mater. Lett.* **183**, 268–271 (2016)
22. B. Kempken, A. Erdt, J. Parisi, J. Kolny-Olesiak, *J. Nanomater.* (2015). <https://doi.org/10.1155/2015/826743>
23. N.K. Pal, C. Kryschi, *Phys. Chem. Chem. Phys.* **17**, 1957–1965 (2015)
24. C. Aprile, M.A. Herranz, E. Carbonell, H. Garria, N. Martin, *Dalton Trans.* (2009). <https://doi.org/10.1039/B814384F>
25. C. Dablemont, P. Lang, C. Mangeney, J.Y. Piquemal, V. Petkov, F. Herbst, G. Viau, *Langmuir* **24**, 5832–5841 (2008)
26. A. Singh, H. Geaney, F. Laffir, K.M. Ryan, *J. Am. Chem.* **134**, 2910–2913 (2012)
27. Y. Park, H. Jin, J. Park, S. Kim, *CrystEngComm* **16**, 8642–8645 (2014)
28. C. Steinhagen, M.G. Panthani, V. Akhavan, B. Goodfellow, B. Koo, B.A. Korgel, *J. Am. Chem. Soc.* **131**, 12554–12555 (2009)
29. K. Woo, Y. Kim, J. Moon, *Energy Environ. Sci.* **5**, 5340–5345 (2012)
30. J. Zhi, W. Shurong, L. Zhishan, Y. Min, L. Sijia, L. Yilei, Z. Qichen, H. Ruiting, *Mat. Sci. Semin. Proc.* **57**, 239–243 (2017)
31. M. Shakban, P.D. Matthews, N. Savjani, X.L. Zhong, Y. Wang, M. Missous, P. O'Brien, *J. Mater. Sci.* **52**, 12761–12771 (2017)
32. A. Aldabahi, E.M. Mkawi, K. Ibrahim, M.A. Farrukh, *Sci. Rep.* **6**, 32431 (2016)



ICSEP 2016

Synthesis and Characterization of amine capped $\text{Cu}_2\text{ZnSnS}_4$ (CZTS) nanoparticles (NPs) for Solar cell application

C. Imla Mary, S. Ananthakumar, M. Senthilkumar, and S. Moorthy Babu*

Crystal Growth Centre, Anna University, Chennai – 600 025, India

Abstract

The CZTS nanoparticles in Oleylamine (OAm) were successfully prepared via hot injection method. In this process, Oleylamine act as the electron donor at elevated temperature in addition to the role of a solvent. Kesterite phase formation was confirmed from XRD and Raman results. SEM results reveal that the range of monodispersed poly-crystalline CZTS nanoparticles was $1\mu\text{m}$ with agglomeration extensively. The capping property of OAm was confirmed with ATR- Fourier Transform infrared Spectroscopy (ATR-FTIR) and the functional groups adsorbed over the surface of CZTS nanoparticles were identified from the FTIR spectra. Optical absorption measurements show the direct band gap of 1.45eV, which was optimized for low-cost solar cells. Furthermore, the electrochemical measurements were carried out for the CZTS NPs to understand the electrochemical storage properties.

© 2017 Elsevier Ltd. All rights reserved.

Selection and/or Peer-review under responsibility of 2nd International Conference on Solar Energy Photovoltaic

Keywords: CZTS NPs; Oleylamine; hot injection method; solar cell material; shape control;

1.Introduction:

Thin film ternary semiconductors like CuInS_2 , AgInS_2 have attracted much attention due to their optical and electrical properties for devices, including solar cells, photovoltaic and optoelectronic applications, and have been widely demonstrated. However, the scarcity of rare metal indium in future has become a dilemma [1]. Recently, several works on compounds of earth- abundant elements with low toxicity revealed that they are reliable for low-cost and sustainable solar cells. $\text{Cu}_2\text{ZnSnS}_4$ (CZTS) is an emerging solar cell material that has earth-abundant elements which have a direct band gap of 1.4 to 1.6 eV and large absorption coefficient of $\sim 10^4\text{cm}^{-1}$ [2, 3]. A rapid development of copper zinc tin sulfide (CZTS) and selenide based CZTS thin-film solar cells show the power conversion efficiency from 8-12.6% range and the prominent potential of this material. CZTS thin films could be synthesized in many ways, including low cost throughput sputtering and co-evaporation from an elemental source in vacuum technique, which yield high conversion efficiencies up to 8% [2, 4-5]. While most methods rely on the traditional vacuum deposition, new scaling production based on nanocrystals (NCs) dispersion (ink) has also received much attention because of the potential to be less expensive than vacuum based deposition. Recently, several methods were reported for synthesizing CZTS nanocrystals dispersion. These dispersions indicated the potential of increasing the efficiency above 7% and concentrated research on the dispersions improved the efficiency above 9% [2,6-7,18]. The highest efficiency with $\text{Cu}_2\text{ZnSnS}_4\text{Se}_{4(1-x)}$ (CZTSSe) solar cells were from

* Corresponding author. Tel.: +91-44-22358333/22359112 ; fax: +91-44-22352774 . E-mail address: babu@annauniv.edu

molecular precursor solution or NCs dispersion. Although the molecular inks are readily scalable and also having the highly toxic solvent, such as hydrazine. Therefore, an alternative to these approaches in regard to numerous semiconductor NCs have proven that such NCs made from the hot injection technique have become competitive with molecular based ink for commercial- scale application [8-10]. The spearheading work was furnished by Guo et al., utilizing a dissolvable elemental sulfur as a source material. Further, the sulfur source was injected into the metal precursor and it was kept at 225°C for 30 min. Besides, the arranged nanocrystals (NCs) display kesterite structure with a stoichiometric ratio of 2.12:0.84:1.06:4 (Cu: Zn: Sn: S); and the outcome demonstrates that the band gap was marginally higher because of copper-rich composition compared with Zn/Sn ratio in the compound. Furthermore, the TEM picture for the blended NPs indicates gentle polydispersity with the particle size of 15-25 nm. In addition, Zn-rich and Cu-poor compositional modification were demonstrated by changing the metal cation ratio with the power conversion efficiency of 7.2% using this NPs [11-12]. Shannon et al., already reported the synthesis of CZTS NPs via hot injection method using two different surfactants such as Oleylamine (OAm), Trioctylphosphine oxide (TOPO). Initially, Oleylamine was used as solvent to form a metal complex between the cations in the range of 150°C, and the sulfur source was sonicated in oleylamine until the orange-red solution was obtained. Further the metal complex temperature reduces to 125°C after 0.5 h. Then, the TOPO solvent was heated up to 300°C with both metal precursor and sulfur source injected into it, for about 75 min. The reported TEM images show the triangular and spherical CZTS nanoparticles with average size of 12.8 ± 1.8 nm [2]. Typically, inorganic CZTS NPs were synthesized from metal ion complex as precursor materials, coordinating organic ligand with high boiling like oleylamine (OAm) as stabilizer, which also solubilize the nanoparticles. In the present work, efforts were made to synthesize CZTS nanoparticles using amine as stabilizer and its structural, optical and electrical properties were investigated for application in solar cell devices.

2. Experimental Procedure:

All the chemicals, reagents, and solvents were used without further purification. In a typical synthesis process 2mmol of Cu₂Cl, 1.2 mmol of Zn(CH₃COO)₂, 1 mmol of SnCl₂.2H₂O and 10 ml of OAm were added to three neck flasks with N₂ bubbling. The mixture was heated up to 140°C for 30 min. The elemental source of 4mmol sulfur and 10 ml of OAm were added to another 100 ml three neck flasks with N₂atm; the mixture was kept at 140 °C for 30 min. Further, it was rapidly injected into the metal ion complex. Then the temperature was increased to 240 °C and kept for 90 min under vigorous stirring. After that the mixture was cooled to 60 °C, 20 ml of isopropanol was added to the flask and it was kept for a day. Furthermore, ethanol was added thrice to remove the supernatant via centrifugation at 5000 rpm for 10 min. The precipitate was dried at room temperature and normal atmosphere (atm). The CZTS nanoparticles could be dispersed in n-hexane to form a stable ink.

2.1. Characterization

The Crystallinity of CZTS NPs were analysed with X-ray diffraction (XRD) by using Burker D8 advance. Raman spectrum were taken using nanophoton - Raman 11 with the wavelength of 532 nm excitation line in our laser. The microstructure and elemental analysis of NPs were analysed using Carl Zeiss MA15/EVO 18 scanning electron microscope (SEM) which was equipped with energy dispersive X-ray analysis (EDX). The capping property of as-synthesized NPs was examined by ATR-FTIR method using JASCO FTIR 6300. Optical measurements were carried out with JASCO UV- 650 spectrophotometer. Cyclic voltammetry measurements were carried out using BIOLOGIC VSP MODEL EC-LAB 10.40 workstation.

3. Results& Discussion:

3.1. Structural Characterization

CZTS nanoparticles were synthesized using Oleylamine as a solvent. Oleylamine act as an electron donor at the elevated temperature. In earlier works on amines, it was found that elemental sulfur reacts with OAm in room temperature and forms alkylammonium polysulfide. At the elevated temperature these polysulfide ion interacts with excess amine and it produces H₂S [13-14]. In this reaction OAm-S mixture is injected into the metal complex solution kept at above 240 °C, after the injection, the color of the mixture turns dark simultaneously. The H₂S produced in OAm-S, rapidly react with Cu-, Zn-, Sn-OAm metal complexes, which lead to the formation of

kesterite phase [15]. XRD pattern of as-synthesized CZTS nanoparticles is shown in Fig 1. All the diffraction peaks were indexed and matches well with JCPDS-260525. The three major peaks at 28.57° , 47.4° , 56.3° may be attributed to (112), (220), and (312), planes respectively. Raman spectrum was measured to identify the phase of the as-prepared CZTS NPs. Fig 2, shows the existence of kesterite CZTS NPs with an intense peak at 333 cm^{-1} [10]. The line broadening and the peak shift in the Raman spectrum indicate the interaction of crystallite size distribution and the phonon dispersion [16-17].

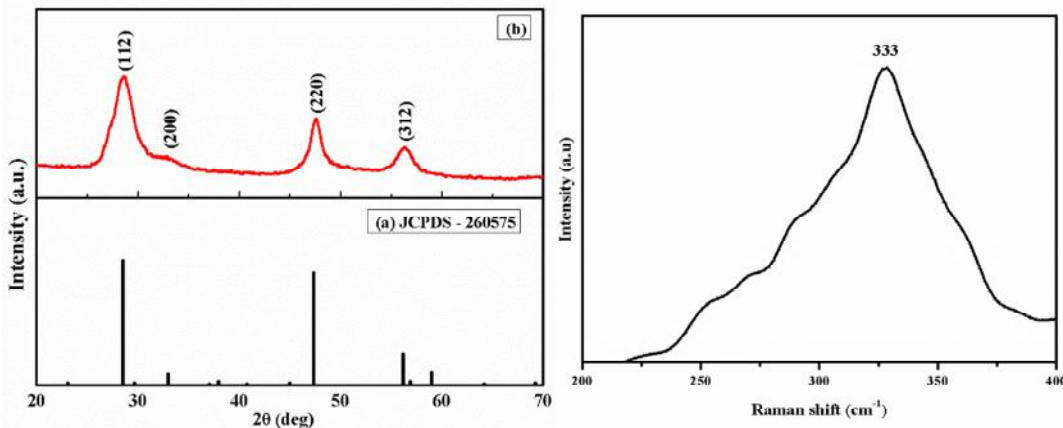


Fig 1. PXRD Pattern of (b) as-synthesized CZTS NPs Fig 2. Raman spectrum of as-prepared NPs

3.2. Surface morphological properties:

Fig 3.(a,b) represents the SEM micrographs of as-synthesized CZTS NPs. The morphology of as-synthesized CZTS NPs reveal uniformly agglomerated nanoparticles, with the average size of the particles in the range of $1\mu\text{m}$. Fig 3. (c) indicates the average composition of CZTS nanoparticles determined by EDX analysis ($\text{Cu}_{1.8}\text{Zn}_1\text{Sn}_{0.99}\text{S}_{4.2}$). The Zn-rich and Cu- poor composition was observed from the stoichiometric ratio, this may be due to the reactivity of different metal precursors [18-21].

3.3. Optical studies:

The absorption spectrum of as-synthesized CZTS NPs was obtained using UV-Visible spectroscopy. Insert of Fig 4.shows the band gap of as-prepared samples estimated from the UV-Visible spectra, as 1.45 eV by the extrapolation of a linear region of the plot of the energy (E) Vs $(\alpha h\nu)^2$ [3]. The band gap energy of as-prepared CZTS NPs are close to the optimum value for photovoltaic solar cells and deserve further research [12, 20]. The role of capping agent over the surface was analysed using ATR- FTIR spectra. Fig 5, shows the ATR-FTIR spectra for as-synthesized CZTS NPs as well as pure OAm. The IR absorption band that exhibit in the range of $1330\text{-}1650\text{ cm}^{-1}$ are due to $-\text{NH}_2$ bending mode [22]. The synthesized CZTS NPs exhibit IR absorption at 2914 cm^{-1} , 2846 cm^{-1} which correspond to the vibration of C-H bond in the surface of as- synthesized CZTS NPs in OAm. The adsorbed C-H bond on the surface shows that OAm is acting as a capping ligand over the particles [23-26].

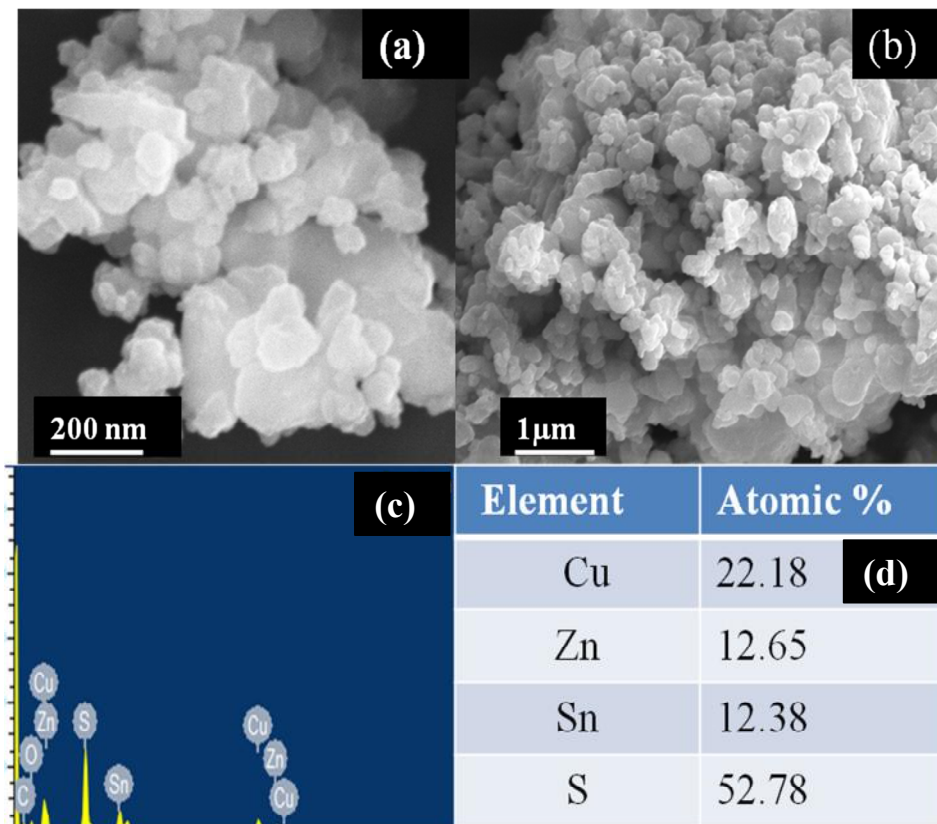


Fig 3. (a, b) SEM micrograph of CZTS NPs with agglomerated sphere in different scale. (c) EDX Spectrum of as-prepared CZTS NPs and (d) Compositional ratio of the elements

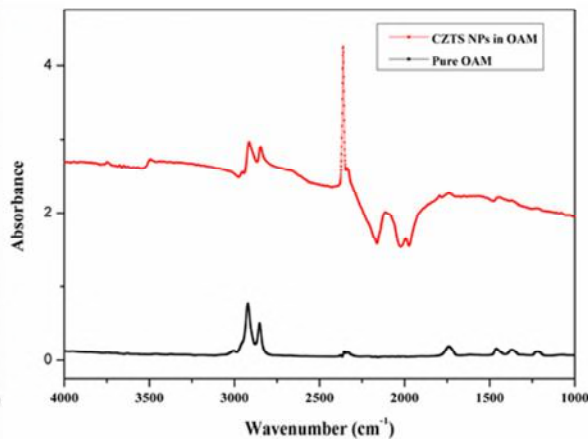
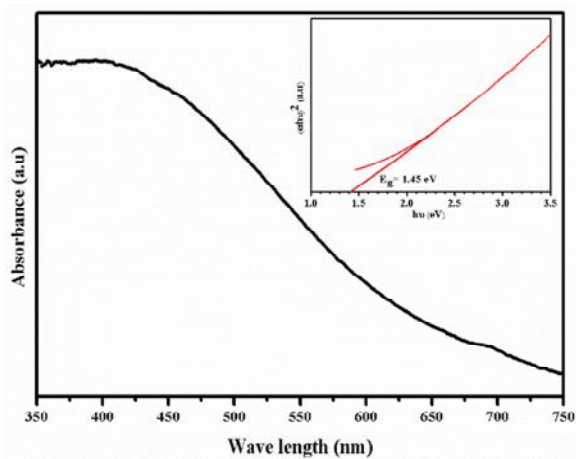


Fig 4. UV-Vis absorption spectrum of CZTS nanoparticles., Fig 5. ATR- FTIR spectra of as-synthesized CZTS NPs
The band gap of the CZTS NPs was plotted at the right corner

3.4. Electrical studies:

The CV measurement was used to identify the conduction band and valence band levels of kesterite CZTS NPs. In the earlier work, Yeng et al., reported the VB and CB energy levels as -5.40 eV and -3.85 eV using cyclic voltammetry measurements. Fig (6) represents the CV results of as-prepared CZTS NPs. The reduction potential (E_{red}), and the oxidation potential (E_{ox}) was calculated from Fig 6. The conduction band energy level (E_{CB}), valence band (E_{VB}) and electrical band gap energy (E_g) were then calculated [27-28]. The oxidation potential (1 V) and the reduction potential (-0.6 V) were determined and the band gap was calculated using the following equation. The calculated VB and CB energy levels are -5.4 eV and -3.8 eV for the as-prepared samples.

$$E_{CB/VB} = [(E_{red/ox} - E_{ferrocene}) + 4.7] \text{ eV}$$

The electrochemical band gap was determined by the difference between VB and CB. The estimated electrical band gap was 1.6 eV. This higher electrical band gap may be due to the interfacial energy barrier between CZTS samples and the electrode [28].

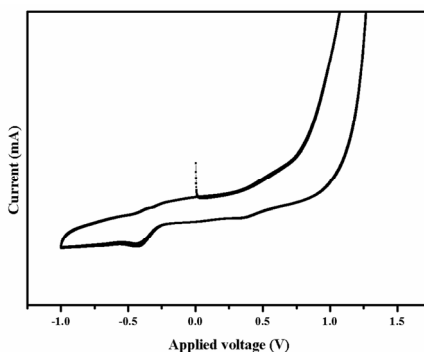


Fig 6. Cyclic Voltammograms of kesterite CE with a scan rate of 20 mVs^{-1}

4. Conclusion:

Hot injection method was used to synthesis CZTS nanoparticles. XRD reveals the kesterite phase. Phase purity of CZTS NPs were confirmed from the Raman results. The EDX results confirm the stoichiometric composition of the synthesized NPs. SEM micrographs reveal that as-synthesized CZTS nanoparticles are uniformly distributed with agglomeration. ATR-FTIR spectra confirm the presence of capping agent over the surface of as-synthesized CZTS NPs. The UV-Vis results indicate that the optical band gap of as-synthesized CZTS nanoparticles is 1.45 eV. The electrical energy band gap were determined by CV measurements and the band gap was found to be 1.6 eV. The developed kesterite CZTS nanoparticles are suitable for solar cell devices.

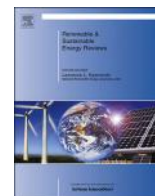
Acknowledgement:

The authors would like to acknowledge DST (DST-TM /SERI /FR /90 (G)) and UGC (F. No.42-855/2013) for their financial support

References:

- [1] Chao Zou, Lijie Zhang, Deshang Lin, Yun Yang, Qiang Li, Xiangju Xu, Xi'an Chen and Shaoming Huang "Facile synthesis of $\text{Cu}_2\text{ZnSnS}_4$ nanocrystals" *CrystEngComm.*, 2011, 13, 3310
- [2] Shannon C. Riha, Bruce A. Parkinson, and Amy L. Prieto "Solution-Based Synthesis and Characterization of $\text{Cu}_2\text{ZnSnS}_4$ Nanocrystals" *J. Am. Chem. Soc.*, 2009, 131, 34, 12055
- [3] Youngwoo Kim, Kyoohye Woo, Inhyuk Kim, Yong Soo Cho, Sunho Jeong and Jooho Moon "Highly concentrated synthesis of copper-zinc-tin-sulfide nanocrystals with easily decomposable capping molecules for printed photovoltaic applications" *Nanoscale.*, 2013, 5, 10183
- [4] B. Selin Tosun, Boris D. Chernomordik, Aloysius A. Gunawan, Bryce Williams, K. Andre Mkhoyan, Lorraine F. Francis and Eray S. Aydil " $\text{Cu}_2\text{ZnSnS}_4$ nanocrystal dispersions in polar liquids" *Chem. Commun.*, 2013, 49, 3549
- [5] B. Shin, O. Gunawan, Y. Zhu, N.A. Bojarczuk, S. Jay Chey and S. Guha, "Thin film solar cell with 8.4% Power conversion efficiency using an earth-abundant $\text{Cu}_2\text{ZnSnS}_4$ absorber" *Prog. Photovolt. Res. Appl.*, 2011, 1174
- [6] Uma Ghorpade, Mahesh Suryawanshi, Seungwook Shin, Kishor Gurav, Pramood Patil, Sambhaji Pawar, Chang Woo Hang, Jin Hyeok Kim and Sanjay Kolekar "Towards environmentally benign approaches for the synthesis of CZTSSe nanocrystals by a hot injection method: a status review" *Chem. Commun.*, 2014, 50, 11258-11273
- [7] C. Miskin, W-C. D. Yang, C J. Hages, N J. Carter, C. Joglekar, E A. Starch and R. Agrawal "9.0% efficient $\text{Cu}_2\text{ZnSn}(\text{S}, \text{Se})_4$ solar cells from selenized nanoparticle inks" *Prog. Photovolt. Res. Appl.*, 2014, DOI: 10.1002/pip. 2472
- [8] Joel van Embden, Anthony S.R. Chesman, Enrico Della Gaspera, Noel W. Duffy, Scott E. Watkins, and Jacek J. Jasieniak " $\text{Cu}_2\text{ZnSnS}_4\text{Se}_{4(1-x)}$ Solar Cells from Polar Nanocrystal Inks" *J. Am. Chem. Soc.*, 2014, 136, 5237–5240
- [9] Trevor R. Martin, John K. Katahara, Cori N. Bucherl, Benjamin W. Krueger, Hugh W. Hillhouse, and Christine K. Luscombe "Nanoparticle Ligands and Pyrolyzed Graphitic Carbon in CZTSSe Photovoltaic Devices" *Chem. Mater.*, 2016, 28, 135–145
- [10] Hao Wei, Wei Guo, Yijing Sun, Zhi Yang and Yafei Zhang "Hot-injection synthesis and characterization of quaternary $\text{Cu}_2\text{ZnSnSe}_4$ nanocrystals" *Materials Letter.*, 2010, 64, 1424-1426
- [11] Q. Guo, H.W. Hillhouse, and R. Agrawal "Synthesis of $\text{Cu}_2\text{ZnSnS}_4$ nanocrystal ink and its use for solar cells" *J. Am. Chem.*, 2009, 131, 11672
- [12] Q. Guo, G.M. Ford, W. C. Yang, B.C. Walker, E.A. Starch, H.W. Hillhouse, and R. Agrawal, "Fabrication of 7.2% Efficient CZTSSe Solar Cells Using CZTS Nanocrystals" *J. Am. Chem. Soc.*, 2010, 132, 17384
- [13] R.E. Davis, H. F. Nakshbendhi "Sulfur in Amine Solvents" *J. Am. Chem. Soc.*, 1962, 84, 2085-2090
- [14] J.W. Thomson, Nagashima. K, Macdonald. PM, Ozin. GA. "From Sulfur-Amine Solutions to Metal Sulfide Nanocrystals: Peering into the Oleylamine-Sulfur Black Box" *J. Am. Chem. Soc.*, 2011, 133, 5036-5041
- [15] Z. Li, A.L.K. Lui, K.H. Lam, L. Xi and Y.M. Lam "Phase-Selective Synthesis of $\text{Cu}_2\text{ZnSnS}_4$ Nanocrystals using different Sulfur Precursors" *Inorg. Chem.*, 2014, 53, 10874-10880
- [16] Mei Li, Wen – Hin Zhou, Jie Guo, Yang- Li Zhou, Ze-Liang Hou, Jie Jiao, Zheng-Ji Zhou, Zu-Liang Du, and Si-Xin Wu, "Synthesis of Pure Metastable Wurtzite CZTS Nanocrystals by Facile One-Pot Method" *J. Phys. Chem. C.*, 2012, 116, 26507- 26516
- [17] Prashant K. Sarswat, Michael L. Free, "An Investigation of rapidly synthesized $\text{Cu}_2\text{ZnSnS}_4$ nanocrystals" *J. Crystal. Growth*, 2013, 372, 87-94
- [18] R. Saravana Kumar, Beo Deul Ryu, S. Chandramohan, Jin Kyung Seol, Sang-Kwon Lee, Chang-Hee Hong, "Rapid synthesis of sphere-like $\text{Cu}_2\text{ZnSnS}_4$ microparticles by microwave irradiation" *Materials letters.*, 2012, 86, 174-177
- [19] Mou Pal, N.R. Mathews, R. Silva Gonzalez, X. Mathew, "Synthesis of $\text{Cu}_2\text{ZnSnS}_4$ nanocrystals by solvothermal method", *Thin Solid Films.*, 2013, 535, 78-82
- [20] M. Dimitrievska, A. Fairbrother, X. Fontane, T. Jawhari, V. Izquierdo-Roca, E. Saucedo and A. Perez-Rodriguez "Multiwavelength excitation Raman scattering study of polycrystalline Kesterite $\text{Cu}_2\text{ZnSnS}_4$ thin films" *Appl. Phys. Lett.*, 2014, 104, 021901
- [21] S. Ananthakumar, J. Ram Kumar, S. Moorthy Babu "Influence of co-ordinating and non-coordinating solvents in structural and morphological properties of $\text{Cu}_2\text{ZnSnS}_4$ (CZTS) nanoparticles" *Optik.*, 30, 2017, 99-105

- [22] Z. Xu, C. Shen, Y. Hou, H. Gao, and S. Sun “Oleylamine as both reducing agent and stabilizer in a facile synthesis of magnetite nanoparticles”, *Chem. Mater.*, 2009, 21, 1778-1780
- [23] Shri Kant Verma, Vikash Agrawal, Kiran Jain, Renu Pasricha, and Suresh Chand “ Green Synthesis of Nanocrystalline $\text{Cu}_2\text{ZnSnS}_4$ powder using Hydrothermal Route” *J. Nanoparticles.*, 2013, 685836- 685843
- [24] Xianzhong Lin, Jaison Kavalakkatt, Kai Kornhuber, Sergiu Levchenko, Martha Ch. Lux-Steiner, Ahmed Ennaoui “Structural and optical properties of $\text{Cu}_2\text{ZnSnS}_4$ thin film absorber from ZnS and Cu_3SnS_4 nanoparticles precursors” *J. TSF.*, 2012, 10, 034
- [25] B. Selin Tosun, Boris D. Chernomordik, Aloysius A. Gunawan, Bryce Williams, K. Andre Mkhoyan, Lorraine F. Franics, and Eray S. Aydil, “ $\text{Cu}_2\text{ZnSnS}_4$ nanocrystal dispersions in polar liquids” *Chem. Commun.*, 2013, 49, 3549-3551
- [26] Stefanos Mourdikoudis, and Luis M. Liz- Marzan “Oleylamine in nanoparticle synthesis” *Chem. Mater.*, 2013, 25, 1465-1476
- [27] J. Kong, Z. Zhou, M. Li, W.H. Zhou, S.J. Yuan, R.Y. Yao, Y. Zhao and S.X. Wu, “Wurtzite copper- zinc-tin sulfide as a superior counter electrode material for dye-sensitized solar cells” *Nano research letters.*, 2013, 8, 64
- [28] Z. Li, A.L.K. Lui, K.H. Lam, L. Xi, and Y.M. Lam “Phase-Selective Synthesis of $\text{Cu}_2\text{ZnSnS}_4$ Nanocrystals using different sulfur precursor” *Inorg. Chem.*, 2014, 53, 10874-10880



Semiconductor nanoparticles sensitized TiO₂ nanotubes for high efficiency solar cell devices



S. Ananthakumar, J. Ramkumar, S. Moorthy Babu*

Crystal Growth Centre, Anna University, Chennai 600025, India

ARTICLE INFO

Article history:

Received 15 April 2014

Received in revised form

1 October 2015

Accepted 17 December 2015

Available online 8 January 2016

Keywords:

TiO₂ nanotubes

Sensitization

Semiconductor nanoparticles

Co-sensitization

ABSTRACT

Titanium di-oxide (TiO₂) nanotubes (NTs) based solar cells are currently analyzed for the high efficiency solar cell devices due to its efficient electron transport. In this context, the present review deals about the recent advances made through the semiconductor nanoparticles sensitization on well aligned, vertically oriented TiO₂ NTs for fabrication of high efficiency third generation solar cells architecture. This review also deals with the efficient methods which are currently used to sensitize TiO₂ NTs by semiconductor nanoparticles. Special attention has been paid to the sensitization effect of cadmium chalcogenides based nanoparticles (CdS, CdSe, CdTe) on TiO₂ nanotubes in improving the efficiency of the solar cell. The expectations on TiO₂ NTs to face the 20 Terawatt (20 TW) challenge is examined.

© 2015 Elsevier Ltd. All rights reserved.

Contents

1. Introduction	1307
2. TiO ₂ nanotubes preparation	1308
3. Sensitization of TiO ₂ nanotubes	1308
4. Sensitization of TiO ₂ nanotubes by semiconductor nanoparticles for solar cells	1309
4.1. Cadmium chalcogenides	1309
4.2. Titania nanoparticles	1313
4.3. Lead chalcogenides nanoparticles	1314
4.4. Chalcopyrites nanoparticles	1314
4.5. Miscellaneous	1314
5. Co-sensitization on TiO ₂ nanotubes	1315
6. Conclusion and future perspectives	1318
Acknowledgments	1320
References	1320

1. Introduction

Titanium di-oxide (TiO₂) based nanomaterials have proven potential candidates for several applications including photo-catalysis to degrade the pollutants in water, solar cells, sensors, transducer, hydrogen generation etc [1–3]. Due to its bio-compatibility, much more research are being devoted for implantation and drug delivery applications [4,5]. In recent years, one dimensional tubular structures

are widely analyzed for various applications due to their high advantages in electronic, structural and optical properties compared to the zero dimensional materials. In this view, synthesis of vertically oriented TiO₂ nanotubes (NTs) were strongly researched. The main advantage here is the current flow in nanotubular architecture which dominates particles, due to the one-dimensional structure (Fig. 1). TiO₂ NTs were widely studied for several applications for the past decades mostly for photoelectrochemical water splitting applications by doping, artificial photosynthesis, hydrogen sensing etc. [6–9]. After the pioneering work done by Shankar, Grimes, Schmuki [10–13(a,b)], the applications of these TiO₂ NTs has turned out into large interest in photocatalysis, dye-sensitized solar cells etc. Hence, research work on

* Corresponding author. Tel.: +91 44 22358333; fax: +91 44 2235 2774.

E-mail addresses: babu@annauniv.edu, babum@yahoo.com (S.M. Babu).

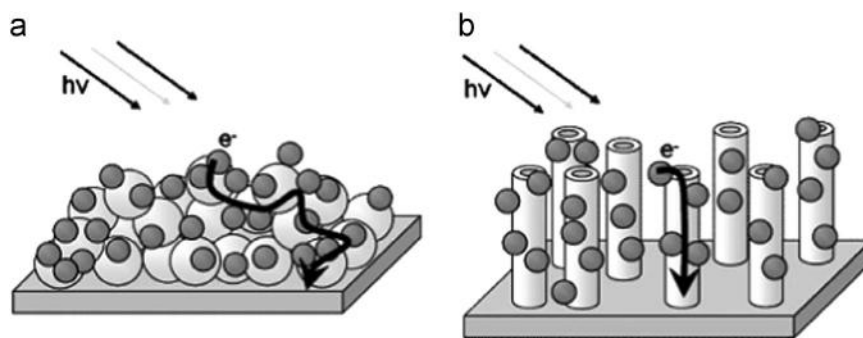


Fig. 1. Schematic diagram of transport of electron in (a) nanoparticles and (b) nanotubes. Reprinted with permission from Ref. [53] Copyright©2009 American Chemical Society.

flexible, low cost, high electron transport TiO_2 NTs array based solar cell fabrication was much motivated. But due to the wide band gap of TiO_2 (3.2 eV), its photon harvesting ability is limited only with UV region. In order to improve the photoresponse of TiO_2 , some additional ways of attaching the molecules or compounds on the surface of TiO_2 which could harvest photons at visible range is followed. For the dye sensitized solar cells (DSSCs), this process is done by ruthenium based organo-metallic complexes and for quantum dot sensitized solar cells (QDSSCs), it is done by semiconductor nanoparticles on the mesoporous TiO_2 nanoparticle layer [14–17]. This process of making the extension of spectral absorption region of TiO_2 from UV to Visible is called sensitization. Gratzel et al. [18] fabricated the first dye sensitized solar cell based on the sensitization of TiO_2 mesoporous film on the conducting substrate. Several excellent reviews deal about the dye sensitized, quantum dot sensitized TiO_2 solar cell architectures [19–23]. Compared to the nanoparticles, nanotubular arrangement has several advantages in terms of electron transport. The decoration or sensitization of semiconductor nanoparticles on TiO_2 NTs is considered one of the best strategy to improve the charge transfer as well enhanced light absorption. Their high mobility of electrons over nanoparticles have good advantage for various applications like photocatalysis, photoelectrochemical analysis etc. For the future generation high efficiency solar cells, photon harvesting over visible region is much desirable one. Hence, the sensitization of TiO_2 NTs by visible to infrared harvesting semiconductor nanoparticles plays a major role for the enhanced photon collection. Moreover, the role of surface capping agent (or) ligand of the nanoparticles to anchor on the surface of the TiO_2 NTs is very important one for the improved photoelectrochemical, photocatalytic performance. Understanding the interaction of semiconductor nanoparticles with the TiO_2 NTs surface is essential one in order to achieve high efficiency solar cells. In this view, the detailed analysis of the attachment of semiconductor nanoparticles on the surface of TiO_2 NTs and the charge transfer between ligand of the nanoparticles and TiO_2 NTs are highly encouraged. The recent advances of TiO_2 NTs solar cells based on semiconductor nanoparticles sensitization are the crucial one in order to make high efficiency solar cell assembly. This process have shown potential impact for the dye-sensitized solar cells to currently emerging hybrid-perovskite solar cells [24]. Here in this review, the importance and present scenario of sensitization process of TiO_2 NTs by semiconductor nanoparticles for high efficiency solar cell devices are discussed. The influence of sensitization (or) decoration of nanoparticles in terms of efficiency are also discussed.

2. TiO_2 nanotubes preparation

Preparation of tubular structure of oxides were widely focused due to their superior advantages over particle structure. Several methods were utilized for the synthesis of TiO_2 nanotube arrays including

solvothermal, hydrothermal, sol-gel, template based process and electrochemical anodization [25–29]. After the major breakthrough work done by Masuda and Fukuda [30], the view of anodization of metals were turned into large interest. Among other techniques used to produce TiO_2 NTs, electrochemical anodization is widely used particularly for the solar cell applications due to its simplicity in experimental arrangement, tuning of pore size and length by altering the voltage, electrolyte and anodization process duration. TiO_2 NTs produced through electrochemical anodization possesses good alignment with large aspect ratio (surface area) with length that varies from 100–1000 μm [31–33]. Since the reduced recombination process compared to nanoparticles made the nanotubes preparation more interesting one, this method is highly encouraged for the solar cell applications. Furthermore, the double walled, free standing membrane approaches of producing TiO_2 NTs through this method has shown a promising way to achieve high efficiency in solar cells [34]. The first generation formation of TiO_2 NTs were mainly oriented with non-organic electrolytes which made a ripples on the sides of the TiO_2 NTs. Moreover, the length of the formation of nanotubes using water as the medium was very low [35]. So far, only non-aqueous electrolytes such as dimethyl formamide (DMF), DMSO (Dimethyl Sulphoxide), ethylene glycol, and ionic liquids containing small amount of HF were examined to make the ordered, debris free, highly oriented TiO_2 NTs [36–40]. Interestingly, ethylene glycol motivates double walled NTs and DMSO results single walled TiO_2 NTs [41]. Various parameters such as pH, applied electric field, nature of the electrolyte, time for the anodization strongly influence in the formation of TiO_2 NTs. The organic medium oriented preparation of TiO_2 NTs follows the plastic-flow model whereas in aqueous medium it follows the chemical-dissolution process. There are some excellent reviews that deals with the mechanism, kinetics of the formation of the TiO_2 NTs and influence of various parameters in its structure through the anodization method [42,43]. Typically fluoride based electrolytes with small amount of water has emerged as the best electrolyte system to get the rib free, self-organized third-generation TiO_2 nanotubular architectures.

3. Sensitization of TiO_2 nanotubes

Sensitization of TiO_2 NTs are usually carried out in order to enhance the various properties of TiO_2 including the photocurrent, absorption etc. Generally for dye sensitized solar cell applications, the sensitization of any kind of TiO_2 morphology is done by the ruthenium based metal complexes [44]. However, the ruthenium dyes have a very weak absorption in shorter wavelengths and also the stability related issues. In solving this, the semiconductor nanomaterials have emerged as a new sensitizers and they have many advantages, which includes (i) tuning capability of absorption onset, (ii) size dependent band gap, (iii) high extinction co-efficient, (iv) large intrinsic dipole

moment, (v) multiple exciton generation effects (MEG), which potentially lead to high theoretical quantum efficiencies, (vi) effective charge transfer to the conduction band of TiO_2 upon visible light irradiation, (vii) high photochemical stability etc. [45]. The sensitization process of the semiconductor nanoparticles on TiO_2 NTs is done by the following methods (a) Pre-synthesis method (through linker), (b) Insitu deposition (without linker), (c) electrochemical/electrophoretic deposition method, (d) Successive Ionic Layer Absorption (SILAR) method, (e) chemical bath deposition (CBD), (f) solvothermal process, (g) spray pyrolysis, (h) atomic layer deposition method (i) drop-casting method etc. Even though all these methods are followed for the sensitization of TiO_2 NTs, chemical bath deposition (CBD) and SILAR method are the widely followed one by many groups due to the simplicity in experimental arrangement and for efficient sensitization. The growth mechanism of the SILAR method has three steps [46] (i) specific adsorption of the most strongly adsorbed ions of the compound to be grown by the substrate immersed in a solution of one of its cationic precursors, (ii) water rinsing of the excess solution still adhering to the substrate and (iii) chemical reaction between the most strongly adsorbed cations and less strongly adsorbed anions by subsequent substrate immersion in the solution. In case of CBD technique, the direct formation of nanoparticles on the desired substrate from the precursor solution is the possible one. Electrochemical deposition technique is the another versatile method to deposit the nanoparticles on the TiO_2 nanotubes. The electron transfer mechanism of the sensitization of nanotubes by nanoparticles are not well understood yet. But, the sensitization is practically always carried out through the linker assisted method (exsitu) or by direct adsorption method without linker (insitu) (Fig. 2). As prepared TiO_2 NTs will be amorphous in nature, so usually annealing at higher temperature (around 400–500 °C) is carried out to improve the crystalline nature of TiO_2 NTs before the sensitization by nanoparticles.

4. Sensitization of TiO_2 nanotubes by semiconductor nanoparticles for solar cells

4.1. Cadmium chalcogenides

Cadmium based II–VI semiconductor nanomaterials are widely used for solar cell applications due to their effective light harvesting ability in visible region. Semiconductor nanomaterials sensitization on TiO_2 NTs are usually carried out either through ligand or without linker molecule. Through the linker assisted method, short chain ligands such as thioglycolic acid (TGA),

mercapto propionic acid (MPA) are much preferable than others. The mechanism for the conduction process of electrons from TiO_2 to CdS could be described based on their band edge levels and their geometry. The primary condition is the conduction band edge of TiO_2 should be more anodic than the sensitizer CdS [47] (Fig. 3). Recently, this charge transport and conduction of quantum dot sensitized solar cells for CdS sensitized TiO_2 NTs through the $dx^2 - y^2$ and dz^2 orbitals of titanium was also analyzed through the density functional theory [48]. The sensitization effect of nanoparticles in solar cell efficiency normally depends upon their size. For the CdSe/ TiO_2 heterojunction, the 3.0 nm size nanoparticles photocurrent was about 1.8 mA/cm² which is higher than the 4.5 nm sized one ($J_{sc} = 1.5$ mA/cm²) [49]. Seabold et al. [50] analyzed the heterojunction of CdTe/ TiO_2 NTs made by the modified dipping and deposition method and through the normal method (Fig. 4). It was found that the former one was the suitable one to make a well distributed nanoparticles coated TiO_2 nanotube arrays. The heterojunction formation of semiconductor nanoparticles/ TiO_2 NTs can be achieved through various methods. Several techniques were followed to make a good heterojunction with TiO_2 NTs. The ex-situ deposition of CdS nanoparticles on TiO_2 NTs have shown improved visible light absorption [51]. Gao et al., formed a CdS/ TiO_2 NT hetero-junction through the closed space sublimation technique which resulted in 5.6 mA/cm² current density for the CdS modified TiO_2 NTs [52]. Baker et al. [53] analyzed the effect of CdS nanoparticles sensitization on TiO_2 NTs through SILAR method. It was concluded that the CdS nanoparticles sensitized arrays showed the photocurrent which was 20% higher than the CdSe nanoparticles sensitized TiO_2 nanoparticles electrode. When TiO_2 NTs are sensitized by CdS nanoparticles comprised with other harvesting materials like graphene, improved photoelectric performance can be achieved [54]. Interestingly, CdS NPs decoration on reduced TiO_2 NTs resulted considerable enhancement of the photocurrent density [55]. Also, CdS nanoparticles deposition on TiO_2 NTs by pulsed laser also have generated much attraction for future energy applications [56]. The methodology of deposition of nanoparticles on TiO_2 also influence considerably the quantum of photocurrent production. Yang et al. [57] studied the effect of CdSe, CdTe nanoparticles sensitization in photocurrent through electrophoretic deposition and in-situ deposition (Fig. 5). It was found that there was a remarkable enhancement of photocurrent for the in-situ deposited aqueous CdTe nanoparticles on TiO_2 NTs. This behavior was due to the direct contact of the particles with TiO_2 NTs in in-situ synthesis process. Further, this enhancement of the photocurrent was found

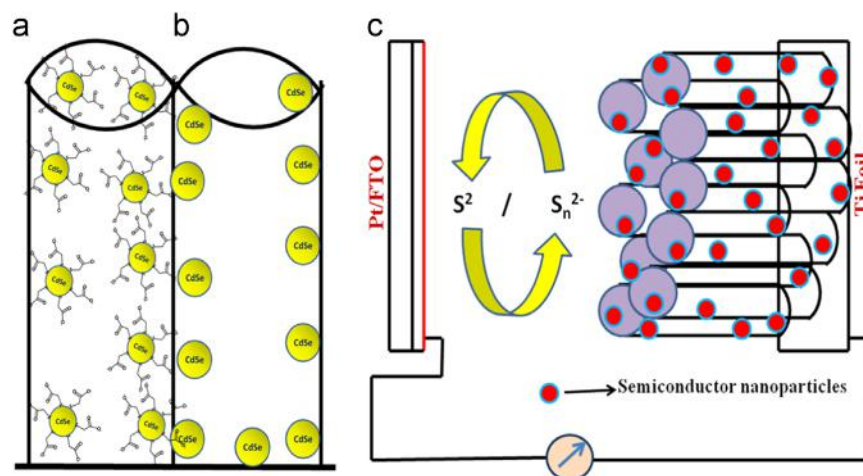


Fig. 2. Schematic representation of a construction of (a) Linker assisted CdSe nanoparticles sensitization on TiO_2 NTs, (b) non-linker assisted deposition of CdSe nanoparticles on TiO_2 NTs and (c) typical construction of a TiO_2 NTs solar cell sensitized by semiconductor nanoparticles.

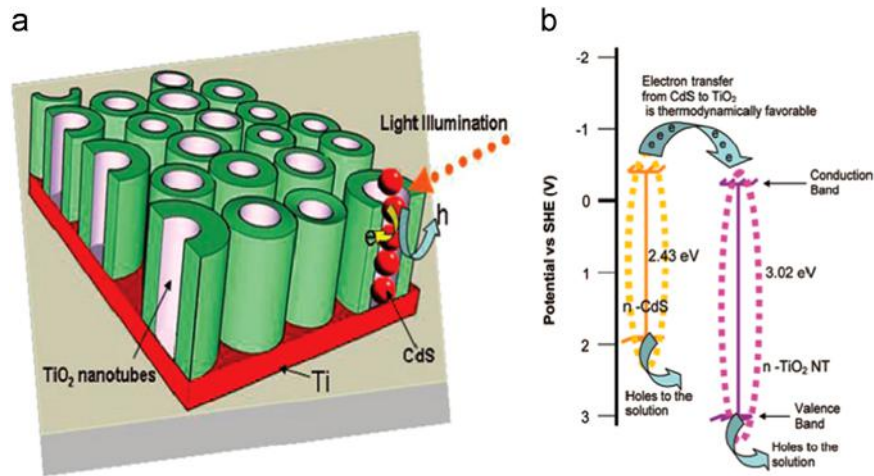


Fig. 3. Sensitization of TiO_2 nanotubes by CdS nanoparticles (a) and the energy level of CdS and TiO_2 (b). Reprinted with permission from Ref. [47] Copyright©2008 American Chemical Society.

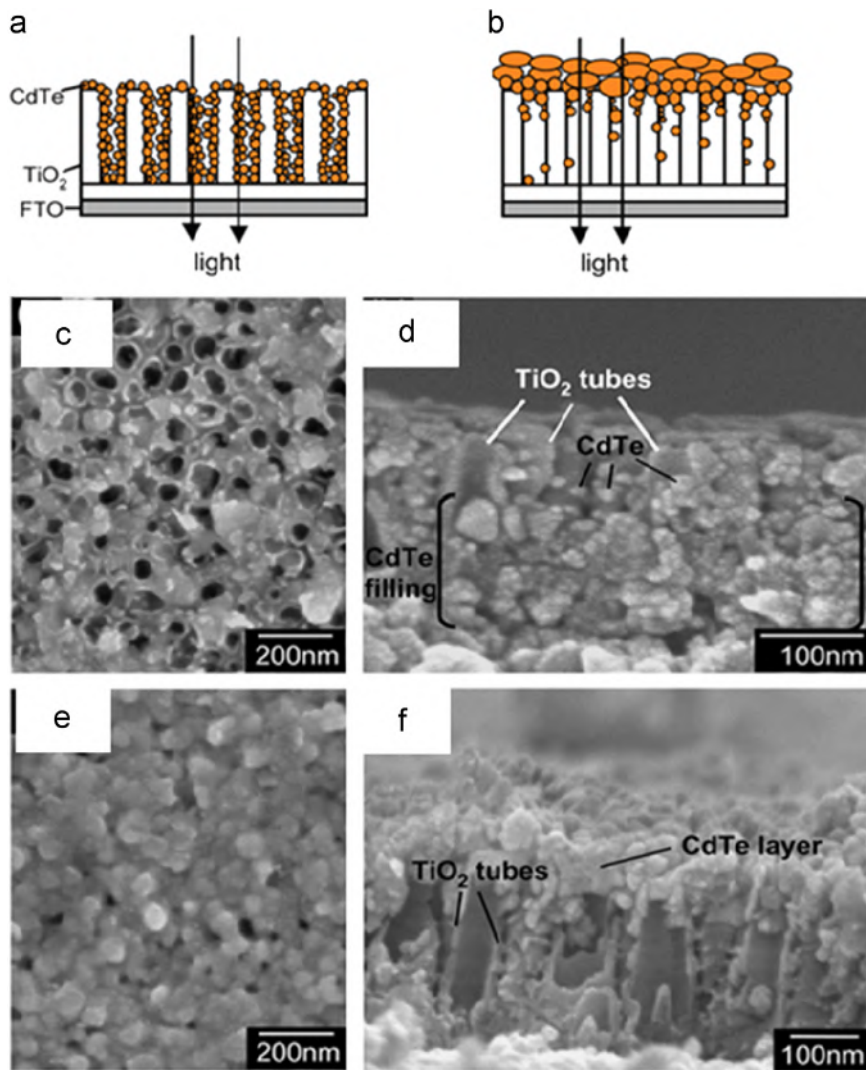


Fig. 4. (i) Schematic representation for deposition of CdTe nanoparticles through (a) dipping and deposition method and (b) regular method (ii) Top and side view SEM images of prepared CdTe/ TiO_2 electrodes through dipping and deposition method (c,d) and regular method (e,f). Reprinted with permission from Ref. [50] Copyright©2008 American Chemical Society.

to be size dependent one. CdTe nanoparticles having the diameter 2.3 nm produced more photocurrent than the nanoparticles having the diameter 3.1 nm. The initial coordination of Cd^{2+} with Ti-

O- was acting as the nucleation site for the growth of the quantum dots. This makes the enhancement in photocurrent compared to the electrophoretic deposition where the linker plays a role for the

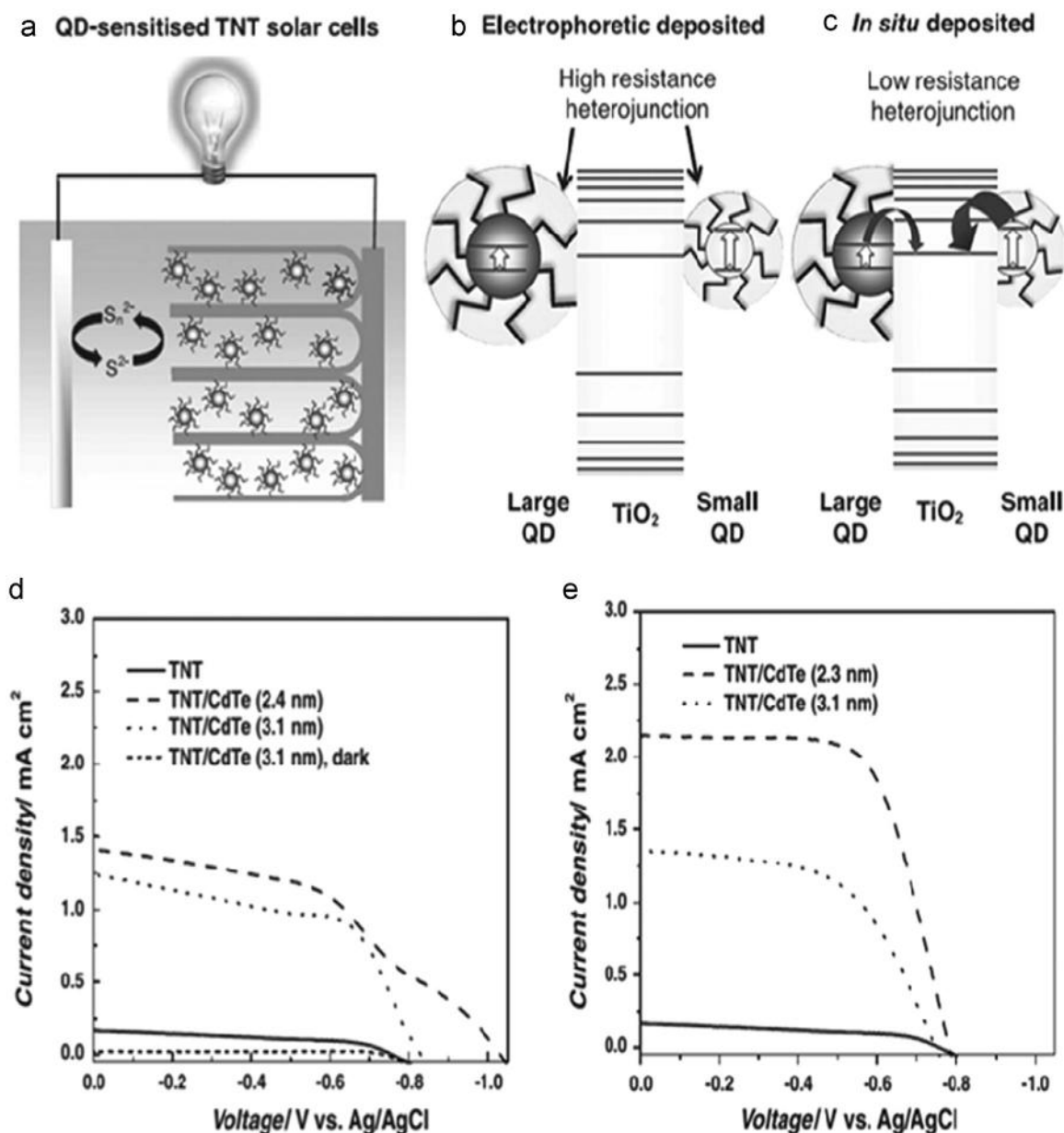


Fig. 5. (i) Illustration of typical semiconductor nanoparticles sensitized TiO_2 nanotubes solar cell (a) (ii) sensitization process of CdTe nanoparticles through electrophoretic (b) and In situ deposited method (c) . (iii) I–V curves of bare Ti NTs and sensitized by different size of CdTe nanoparticles by electrophoretic deposition (d) and in situ deposition (e) . Reprinted with permission from Ref. [57] Copyright©2012 Jhon Wiley and Sons.

conduction. Hossain et al. [58] studied the effect of bubble like CdSe nanoparticles on TiO_2 NTs through chemical bath deposition. They found that the time taken for the deposition time played a crucial factor in the efficiency of the solar cell. For the 20 min deposited TiO_2 NTs, the efficiency of $\eta=0.81\%$ ($V_{oc}=383$ mV; $J_{sc}=4.08$ mA/cm²; FF=52.1) was observed whereas for the 60 min deposited TiO_2 NTs, the efficiency was 1.56% ($V_{oc}=438.0$ mV; $J_{sc}=7.19$ mA/cm²; FF=49.5). But, in this method the cluster of CdSe particles which were deposited on the TiO_2 NTs were not fully sensitized inside of the nanotubes, which may be the reason for the low efficiency. Sun et al. [59] studied the effect of CdS nanoparticles on the TiO_2 NTs array through the sequential chemical bath deposition (S-CBD) method (Fig. 6) Interestingly, in this method, the photocurrent of CdS sensitized TiO_2 NTs produced 35 times higher current density than the (from 0.22 to 7.82 mA/cm² with the efficiency 4.15%) plain TiO_2 nanotubes. Moreover, there was no aggregation found on the surface of the nanotubes which

clearly predicts the suitability of this method for solar cells. In advance, Ma et al. [60] and Xie et al. [61] investigated the influence of CdS nanoparticles deposited on TiO_2 NTs through sonication assisted sequential chemical bath deposition method. It was found that this method effectively prevent clogging of CdS nanoparticles and produces more uniform nanoparticles-nanotubes structure with good intimate contact compared to S-CBD method. Similar results were also obtained earlier for CdTe nanoparticles sensitized TiO_2 photoanodes by Gao et al., [62] using presynthesized nanoparticles sensitization (exsitu) method (Fig. 7) Here, the enhancement of photocurrent was found about 10 times (from 0.17 mA/cm² to 6 mA/cm²). Further, it was found that the electron injection rate was also very high for smaller sized nanoparticles compared with bigger one. Hence, the presynthesized sensitization method was normally not encouraged for the sensitization process which always results the low efficiency in solar cells which may be due to the partial coverage of the nanoparticles on the

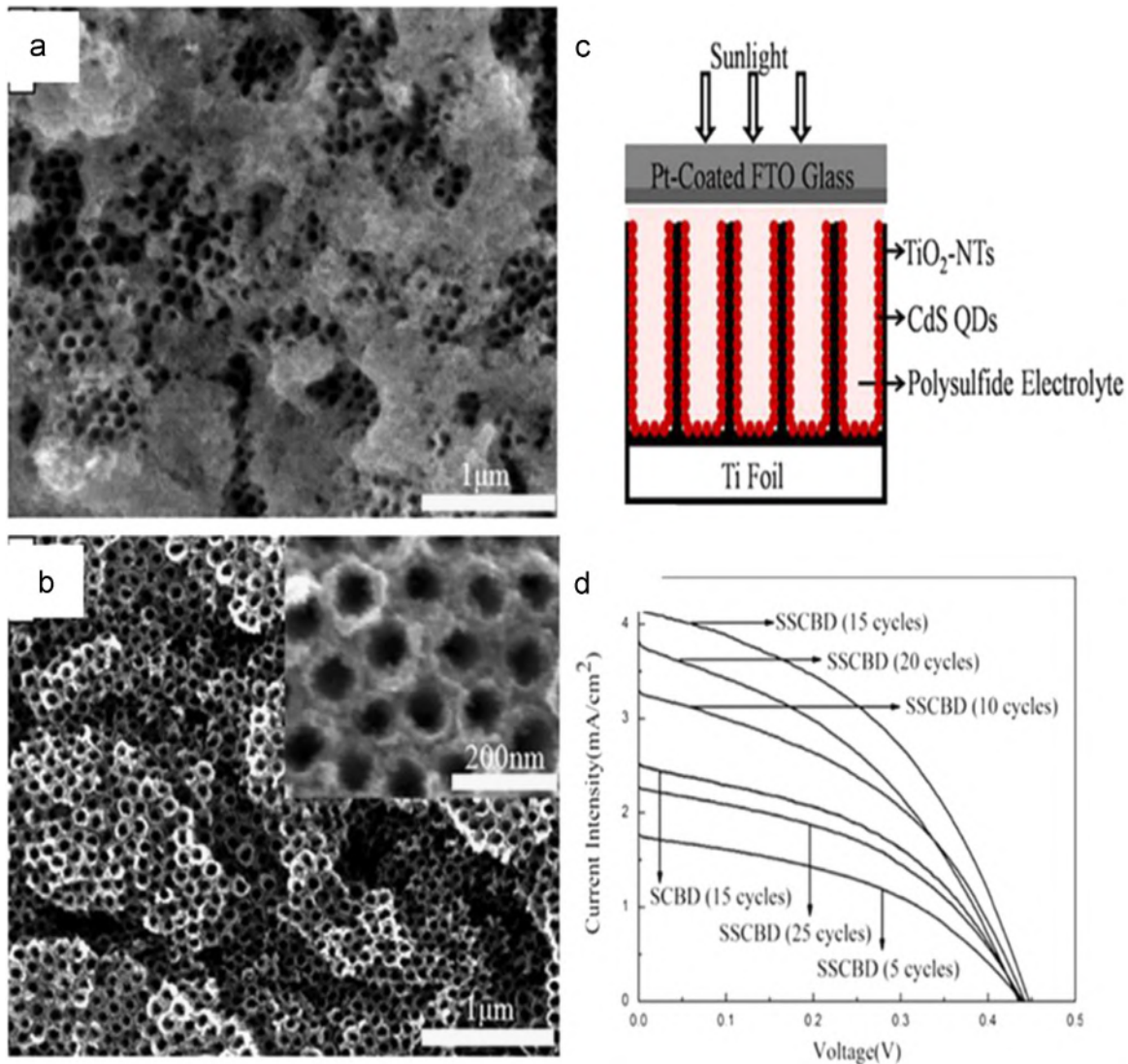


Fig. 6. (i) SEM images of CdS/TiO₂ NTs and S-CdS/TiO₂ NTs (a,b) (ii) Schematic diagram of CdS nanoparticles sensitized TiO₂ NTs solar cell (c) and (iii) I–V curves of prepared solar cells through various cycles of deposition (d). Reprinted with permission from Ref. [59] Copyright©2008 Elsevier.

surface of the nanotubes. However, in CBD method the increased time of deposition of the nanoparticles on the TiO₂ nanotubes may be a negative factor in efficiency. Shen et al. [63] found that the efficiency and IPCE of the solar cell was decreased when the deposition time of CdSe nanoparticles get increased from 36 h to 48 h. For the 36 h the efficiency was 1.7% whereas it was 0.94% for 48 h (Fig. 8). The decrease of efficiency in this case was due to the increase of CdSe–CdSe boundaries which cause the increasing loss of e–h’s from CdSe nanoparticles to TiO₂ nanotubes. This also enhances the exciton recombination and trapping at the interface. Hence an optimal range for deposition of nanoparticles on TiO₂ NTs is required to attain the high efficiency solar cell. In most of the cases, the electrolyte system employed for the fabrication of TiO₂ NTs solar cells is a polysulfide electrolyte (S²⁻/S_x²⁻) which differs from the traditional iodine/triiodide redox couple which lead to corrosion on the quantum dot surface [64].

Generally, the major problem associated with the TiO₂ NTs sensitization with the nanoparticles is clogging of the nanoparticles on the surface. This phenomena can happen at the NTs surface due to the agglomeration of the nanoparticles. Usually, large size of the nanoparticles make aggregation on the surface of the TiO₂ NTs. This prevents the deposition of nanoparticles on NTs further and also suppresses the conductivity hence results

poor efficiency in solar cell. However, electrochemical deposition of semiconductor nanoparticles on TiO₂ NTs has found to be fruitful remedy for this problem. Electrochemical deposition of CdSe nanoparticles on TiO₂ NTs proven that this method help to make a uniformly distributed nanoparticles on the TiO₂ NTs and thereby increase the contact surface area [65]. This method also prevents the clogging or assembling of the nanoparticles on nanotubes. Pulsed electrode deposition method was also found to be an useful method to fabricate the CdTe/TiO₂ NT core–shell solar cell structure [66]. In this method, the pulsed potential was applied in order to avoid the depletion of HTeO²⁺ inside the tube and to reduce the deposition of particles at the pore openings. With the open-circuit voltage of 0.23 V, fill factor 30%, the efficiency ~0.1% was obtained using this method with the higher external quantum efficiency. For the CdTe/TiO₂ NTs heterojunction, the ZnS layer coating through SILAR method was found as the best choice to protect the photoelectrode against photocorrosion [67]. Compared with these methods, the solvothermal method offers high efficiency of the sensitization which clearly shows its promising application for sensitization process. Pang et al. [68] investigated the effect of CdSe nano tetrapods sensitized TiO₂ nanotube array using pre synthesized linker assisted method through mercaptopropionic acid (MPA)

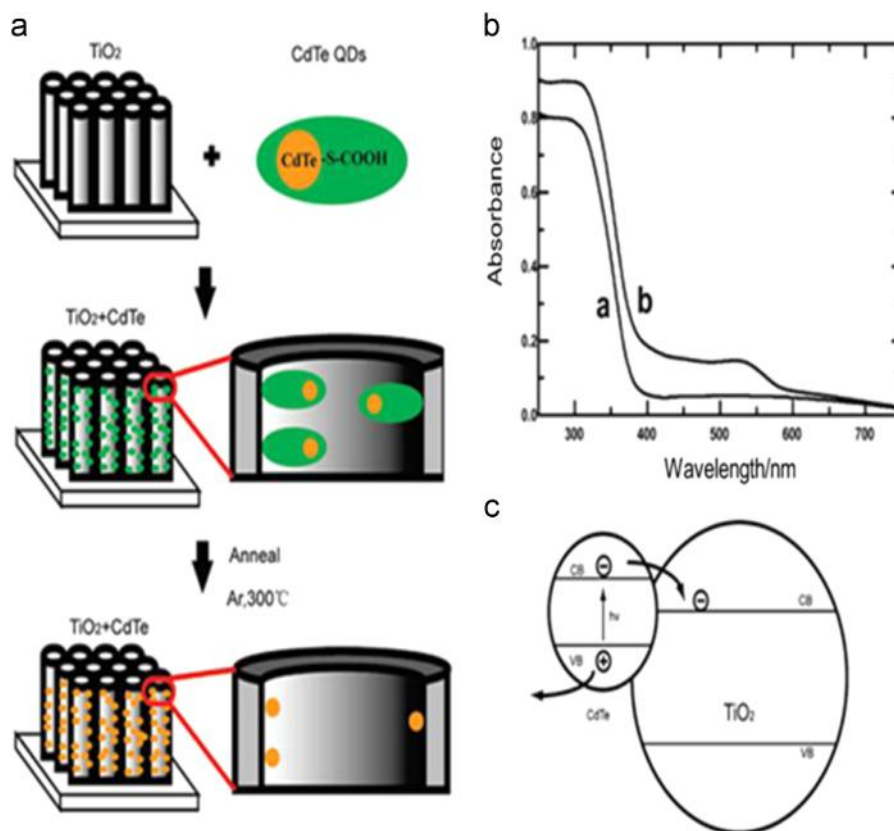


Fig. 7. (a) Sensitization of CdTe nanoparticles on TiO₂ nanotubes (b) Absorption spectra of plain TiO₂ NTs and CdTe nanoparticles sensitized TiO₂ NTs and (c) Schematic diagram of charge transfer process between CdTe and TiO₂. Reprinted with permission from Ref. [62] Copyright©2009 American Chemical Society.

as the capping ligand. The device performance results the bare TiO₂ nanotube array shows the photocurrent density of 0.40 mA/cm², whereas the CdSe nanotetrapods sensitized electrode shows the density of about 0.86 mA/cm² which clearly indicates the influence of branched structure of chalcogenides on TiO₂ nanotubes for enhanced solar cell efficiency. The new look on constructing a rainbow solar cell based on the different sized CdSe nanoparticles inside the TiO₂ nanotubes also opened a way to enhance the efficiency. Kongkanand et al. [69] has proposed this concept and the faster electron injection and greater absorption range is now become a feasible one (Fig. 9). Recently, Kalanur et al. [70] observed that under simulated conditions, the solvothermal sensitization of CdS nanoparticles on TiO₂ NTs clearly showed the 10 times higher photocurrent than the particles sensitized by chemical bath deposition (CBD) method. This facile method also would open a new way to sensitize the TiO₂ NTs through solvothermal process. In contrast to the one side closed TiO₂ NTs, two ends opened TiO₂ nanotubes can increase the efficiency considerably due to efficient decoration. For CdS nanoparticles, it was found that when the particles were deposited through SILAR method, the incident photon to current conversion efficiency (IPCE) was improved from 41% to 68% under front side illumination [71]. Here, oxalic acid was used to remove the bottom caps of the pre-crystallized TiO₂ nanotubes. Gao et al. [72] used similar method for the CdS nanoparticles and found that the double side opened TiO₂ NTs prevents the clogging of CdS nanoparticles on the surface and enhances the efficiency. The C(closed end)-Ti NT/CdS photoelectrodes shows the efficiency of 0.46% whereas the O (opened end)-Ti NT/CdS photoelectrodes shows about 1.46% which clearly reflects the three fold enhancement in efficiency. Advanced techniques like RF magnetron sputtering has been

found one of the best method to sensitize the TiO₂ nanotubes. Fernandes et al. [73], fabricated CdSe sensitized TiO₂ nanotube array photoelectrode solar cell through RF sputtering. For the 30 min sensitized samples, the photocurrent of 1.9 mA/cm² was observed for the 400 °C annealed sample under 1 sun illumination. Alloyed systems such as CdS_{0.54}Se_{0.46} [74], Zn_xCd_{1-x}Se, Mn_xCd_{1-x}Se [75–78], and Zn_xIn_{1-x}S [79] have shown best results for the absorption in visible range when they undergo sensitization on TiO₂ nanotubes. Further studies in this direction would explore the efficiency enhancement in TiO₂ NTs based solar cells.

4.2. Titania nanoparticles

For the sensitization of TiO₂ NTs by TiO₂ nanoparticles TiCl₄ treatment was the best one to increase the surface area, to improve the electron transport etc. In this method, the annealed TiO₂ NTs are immersed with TiCl₄ and then rinsed on H₂O. The hydrolysis reaction of TiCl₄ with water produces uniformly formed TiO₂ nanoparticles inside as well as outside of the TiO₂ NTs. The TiCl₄ treatment of nanotubes after anodization enhances several times the photocurrent production. The incorporation of TiO₂ nanoparticles on TiO₂ nanotubes by this method has already given successful outcome for dye sensitized solar cell (DSSC) devices [80,81]. Pan et al. observed the length dependent enhancement of photocurrent of TiO₂ NTs after TiO₂ nanoparticles infiltration [82] (Fig. 10). Roy et al. [83] investigated the effect of TiO₂ decoration through TiCl₄ treatment in efficiency of the solar cell. The increase of the thickness of the TiO₂ layer was found after surface treatment with the maximum conversion efficiency upto 3.8%. Infiltration of titania nanoparticles through suitable method could also produce better results. The infiltration of titania nanoparticles on

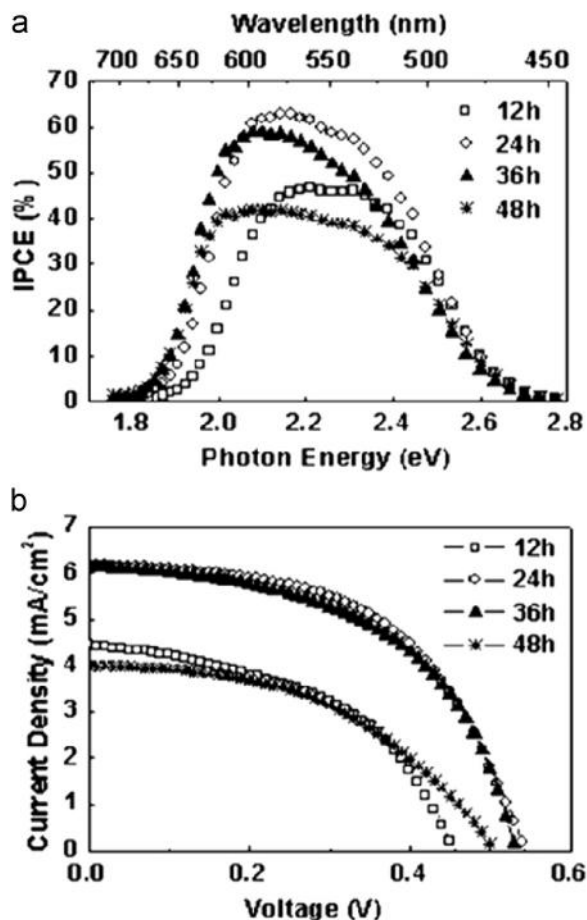


Fig. 8. (a) IPCE and (b) I–V characteristics of CdSe nanoparticles deposited TiO₂ NTs solar cell at different time intervals. Reprinted with permission from Ref. [63] Copyright©2010 American Chemical Society.

TiO₂ NTs through the newly developed dipping–rinsing–hydrolysis process (DRH) could also provide the considerable efficiency enhancement [84]. In this method, the TiO₂ nanoparticles were grown directly on the sides of the nanotubes through hydrolysis of the precursors tetrabutyl titanate (Ti(O–nBu)₄) and anthracene-9-carboxylic acid (9–AnCOOH). Toluene was employed as the solvent medium for the rinsing process.

For the best cycle, around 6.45% conversion efficiency with the photocurrent density (J_{sc}) of 16.25 mA cm^{–2} was obtained through this method. Recently, the anodized TiO₂ NTs decorated by the double layer of 1D&3D TiO₂ nanoparticles have given the highest efficiency about 9.10% with high J_{sc} value (17.90 mA/cm²) [85]. This assures that future developments through novel approaches would give better efficiency results.

4.3. Lead chalcogenides nanoparticles

Lead chalcogenide nanomaterials have proven as viable candidates for the solar cell applications due to their exemplary light collection ability at NIR region. Among the PbS, PbSe nanoparticles, only a few reports available for PbS ($E_g=0.41$ eV in bulk form) for the sensitization of TiO₂ NTs. The first successful work on the coating of the controlled size of PbS nanoparticles on inside and outside of the TiO₂ nanotubes was done by Ratanatawanate et al. [86] using the thiolactic acid as the linker molecule through dip coating process. A cationic surfactant PDDDB, was utilized to block the external surfaces of the nanotubes. Fanggong Cai et al. observed that when size of the PbS nanoparticles exceeds over 15 nm, it motivates agglomeration on the surface of TiO₂ NTs

which strongly reduces its performance [87]. Kang et al. [88] found that the PbS nanoparticles deposited by SILAR method showed an enhanced photocurrent (11.2 mA/cm²) and absorption than the electrochemically deposited one (5.72 mA/cm²). Interestingly, a recent observation by Tao et al. [89] showed that the insitu electrical field assisted chemical bath deposition (EACBD) of PbS nanoparticles on TiO₂ NTs shows the remarkable efficiency of the solar cell of 3.41% which is 133.6% higher than the previous record (1.46%). This has shown that special emphasis on lead chalcogenide nanomaterials sensitization on TiO₂ NTs could give the fascinating results with higher efficiency in the near future.

4.4. Chalcopyrites nanoparticles

Ternary compound semiconductors such as CuInS₂, AgInS₂ and CuInSe₂ nanomaterials were very rarely utilized for the sensitization of TiO₂ nanotubes. AgInS₂ NPs sensitization on TiO₂ nanotubes have shown promising photo electrochemical results for the solar cell applications [90]. The first report on the deposition of CuInS₂ nanoparticles on TiO₂ NTs for the photocatalytic applications was studied by Liu et al. [91]. For the photovoltaic's applications, Chen et al., [92] demonstrated that the SILAR method deposited CuInS₂ nanoparticles have shown good performance with the CdS nanoparticles sensitized TiO₂ nanotubes. A maximum of 7.3% efficiency of CdS/CuInS₂/TiO₂ NTs was obtained against CdS/TiO₂ NTs (3.3%) which has shown a remarkable 120% of enhancement. This clearly revealed the dual role of CuInS₂ nanoparticles as a barrier layer as well as co-sensitizer. Further, Yuan et al. [93] used pulsed electrochemical deposition to wrap the CuInS₂ nanoparticles on TiO₂ NTs and observed a heterojunction (p–n type) diode formation which has shown a promising approach of depositing chalcopyrites on the walls of TiO₂ NTs for future solar cell device fabrication applications. In case of CuInSe₂ nanomaterials, Liao et al. [94] succeeded in decorating TiO₂ nanotubes with CuInSe₂ nanocrystals through electrophoretic deposition and it was found that the absorption range was expanded after decoration from 400 to 700 nm. Similar kind of observation was achieved through SILAR based deposition of CuInSe₂ NPs on TiO₂ NTs recently [95]. But, up to till date, there are no report available on solar cell devices based on this CuInSe₂ nanoparticles sensitized TiO₂ nanotubes array. Nevertheless, it is expected that future development through this chalcopyrites nanomaterials sensitization on TiO₂ NTs array could give improved efficiency.

4.5. Miscellaneous

Other than mentioned above, there are some semiconductor systems such as MnTe, Ag₂S, Bi₂S₃, In₂S₃, SnS, CdO, Cu₃BiS₃, Co₃O₄ and Cu₂O were also newly studied for the sensitization of TiO₂ nanotube arrays for solar cell applications. Recently, Tubtintae et al. [96] analyzed the effect of boron doped MnTe nanoparticles on TiO₂ NTs through SILAR method. It was found that the efficiency of the solar cell got increased compared with the undoped system. For the undoped system the efficiency was found to be 0.006% (with the $V_{oc}=0.39$, $J_{sc}=0.038$ mA/cm², FF=43.80) and for the doped system the efficiency was about 0.040% (with the $V_{oc}=0.64$, $J_{sc}=0.097$ mA/cm²; FF=62.80) for the best SILAR cycle $n=5$. In spite of various architecture, recombination is the major obstacle in achieving higher solar cell efficiency. An improved photo electrochemical performance is possible when Ag₂S nanoparticles are co-sensitized with CdS nanoparticles on TiO₂ NTs [97]. Sensitizing the TiO₂ NTs by semiconductor nanoparticles with a recombination barrier layer like ZnO, a considerable enhancement of the efficiency of solar cell could be achieved. In case of the Ag₂S nanoparticles, it was found that the increased efficiency was possible only when the recombination layer of ZnO is coated

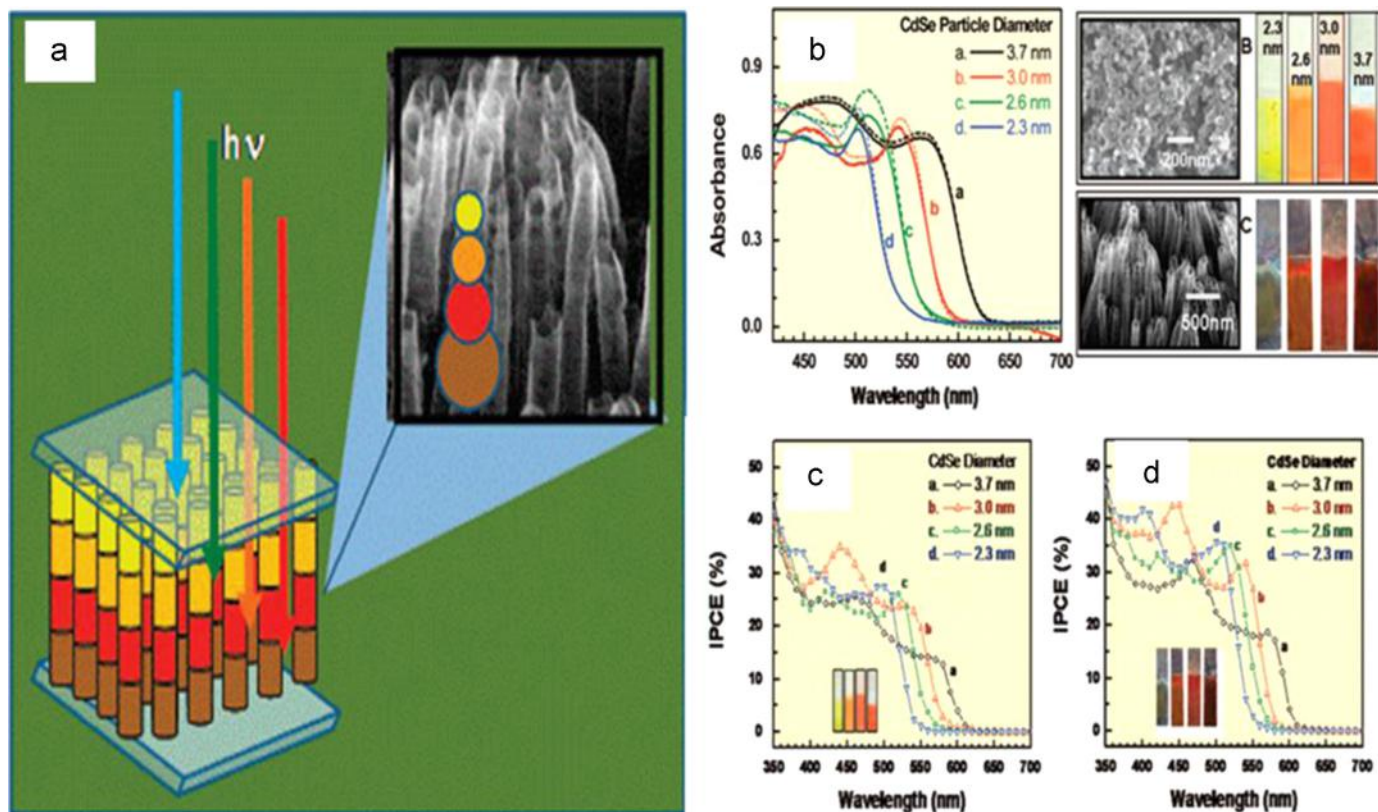


Fig. 9. Fabrication of rainbow solar cell using TiO₂ NTs array (a) and the UV-visible spectra of different size of CdSe nanoparticles sensitization on TiO₂ nanoparticles and TiO₂ nanotubes (b,c,d). Reprinted with permission from Ref. [64] Copyright©2011 American Chemical Society.

around it [98]. For the Ag₂S/ZnO/Ti NTs electrode, the efficiency obtained was 0.28% whereas for the Ag₂S/Ti NTs electrode it was about 0.22% only (Fig. 11). This method was successfully applied for the other systems like CdS/ZnO/TiO₂ NTs and CdSe/ZnO/TiO₂ NTs and similar kind of the enhancement was observed [99,100]. Similar kind of surface recombination can also be avoided by coating Al₂O₃, Y₂O₃ on the inner walls of TiO₂ NTs [101,102]. Solis et al. [103] observed that when TiO₂ NTs are sensitized by Bi₂S₃ nanoparticles using CBD method, there was a comparable improvement in fillfactor (0.78). However, the Bi₂S₃ sensitization has to be optimized in order to get high efficiency solar cell architecture. Sarkar et al. [104] successfully deposited In₂S₃ on TiO₂ NTs through Atomic Layer Deposition (ALD) method. When Co²⁺/Co³⁺ electrolyte was employed for the In₂S₃ sensitized TiO₂ NTs solar cell, the efficiency was obtained around 0.36% (V_{oc}=0.22 V) under AM 1.5 conditions. Further, the low quantum efficiency of this cell (~10%) indicates that there was a charge recombination in the system which has to be eliminated to obtain good efficiency. Jia et al. [105] utilized SILAR method to decorate TiO₂ NTs using SnS nanoparticles for the fabrication of solar cell. The resultant cell had a 0.75% efficiency (J_{sc}=1.55 mA/cm²) which was higher than the pristine SnS nanoparticles (0.03%, J_{sc}=0.26 mA/cm²) and unmodified TiO₂ NTs (0.14%, J_{sc}=0.65 mA/cm²). Sarma et al. [106] made a CdO sensitized TiO₂ NTs heterojunction through normal room temperature dipping method. It was observed that the photocurrent densities of CdO/TiO₂ NTs composite (1–1.2 mA/cm² at 1.4 V) was higher than the bare TiO₂ NTs (~0.7 mA/cm²). A recent analysis by Zhong et al., has revealed that flower like Cu₃BiS₃ nanoparticles has shown improved photoelectrochemical performance of TiO₂ NTs and it is expected that this kind of copper based new type of nanoparticles can be preferred for photovoltaic applications [107]. In the case of Cu₂O nanoparticles, the sensitization was mostly done by

electrochemical deposition method and the efficient charge separation was confirmed through impedance spectroscopy [108]. Moreover, the morphology of the Cu₂O particles on TiO₂ nanotubes was found to be a pH dependent one [109]. Li et al., [110] fabricated a proto type core-shell Cu₂O-TiO₂ NTs solar cell through electrochemical method and used NH₄Cl treatment to increase the conductivity of the barrier layer of the TiO₂ nanotubes. This resulted a uniform growth of Cu₂O nanoparticles on TiO₂ nanotubes and an efficiency of about 0.01% was achieved with V_{oc}=0.1 V, J_{sc}=0.33 mA/cm². Tsui et al. [111] fabricated Cu₂O/TiO₂ NTs solar cell using a 3-step pulsed plating method. A plasma treatment was applied to remove the hydrocarbons on the surface of the nanotubes to prevent clogging and the efficiency was achieved about 1.1% which was 2.5 times higher than the bare TiO₂ nanotubes (0.5%). These results clearly explores the possibilities of effective sensitization through novel materials.

5. Co-sensitization on TiO₂ nanotubes

Co-sensitization is an attractive novel way to utilize the maximum area of the solar spectrum. In co-sensitization process, two different components which are absorbing the light at two different wavelengths are mixed together for the sensitization. Co-sensitization has been successfully examined in two different dyes, dye and quantumdots [112–115]. In case of the semiconductor co-sensitization, the condition to be noted is the conduction band of either of sensitizers should be higher than the other one (Fig. 12) and both edges should be higher than the valence band edge of TiO₂. Further, the Fermi level alignment of the nanoparticles must be favorable for the charge separation and transformation [116]. This is the primary requirement of the co-sensitization process in quantumdot sensitized solar cells. Co-sensitization process was

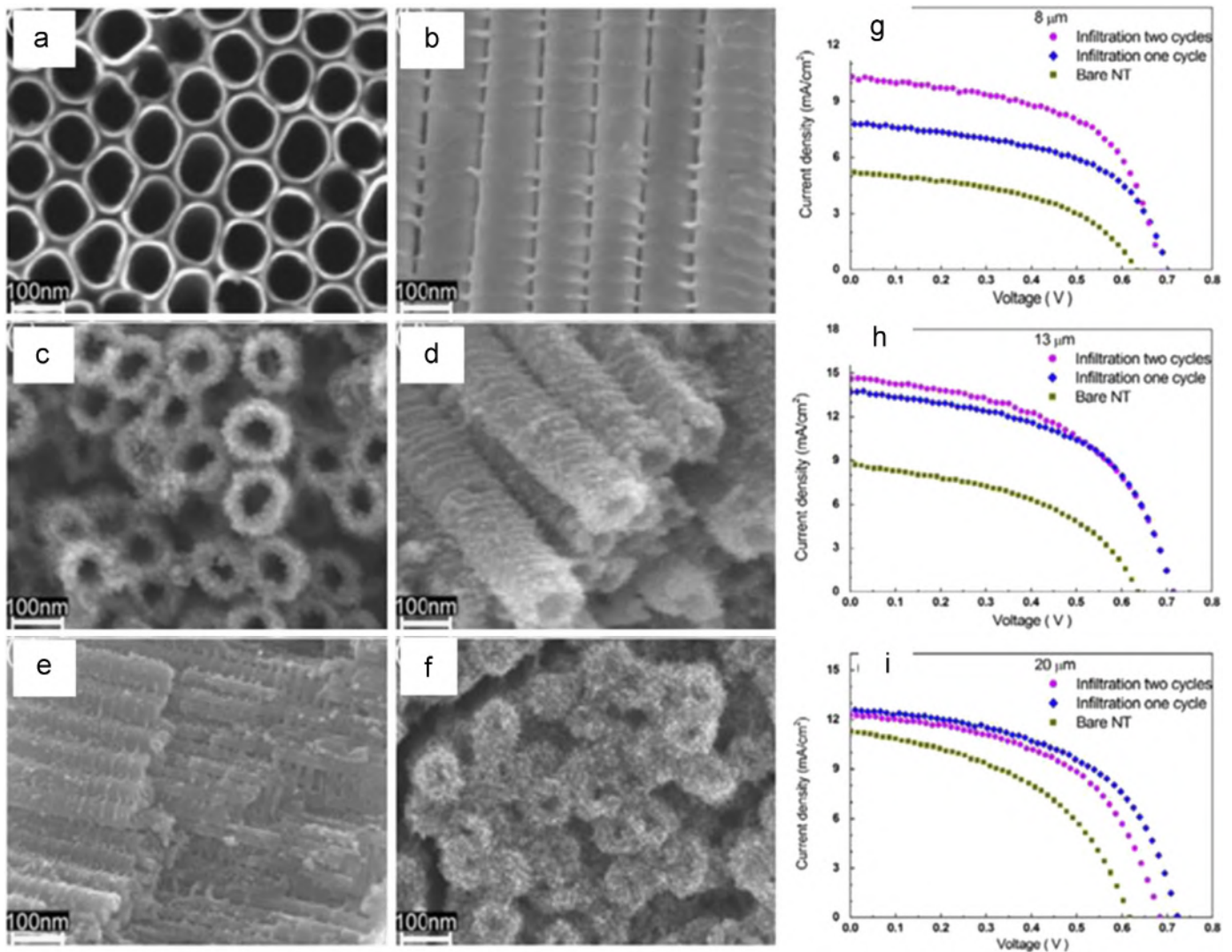


Fig. 10. (i) SEM images of the TiO₂ nanotubes (a,b) (ii) top, tilt and inside view of the split TiO₂ NTs after once cycle-infiltration (c,d,e) (iii) NTs and NPs mixed structure after two-cycle infiltration (f) and (iv) I–V measurement of fabricated DSSCs with different lengths (8 μm, 13 μm, 20 μm) of NTs (g,h,i). Reprinted with permission from Ref. [82] Copyright©2011 IOP Publishing. All rights reserved.

widely studied for quantumdot sensitized solar cells, and dye sensitized-solar cells [117, 118]. A metal-semiconductor NPs co-sensitization and core-shell type based co-sensitization on TiO₂ NTs is another kind of interesting approach to improve the photoelectrochemical performance [119–121]. In case of quantumdot sensitization, techniques such as sequential assisted chemical-bath deposition has been found as efficient for the visible light absorption of TiO₂ NTs when co-sensitized by CdS and CdSe nanoparticles [122]. For the TiO₂/CdS/CdSe system the short circuit current density was found to be about 13.0 mA/cm² whereas for TiO₂/CdSe/CdS it was found to be 1.8 mA/cm². Due to the proper Fermi level position of CdS and CdSe with TiO₂, it provided the larger charge collection that was the reason for higher value of photocurrent in TiO₂/CdS/CdSe system. Co-sensitization of CdX (X=Se,Te) nanoparticles with CdS nanoparticles on TiO₂ NTs was found more efficient one for many applications including the immunosensor [123], photocathodic protection of metals [124]. In case of co-sensitization on TiO₂ NTs for solar cells, several attempts were made in enhancing the solar cell efficiency. Lee et al. [125] identified that the cascade structure of TiO₂/CdS/CdSe was found to be more efficient than the TiO₂/CdSe/CdS structure. For this structure, the saturated photocurrent of 14.9 mA/cm² was achieved which is higher than the TiO₂/CdS under standard

conditions. Based on this observation, Huang et al. [126] found that the fibrous TiO₂ NTs photoanode (optimized length was 28 μm) could produce the efficiency of about 3.18% (J_{sc} = 11.48 mA cm⁻²) after the co-sensitization of CdS/CdSe nanoparticles on it. When TiO₂ nanotube arrays were used as the photoanode instead of fibrous TiO₂ NTs, the efficiency was found to be 3.2% for the front side illuminated CdS/CdSe co-sensitized solar cell (FTO/compact TiO₂/CdS/CdSe/Cu₂S) [127] (Fig. 13). In this cell assembly, the free standing membrane of TiO₂ NTs were transferred onto FTO substrate before the co-sensitization process. For the back side illumination (Ti/Ti NT arrays/CdS/CdSe/electrolyte/Pt), the cell efficiency was found to be 1.32% only due to the recombination processes. In the back side illumination mode, the intensity of the incoming light was decreased by the counter electrode and electrolyte used in the cell. Hence, the transfer of electrons is hindered by a blocking layer between the TiO₂ and Ti substrate. So, the TiO₂ NTs membrane was delaminated from the substrate and used for the front side illumination purpose. Not only with two different semiconductors, different sizes of the same one could be utilized for co-sensitization for improved photo conversion efficiency which has been proven in CdSe nanoparticles [128]. Besides, involvement of two different methods involving in co-sensitization process may be an effective tool to

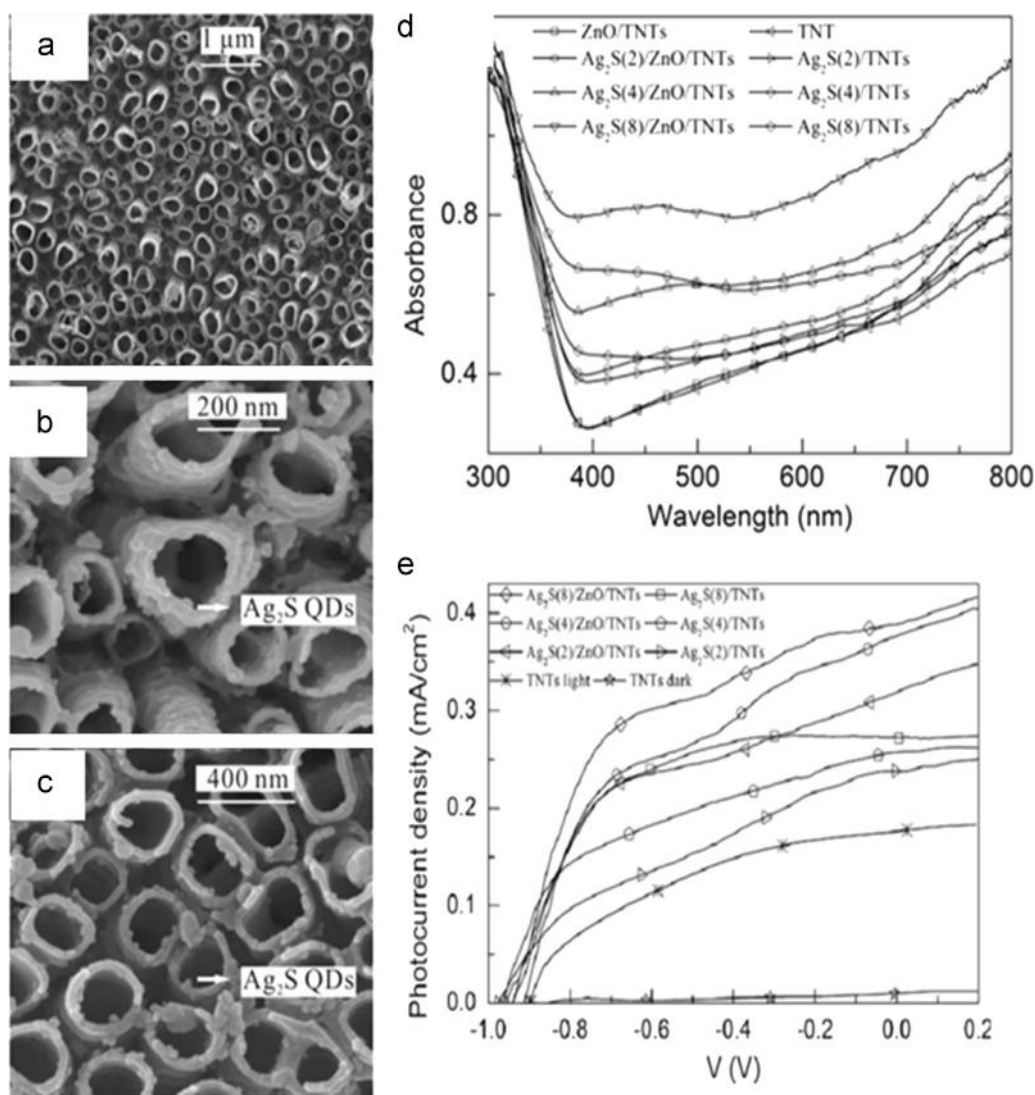


Fig. 11. (i) SEM images (a,b,c) (ii) UV–visible spectra (d) (iii) I–V curves of plain TiO₂ NTs, Ag₂S/TiO₂ NTs and Ag₂S/ZnO/TiO₂ NTs (e). Reprinted with permission from Ref. [98] Copyright©2011 Springer.

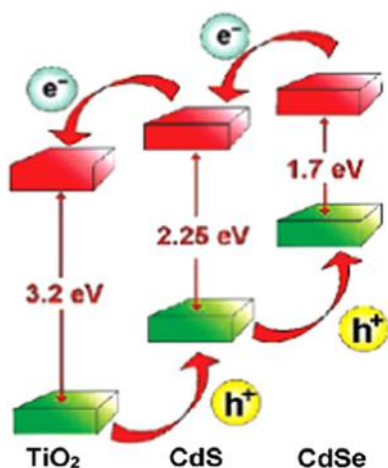


Fig. 12. Ideal band energy levels for efficient transport of excited electrons and holes in CdS/CdSe Co-sensitized electrode. Reprinted with permission from Ref. [116] Copyright©2010 American Chemical Society.

attain the improved efficiency. For example, in the co-sensitization process of CdSe/CdS@TiO₂ NTs, where the sensitization process was done by SILAR (CdS) and CBD (CdSe) methods, the sealed

annealing process of the quantum dots deposited on TiO₂ NTs was found to produce higher efficiency (2.74% for CdSe (40 h)/CdS (5 c)) [129]. Similar kind of approach was also extended towards the photocatalysis applications [130,131]. Co-sensitization by two different group semiconductors through this method also would help to enhance the absorption as well as photocurrent density [132–134]. Further, doped heterostructures such as Mn (or) Co doped CdS, CdS NPs decorated Sb doped SnO₂, PbS sensitized Sb doped SnO₂ on TiO₂ NTs have also proven as this method is a promising way to improve the photoelectrochemical performance of the TiO₂ NTs [135–137]. Li et al., adopted this concept and achieved co-sensitization of Cd S_xSe_{1-x} nanoparticles with Mn doped CdS nanoparticles on TiO₂ NTs for the construction of the solar cell. The resultant device was shown about 3.26% which was much higher than the device made by the Mn–CdS NPs sensitization alone (0.81%) [138].

Template mediated method is also being adopted to make TiO₂ nanotubes due to its low cost, high reproducibility, easy equipment etc. Zhang et al. [139] made an ordered TiO₂ nanotubes on FTO glass substrate using a sol–gel assisted template process (Fig. 14). First, ZnO nanorods were grown on the FTO substrate and then ZnO/TiO₂ structure was created using dip coating technique in TiO₂ sol. Finally the ZnO nanorods were removed using HCl etching treatment to

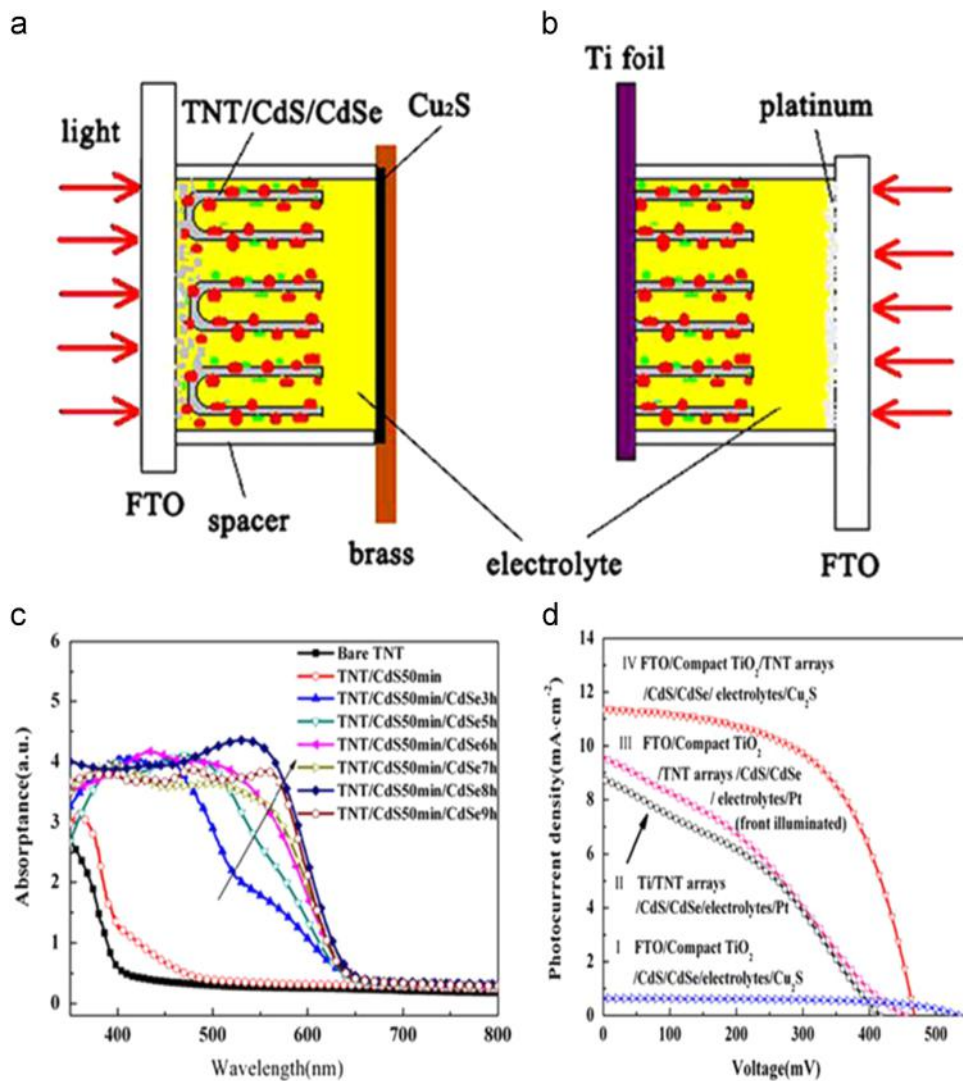


Fig. 13. Schematic diagram of (a) front side illuminated and (b) back side illuminated semiconductor nanoparticles sensitized TiO₂ NTs solar cell. (c) absorption spectra of CdS/CdSe co-sensitized TiO₂ NTs on FTO with various deposition times from 3 to 9 h (d) I–V curves of solar cells for four different structures. Reprinted with permission from Ref. [127] Copyright©2011 American Chemical Society.

obtain highly ordered TiO₂ nanotubes. With TiCl₄ treatment, efficiency upto 4.61% was achieved for 14 h CdS/CdSe co-sensitized photoelectrode. Wang et al. [140] demonstrated CdS/CdSe co-sensitized TiO₂ NTs solar cell using two methods namely SILAR method for the CdS under layer nanoparticles and Electrochemical atomic layer deposition (ECALD) method for top CdSe nanoparticles. Because of the monolayer growth mechanism of the SILAR and ECALD, uniform decoration of the nanoparticles in inner side of TiO₂ nanotubes was a possible one. The maximum of 9.7% of photo conversion efficiency was obtained for the CdSe(6 h)/CdS(4 cycles)/TiO₂ NTs sample. Novel ideas could be a platform to improve the efficiency in TiO₂ NTs based solar cell architectures. Li et al. [141] made a free standing translucent TiO₂ nanowires/TiO₂ NTs film through a two step anodization method. Then, CdS/CdSe co-sensitization was carried out on TiO₂ nanowires/TiO₂ NTs using SILAR method. The release of H⁺ ions in the medium was found to be a major driving force in the formation of nanowires on the surface. For the best SILAR cycle, about 2.41% efficiency was obtained in this structure. Recently, Zhang et al. [142] used atomic layer deposition (ALD) method to make a nanofilm of CdS/CdSe quantum dots on TiO₂ NTs. To passivate quantum dots from the surface to avoid carrier scattering and recombination, ZnS treatment was followed. It was achieved about 4.56% efficiency ($V_{oc}=0.52$ V, $J_{sc}=17.59$ mA/cm², FF=59.82) which was 57.8% higher than that of similar sensitization

process by SILAR method ($\eta=2.89\%$; $V_{oc}=0.49$ V, $J_{sc}=11.72$ mA/cm², FF=50.31). Co-sensitization can also efficiently be achieved through the tri-sensitization mode. The energy level diagram of this case is given in (Fig. 15). Through the sensitization of ZnS with CdS/CdSe, significant improvement of absorption has become a possible one. Cheng et al. [143] investigated CdS/CdSe/ZnS cascade structure and its performance for solar cells for TiO₂ NTs with nanowires (NWs). The sensitization process was achieved through SILAR process. Here, ZnS layer acted as a potential barrier for the CdSe-electrolyte. For the best SILAR cycle, about 2.0% of efficiency was achieved with $V_{oc}=0.95$ V, $J_{sc}=3.91$ mA/cm², FF=0.567. Similar kind of cascade structure was formed by Li et al. [144] through Sequential Chemical Bath Deposition (SQCBD) method on TiO₂ NTs. Maximum IPCE of about 72% was obtained for CdS/CdSe/ZnS system which was comparatively higher than the CdS/CdSe co-sensitization (IPCE=53%). Hence it can be concluded that proper tuning of energy levels in co-sensitization can make a tremendous outcome in efficiency.

6. Conclusion and future perspectives

In conclusion, because of their easy fabrication method, titanium-dioxide (TiO₂) nanotubes based solar cells are showing

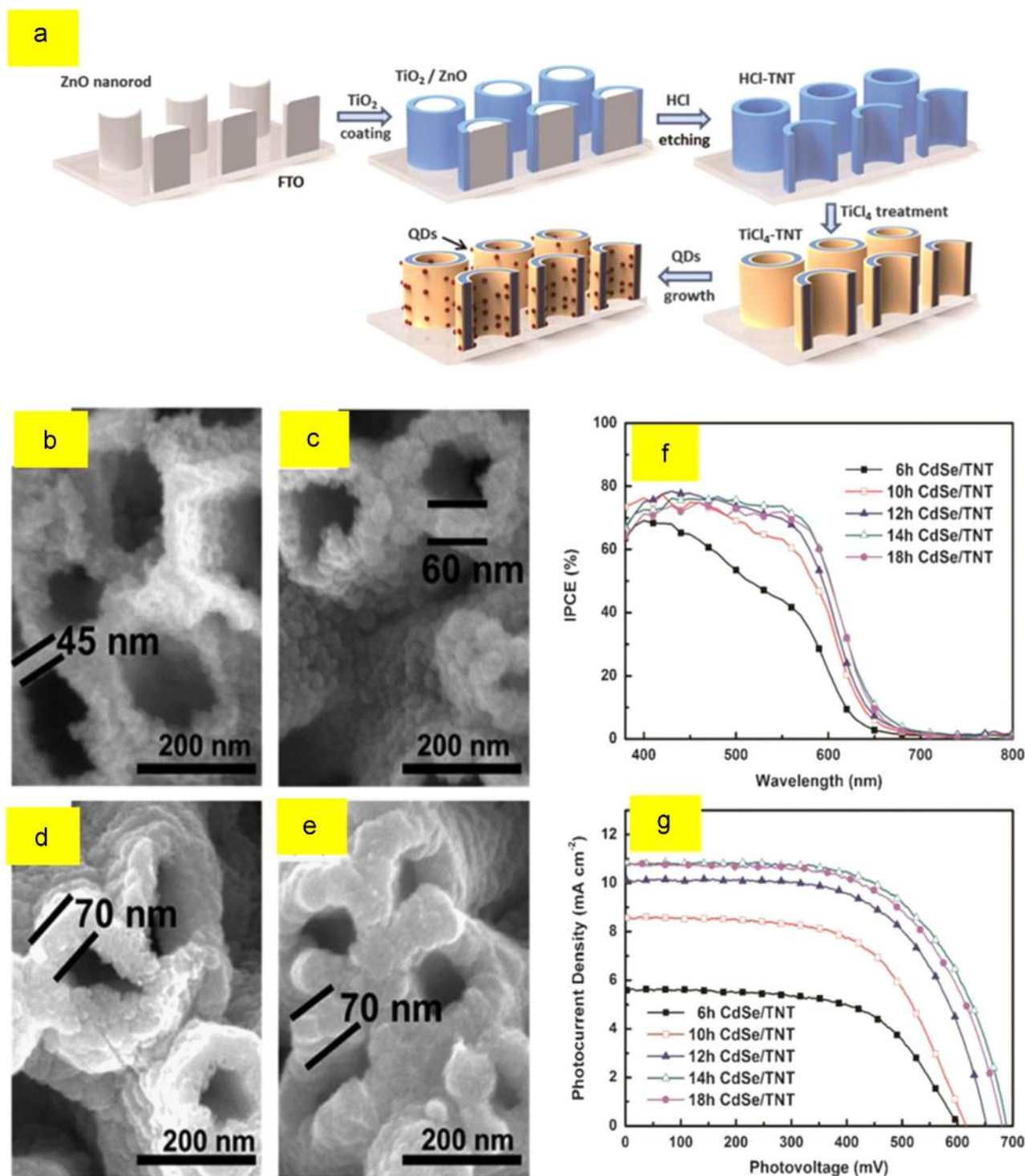


Fig. 14. (i) (a) Schematic process of preparing QDs anchored TiO₂ nanotube arrays directly on FTO glass (ii) SEM images (b,c,d,e) (iii) IPCE and (iv) I–V characteristics of 6 h, 10 h, 14 h, 18 h CdSe/CdSe co-sensitized photoelectrodes. Reprinted from Ref. [139] with the permission of The Royal Society of Chemistry.

attractive results through sensitization by semiconductor nanoparticles. In order to achieve high efficiency, the interface between quantumdots and TiO₂ NTs are to be examined in order to visualize more absorption. The parallel tandem architecture which has been proposed in DSSCs based on this TiO₂ NTs solar cells can be a promising approach for the high efficiency in future direction. Though TiO₂ NTs have more percolation pathway over nanoparticles, the efficiency still to be improved over nanoparticles. Further analysis to be done for the efficient charge transfer from nanoparticles to TiO₂ NTs. Novel approaches in the preparation of

double sided open ended NTs and vertically oriented long range TiO₂ NTs would be a useful one to prepare high efficiency devices. The surface roughness of TiO₂ NTs plays a crucial role in the growth of TiO₂ NTs. Hence, the detailed analysis of the inner surface of TiO₂ NTs and its geometrical parameters are the essential one for the enhanced quantum dots decoration. The defect chemistry of TiO₂ NTs for the charge transport and recombination has to be analyzed well in order to get the complete overview on TiO₂ NTs solar cell. Also, the concentration of oxygen and the optimized diameter, length and thickness of the TiO₂ NTs wall for

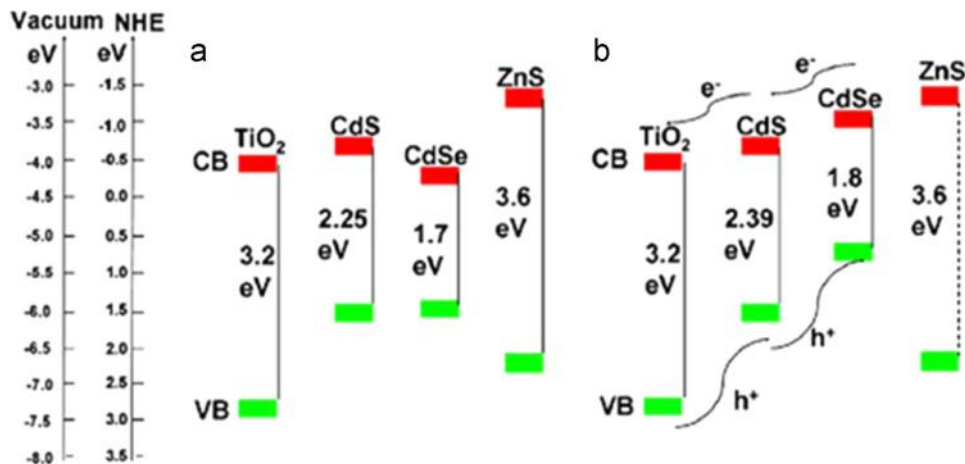


Fig. 15. Relative energy level of (a) bulk phase and (b) nanostructure interface of TiO_2 , CdS, CdSe, ZnS. Reprinted with permission from Ref. [144] Copyright©2011 Elsevier.

the effective nanoparticles sensitization need to be addressed. In addition to this, the life time measurements for the nanoparticles sensitized TiO_2 NTs would ideally provide a way to overcome charge trapping. Moreover, functionalization of TiO_2 NTs also would help to enhance the visible light absorption. Deposition of semiconductor nanoparticles using advanced methods on preferred-oriented TiO_2 NTs (or) a free standing TiO_2 NTs array may be a good option to improve the current efficiency. The improved dye absorption through good anchoring groups of the dye also would enhance the efficiency to some level. Novel materials approach like organic–inorganic hybrid perovskites (ex: $\text{CH}_3\text{NH}_3\text{PbI}_3$) sensitization on highly oriented TiO_2 nanotubes would also be a good way to enhance efficiency. The recently emerging black colored TiO_2 NTs array which efficiently harvest the visible light could also be utilized for the high efficiency solar cell devices. At this juncture, it is concluded that the TiO_2 nanotubes would perhaps holding a promising avenue towards the development of high efficiency solar cells through the sensitization process of semiconductor nanoparticles. It is believed that the future breakthroughs in TiO_2 NTs architecture, materials would definitely solve major obstacles in achieving high efficiency solar devices.

Acknowledgments

The authors sincerely thank UGC- (F.No. 42-885/2013 (SR)), and DST-SERI (DST/TM/SERI/FR/90(G)), Govt of India for funding the research. S. Ananthakumar and J. Ramkumar sincerely thanks Ministry of New and Renewable Energy (MNRE), Govt. of India for providing fellowships under National Renewable Energy Fellowship (NREF) scheme for the doctoral studies.

References

- [1] Chen X, Mao SS. *Chem Rev* 2007;107:2891–959.
- [2] Sreekumar Nair A, Peining Z, Babu VJ, Shengyuan Y, Ramakrishna S. *Phys Chem Chem Phys* 2011;13:21248–61.
- [3] Yang L, Chen B, Luo S, Li J, Liu R, Cai Q. *Environ Sci Technol* 2010;44:7884–9.
- [4] Narayanan R, Kwon TY, Kim KH. *Mater Chem Phys* 2009;117:460–4.
- [5] Signoretto M, Ghedini E, Nichele V, Pinna F, Crocella V, Cerrato G. *Microporous Mesoporous Mater* 2011;139:189–96.
- [6] Park JK, Kim S, Bard AJ. *Nano Lett* 2006;6:24–8.
- [7] Ryu J, Lee SH, Nam DH, Park CB. *Adv Mater* 2011;23:1883–8.
- [8] Das C, Roy P, Yang M, Jha H, Schmuki P. *Nanoscale* 2011;3:3094–6.
- [9] Wang J, Lin Z. *Chem Asian J* 2012;7:2754–62.
- [10] Liu Z, Zhang X, Nishimoto S, Jin M, Tryk DA, Murakami T, Fujishima A. *J Phys Chem C* 2008;112:253–9.
- [11] Shankar K, Basham JI, Allam NK, Varghese OK, Mor GK, Feng X, Paulose M, Seabold JA, Choi KS, Grimes CA. *J Phys Chem C* 2009;113:6327–59.
- [12] Shankar K, Mor GK, Prakasam HE, Yoriya S, Paulose M, Varghese OK, Grimes CA. *Nanotechnology* 2007;18(065707):1–11.
- [13] a) Paramasivam I, Jha H, Liu N, Schmuki P. *Small*, 8; 2012. p. 3073–103; b) Macak JM, Tsuchiya H, Ghicov A, Yasuda K, Hahn R, Bauer S, Schmuki P. *Curr Opin Solid State Mater Sci*, 11; 2007. p. 3–18.
- [14] Hua Y, Chang S, Huang D, Zhou X, Zhu X, Zhao J, Chen T, Wong WY, Wong WK. *Chem Mater* 2013;25:2146–53.
- [15] Han L, Islam A, Chen H, Malapaka C, Chiranjeevi B, Shufang Z, Yang X, Yanagita M. *Energy Environ Sci* 2012;5:6057–60.
- [16] Plass R, Pelet S, Krueger J, Gratzel M. *J Phys Chem B* 2002;106:7578–80.
- [17] Lee YL, Huang BM, Chien HT. *Chem Mater* 2008;20:6903–5.
- [18] Regan BO, Gratzel M. *Nature* 1991;353:737–40.
- [19] Hagfeldt H, Boschloo G, Sun L, Kloo L, Pettersson H. *Chem Rev* 2010;110:6595–663.
- [20] Tetreault N, Gratzel M. *Energy Environ Sci* 2012;5:8506–16.
- [21] Lee JK, Yang MY. *Mater Sci Eng B* 2011;176:1142–60.
- [22] Ruhle S, Shalom M, Zaban A. *ChemPhysChem* 2010;11:2290–304.
- [23] Kramer IJ, Sargent EH. *Chem Rev* 2014;114:863–82.
- [24] Qin P, Paulose M, Dar I, Moehl T, Arora N, Gao P, Varghese OK, Gratzel M, Nazeeruddin MK. *Small* 2015;11:5533–9. <http://dx.doi.org/10.1002/sml.201501460>.
- [25] Jiang Z, Yang F, Luo N, Chu BTT, Sun D, Shi H, Xiao T. *Edwards Chem Commun* 2008;47:6372–4.
- [26] Bavykin DV, Parmon VN, Lapkin AA, Walsh FC. *J Mater Chem* 2004;14:3370–7.
- [27] Zhang M, Bando Y, Wada K. *J Mater Sci Lett* 2001;20:167–70.
- [28] Ghicov A, Schmuki P. *Chem Commun* 2009;20:2791–808.
- [29] Wang D, Yu B, Wang C, Zhou F, Liu W. *Adv Mater* 2009;21:1964–7.
- [30] Masuda H, Fukuda K. *Science* 1995;268:1466.
- [31] Wang J, Lin Z. *Chem Mater* 2008;20:1257–61.
- [32] Yin H, Liu H, Shen WZ. *Nanotechnology* 2010;21(035601):1–7.
- [33] Wang X, Zhang S, Sun L. *Thin Solid Films* 2011;519:4694–8.
- [34] Dubey M, Shrestha M, Zhong Y, Galipeau D, He H. *Nanotechnology* 2011;22(285201):1–9.
- [35] Mor JK, Varghese OK, Paulose M, Mukherjee N, Grimes CG. *J Mater Res* 2003;18:2588–93.
- [36] Yang Y, Wang X, Li L. *J Am Chem Soc* 2008;91:3086–9.
- [37] Ruan C, Paulose M, Varghese OK, Mor GK, Grimes CA. *J Phys Chem B* 2005;109:15754–9.
- [38] Yoriya S, Paulose M, Varghese OK, Mor GK, Grimes CA. *J Phys Chem C* 2007;111:13770–6.
- [39] Shankar K, Mor GK, Prakasam HE, Varghese OK, Grimes CA. *Langmuir* 2007;23:12445–9.
- [40] Wender H, Feil AF, Diaz LB, Ribeiro CS, Machado GJ, Migowski P, Weibel DE, Teixeira SR. *Appl Mater Interfaces* 2011;3:1359–65.
- [41] Liu N, Mirabolghasemi H, Lee K, Albu SP, Tighineanu A, Altomare M, Schmuki P. *Faraday Discuss* 2013;164:107–16.
- [42] Mor GK, Varghese Paulose M, Shankar K, Grimes CA. *Sol Energy Mater Sol Cells* 2006;90:2011–75.
- [43] Regonini D, Bowen CR, Jaroenworarluck A, Stevens R. *Mater Sci Eng R* 2013;74:377–406.
- [44] Gratzel M. *J Photochem Photobiol C: Photochem Rev* 2003;4:145–53.
- [45] Yang Z, Chen CY, Roy P, Chang HT. *Chem Commun* 2011;47:9561–71.
- [46] Hod I, Zaban A. *Langmuir* 2013;30:7264–73. <http://dx.doi.org/10.1021/la403768j>.
- [47] Banerjee S, Mohapatra SK, Das PP, Misra M. *Chem Mater* 2008;20:6784–91.
- [48] Dong C, Li X, Qi J. *J Phys Chem C* 2011;115:20307–15.
- [49] Si HY, Sun ZH, Zhang HL. *Colloids Surf A: Physicochem Eng Asp* 2008;313–314:604–7.
- [50] Seabold JA, Shankar K, Wilke RHT, Paulose M, Varghese OK, Grimes CA, Choi KS. *Chem Mater* 2008;20:5266–73.

- [51] Bjelajac A, Petrovic R, Nedeljkovic JM, Djokic V, Radetic T, Cirkovic J, Janackovic D. *Ceram Int* 2015;41:7048–53.
- [52] Gao XF, Sun WT, Hu ZD, Ai G, Zhang YL, Feng S, Li F, Peng LM. *J Phys Chem C* 2009;113:20481–5.
- [53] Baker DR, Kamat PV. *Adv Funct Mater* 2009;19:805–11.
- [54] Xian J, Li D, Chen J, Li X, He M, Shao Y, Yu L, Fang J. *ACS Appl Mater Interfaces* 2014;6:13157–66.
- [55] Zhang Q, Wang L, Feng J, Xu H, Yan W. *Phys Chem Chem Phys* 2014;16:23431–9.
- [56] Zhang J, Tang C, Bang JH. *Electrochem Commun* 2010;12:1124–8.
- [57] Yang H, Fan W, Vaneski A, Susha AS, Teoh WY, Rogach AL. *Adv Funct Mater* 2012;22:2821–9.
- [58] Hossain MF, Biswas S, Zhang ZH, Takahashi T. *J Photochem Photobiol A: Chem* 2011;217:68–75.
- [59] Sun WT, Yu Y, Pan HY, Gao XF, Chen Q, Peng LM. *J Am Chem Soc* 2008;130:1124–5.
- [60] Ma X, Shen Y, Wu G, Wu Q, Pei B, Cao M, Gu F. *J Alloy Compd* 2012;538:61–5.
- [61] Xie Y, Ali G, Yoo SH, Cho SO. *ACS Appl Mater Interfaces* 2010;2:2910–4.
- [62] Gao XF, Li HB, Sun WT, Chen Q, Tang FQ, Peng LM. *J Phys Chem C* 2009;113:7531–5.
- [63] Shen Q, Yamada A, Tamura S, Toyoda T. *Appl Phys Lett* 2010;97(123107):1–3.
- [64] Chakrapani V, Baker D, Kamat PV. *J Am Chem Soc* 2011;133:9607–15.
- [65] Shao Z, Zhu W, Li Z, Yang Q, Wang G. *J Phys Chem C* 2012;116:2438–42.
- [66] Zhang M, Wang YN, Moulin E, Grutzmacher D, Chien CJ, Chang PC, Gao X, Cariu R, Lu JG. *J Mater Chem* 2012;22:10441–3.
- [67] Wang Q, Yang X, Chi L, Cui M. *Electrochim Acta* 2013;91:330–6.
- [68] Pang Q, Leng L, Liang C, He J, Zhou L, Lan Y, Zhao L. *Integr Ferroelectr* 2012;137:165–72.
- [69] Kongkanand A, Tvrdy K, Takechi K, Kuno M, Kamat PV. *J Am Chem Soc* 2008;130:4007–15.
- [70] Kalanur SS, Hwang YJ, Joo OS. *J Colloid Interface Sci* 2013;402:94–9.
- [71] Liou YH, Kao LC, Tsai MC, Lin CJ. *Electrochem Commun* 2012;15:66–9.
- [72] Gao S, Yang J, Liu M, Yan H, Li W, Zhang J, Luo Y. *J Power Sources* 2014;250:174–80.
- [73] Fernandes JA, Migowski P, Fabrim Z, Feil AF, Rosa G, Khan S, Machado GJ, Fichtner PFP, Teixeira SR, Santos MJL, Dupont J. *Phys Chem Chem Phys* 2014;16:9148–53.
- [74] Gakhar R, Smith YR, Misra M, Chidambaram D. *Appl Surf Sci* 2015;355:1279–88.
- [75] Gakhar R, Smmers K, Palaniappan R, Pillai SK, Chidambaram D. *RSC Adv* 2014;4:49729–36.
- [76] Kang Q, Cai Q, Yao SZ, Grimes CA, Ye J. *J Phys Chem C* 2012;116:16885–92.
- [77] Li Z, Yu L, Liu Y, Sun S. *J Mater Sci: Mater Electron* 2015;26:1625–33.
- [78] Gakhar R, Merwin A, Summers K, Pillai SK, Chidambaram D. *J Mater Chem A* 2014;2:10116–25.
- [79] Wang Q, Qiao J, Gao S. *Mater Lett* 2014;131:354–7.
- [80] Premlal EVA, Dematage N, GRA Kumara, RMG Rajapakse, Murakami K, Konno A. *Electrochem Acta* 2012;63:375–80.
- [81] O'Regan BC, Durrant JR, Sommeling PM, Bakker NJ. *J Phys Chem C* 2007;111:14001–10.
- [82] Pan X, Chen C, Zhu K, Fan Z. *Nanotechnology* 2011;22(235402):1–7.
- [83] Roy P, Kim D, Paramasivam I, Schmuki P. *Electrochem Commun* 2009;11:1001–4.
- [84] Lin LY, Chen CY, Yeh MH, Tsai KW, Lee CP, Vittal R, Wu CG, Ho KC. *J Power Sources* 2013;243:535–43.
- [85] Wu WQ, Xu YF, Rao HS, Su CY, Kuang DB. *J Phys Chem C* 2014;118:16426–32.
- [86] Ratanatawanate C, Xiong C, Balkus KJ. *ACS Nano* 2008;2:1682–8.
- [87] Cai F, Yang F, Zhang Y, Ke C, Cheng C, Zhao Y, Yan G. *Phys Chem Chem Phys* 2014;16:23967–74.
- [88] Kang Q, Liu S, Yang L, Cai Q, Grimes CA. *Appl Mater Interfaces* 2011;3:746–9.
- [89] Tao L, Xiong Y, Liu H, Shen W. *Nanoscale* 2014;6:931–8.
- [90] Cui X, Gu H, Guan Y, Ren G, Ma Z, Yin Y, Liu J, Cui X, Yao L, Yin Y, Wang D, Jin G, Rong S, Tong L, Hou J, Li M. *Sol Energy Mater Sol Cells* 2015;137:101–6.
- [91] Liu R, Liu Y, Liu C, Luo S, Teng Y, Yang L, Yang R, Cai Q. *J Alloy Compd* 2011;509:2434–40.
- [92] Chen C, Ali G, Yoo SH, Kum JM, Cho SO. *J Mater Chem* 2011;21:16430–5.
- [93] Yun JH, Ng YH, Hung S, Conibeer G, Amal R. *Chem Commun* 2011;47:11288–90.
- [94] Liao Y, Zhang H, Zhong Z, Jia L, Bai F, Li J, Zhong P, Chen H, Zhang J. *Appl Mater Interfaces* 2013;5(21):11022–8.
- [95] Wang Q, Qiao J, Zhou J, Gao S. *Electrochim Acta* 2015;167:470–5.
- [96] Tubtintae A, Hongto T, Hongsith K, Choopun S. *Superlattices Microstruct* 2014;66:96–104.
- [97] Liu Z, Ji G, Guan D, Wang B, Wu X. *J Colloid Interface Sci* 2015;457:1–8.
- [98] Chen C, Xie Y, Ali G, Yoo SH, Cho SO. *Nanoscale Res Lett* 2011;6(462):1–9.
- [99] Chen C, Xie Y, Ali G, Yoo SH, Cho SO. *Nanotechnology* 2011;22(015202):1–8.
- [100] Lee W, Kang SH, Kim JY, Kolekar GB, Sung YE, Han SH. *Nanotechnology* 2009;20(335706):1–7.
- [101] Gui Q, Xu Z, Zhang H, Cheng C, Zhu X, Yin M, Song Y, Lu L, Chen X, Li D. *ACS Appl Mater Interfaces* 2014;6:17053–8.
- [102] Lin LY, Yeh MH, Chen CY, Vittal R, Wu CG, Ho KC. *J Mater Chem A* 2014;2:8281–7.
- [103] Solis M, Rincon ME, Calva JC, Alvarado G. *Electrochem Acta* 2013;112:159–63.
- [104] Sarkar SK, Kim JY, Goldstein DN, Neale NR, Zhu K, Elliot CM, Frank AJ, George SM. *J Phys Chem C* 2010;114:8032–9.
- [105] Jia Y, Yang F, Cai F, Cheng C, Zhao Y. *Electron Mater Lett* 2013;9:287–91.
- [106] Sarma B, Smith YR, Mohanty SK, Misra M. *Mater Lett* 2012;85:33–6.
- [107] Zhong JS, Wang QY, Zhu X, Chen DQ, Ji ZG. *J Alloy Compd* 2015;641:144–7.
- [108] Hou Y, Li XY, Zhao QD, Quan X, Chen GH. *Appl Phys Lett* 2009;95(093108):1–3.
- [109] Assauld L, Heresanu V, Hanbucken M, Santinacci L. *C R Chim* 2013;16:89–95.
- [110] Li D, Chien CJ, Chien CJ, Deora S, Chang PC, Moulin E, Lu JG. *Chem Phys Lett* 2011;501:446–50.
- [111] Tsui LK, Zangari G. *Electrochem Acta* 2014;128:341–8. <http://dx.doi.org/10.1016/j.electacta.2013.09.150>.
- [112] Cheng M, Yang X, Li J, Zhang F, Sun L. *ChemSusChem* 2013;6:70–7.
- [113] Kuang D, Walter P, Nuesch F, Kim S, Ko J, Comte P, Zakeeruddin SM, Nazeeruddin MK, Gratzel M. *Langmuir* 2007;23:10906–9.
- [114] Song X, Yu XL, Xie Y, Sun J, Ling T, Du XW. *Semicond Sci Technol* 2010;25(095014):1–5.
- [115] Ananthakumar S, Ramkumar J, Moorthy Babu S. *Sol Energy* 2014;106:136–42.
- [116] Lee YL, Chi CF, Liao SY. *Chem Mater* 2010;22:922–7.
- [117] Chen J, Lei W, Deng WQ. *Nanoscale* 2011;3:674–7.
- [118] Kuang D, Walter P, Nuesch F, Kim S, Ko J, Comte P, Zakeeruddin SM, Nazeeruddin MK, Gratzel M. *Langmuir* 2007;23:10906–9.
- [119] Wang Q, Yang X, Liu D, Chi L, Hou J. *Electrochem Acta* 2012;83:140–5.
- [120] Wang Q, Li S, Qiao J, Jin R, Yu Y, Gao S. *Sol Energy Mater Sol Cells* 2015;132:650–4.
- [121] Huo H, Xu Z, Zhang T, Xu C. *J Mater Chem A* 2015;3:5882–8.
- [122] Gao XF, Sun WT, Ai G, Peng LM. *Appl Phys Lett* 2010;96(153104):1–3.
- [123] Cai J, Sheng P, Zhou L, Shi L, Wang N, Cai Q. *Biosens Bioelectron* 2013;50:66–71.
- [124] Zhang J, Du RG, Lin ZQ, Zhu YF, Guo Y, Qi HQ, Xu L, Lin CJ. *Electrochem Acta* 2012;83:59–64.
- [125] Lee YL, Lo YS. *Adv Funct Mater* 2009;19:604–9.
- [126] Huang S, Zhang Q, Huang X, Guo X, Deng M, Li D, Luo Y, Shen Q, Toyoda T, Meng Q. *Nanotechnology* 2010;21(375201):1–7.
- [127] Guan XF, Huang SQ, Zhang QX, Shen X, Sun HC, Li DM, Luo YH, Yu RC, Meng QB. *Nanotechnology* 2011;22(465402):1–8.
- [128] Lee W, Kang SH, Min SK, Sung YE, Han SH. *Electrochem Commun* 2008;10:1579–82.
- [129] Lai Y, Li Z, Zheng D, Chi L, Du R, Lin C. *Electrochem Acta* 2012;79:175–81.
- [130] Liu L, Hui J, Su L, Lv J, Wu Y, Irvine JTS. *Mater Lett* 2014;132:231–5.
- [131] Lv J, Wang H, Gao H, Xu G, Wang D, Chen Z, Zhang X, Zheng Z, Wu Y. *Surf Coat Technol* 2015;261:356–63.
- [132] Zhu Y, Wang R, Zhang W, Ge H, Li L. *Appl Surf Sci* 2014;315:149–53.
- [133] Lv P, Fu W, Yang H, Sun H, Chen Y, Ma J, Zhou X, Tian L, Zhang W, Li M, Yao H, Wu D. *CrystEngComm* 2013;15:7548–55.
- [134] Lv P, Fu W, Mu Y, Sun M, Su S, Chen Y, Yao H, Ding D, Liu T, Wang J, Yang H. *J Alloy Compd* 2015;621:30–4.
- [135] Smith YR, Gakhar R, Merwin A, Mohanty SK, Chidambaram D, Misra M. *Electrochim Acta* 2014;135:503–12.
- [136] Zhang Q, Xu H, Yan W. *Electrochim Acta* 2012;61:64–72.
- [137] Wu J, Tang C, Xu H, Yan W. *J Alloy Compd* 2015;633:83–91.
- [138] Li Z, Yu L, Liu Y, Sun S. *Electrochim Acta* 2015;153:200–9.
- [139] Zhang Q, Chen G, Yang Y, Shen X, Zhang Y, Li C, Yu R, Luo Y, Li D, Meng Q. *Phys Chem Chem Phys* 2012;14:6479–86.
- [140] Wang H, Zhu W, Chong B, Qin K. *Int J Hydrogen Energy* 2014;39:90–9.
- [141] Li Zhen, Yu L, Sun S. *Electrochem Acta* 2014;129:379–88.
- [142] Zhang X, Yu D, Xiong FQ, Li M, Yang Z, Zhu J, Zhang WH, Li C. *Chem Commun* 2014;50:4364–7.
- [143] Cheng S, Fu W, Yang H, Zhang L, Ma J, Zhao H, Sun M, Yang LJ. *Phys Chem C* 2012;116:2615–21.
- [144] Li ZX, Xie YL, Xu H, Wang TM, Zu ZG, Zhang HL. *J Photochem Photobiol A: Chem* 2011;224:25–30.



Synthesis of thiol modified CdSe nanoparticles/P3HT blends for hybrid solar cell structures



S. Ananthakumar¹, J. Ramkumar¹, S. Moorthy Babu^{*,1}

Crystal Growth Centre, Anna University, Chennai 25, India

ARTICLE INFO

Available online 20 February 2014

Keywords:

CdSe nanoparticles
Phase transfer
Hybrid solar cell

ABSTRACT

Thioglycolic acid (TGA) capped cadmium selenide (CdSe) nanoparticles were synthesised in aqueous medium through wet chemical method using sodium selenite as the selenium source. The synthesised particles were transformed into organic medium using 1-dodecanethiol through efficient partial ligand exchange strategy. The UV–visible spectra recorded for the particles reveal the size distribution in water as well as in organic solvent. TEM analysis of the synthesised particles shows the size and the nature of distribution of the particles in solution. The phase transferred particles were blended with the polymer poly-3-hexyl thiophene (P3HT) in chloroform. UV–visible and photoluminescence spectra of the polymer with various volumes of the nanoparticles clearly indicate the effective coupling and the efficient charge transfer process in the blend. SEM analysis of the CdSe–P3HT blends confirms the effective distribution of the nanoparticles in the polymeric matrix. AFM studies reveal the morphology of the nanoparticles and the phase separation process in the blends.

© 2014 Elsevier Ltd. All rights reserved.

1. Introduction

Semiconductor nanoparticles have a wide variety of applications in optoelectronics particularly in photovoltaics due to their size dependent properties [1,2]. Due to the limitation of the poor charge carrier mobility, organic acceptor molecules like fullerenes and PCBM are being replaced by semiconductor nanocrystals such as CdSe, CdTe, CdS, ZnO and TiO₂ to fabricate the hybrid solar cells based on the bulk heterojunction concept [3–9]. In recent years, the blends of these nanocrystals with semiconducting polymers have shown wide range of applications in the photovoltaics. CdSe is of great interest and useful in hybrid and quantum dot sensitised electrodes for solar cells [10,11] due to the size tunability nature and low bandgap

($E_g=1.74$ eV in bulk form). Moreover, the absorption wavelength of nano sized CdSe could be tuned to near-IR region which shows its applicability in solar cells. CdSe nanoparticles were synthesised mostly in organometallic medium with trioctyl phosphine oxide (TOPO) as the capping ligand. Then surface treatment with pyridine was carried out with polymer, the blend was used as active layer in hybrid solar cells [12–14]. CdSe nanoparticles synthesised with TGA in aqueous system have major setback in many useful applications as they are immiscible in organic solvents. To eliminate this problem, the phase transfer chemistry has been proposed. Phase transfer of semiconductor nanoparticles from aqueous to organic medium is being carried out using different methods [15–17]. Gaponik et al. [18] have proposed a suitable method which helps to transfer the aqueous synthesised CdTe nanoparticles into organic medium through the long chain 1-dodecanethiol. This method is a simple and convenient one for the photovoltaic applications. Also, the 1-DDT capping has shown considerable application in

* Corresponding author.

E-mail addresses: smoorthybabu@yahoo.com, babu@annauniv.edu, babum@yahoo.com (S. Moorthy Babu).

¹ Tel.: +91 44 22358333; fax: +91 44 2235 2774.

HgTe nanoparticles for electroluminescent devices [19]. The ligand TOPO is toxic, hazardous in nature and it requires pyridine treatment of the particles for application as active layer in solar cells. Hence, the alternative pathway to produce CdSe nanoparticles soluble in the organic solvent with the suitable ligand for the active layer application was highly motivated. Recently, 1-DDT ligand capped semiconductor nanoparticles were shown as potential candidates for photovoltaic applications [20]. Since these ligands play a major role in the morphology and the efficiency in charge transport of the active layer, significant efforts were focussed for their selectivity. The non-TOPO based synthesis of the CdSe nanoparticles for hybrid solar cells has been achieved using the Aerosol Flow Growth Technique at high temperature using 1-DDT as the capping agent [21]. Further, the ligand 1-DDT can give a better spatial resolution than the short chain ligand thioglycolic acid (TGA) that can be used effectively for the phase transfer process. Moreover, 1-dodecanethiol acts as the very good additive in the performance of P3HT:PCBM blends [22]. Phase transferred particles capped by 1-DDT can readily be blended with P3HT polymer without surface treatment which eliminates the pyridine treatment (toxic) reaction. In this paper, the synthesis of TGA capped CdSe nanoparticles at low temperature (90 °C) in aqueous medium is reported. The synthesised particles were phase transferred through the partial ligand exchange process using 1-dodecanethiol. The phase transferred particles were blended with the polymer P3HT in chloroform. The optical properties and morphological analysis of the blends were evaluated.

2. Experimental section

2.1. Chemicals

Precursors in the form of cadmium chloride (CdCl_2) SRL (97%), sodium selenite (Na_2SeO_3) CDH (99%), thioglycolic acid (TGA) SPECTROCHEM (95%), sodium borohydride (NaBH_4) MERCK (95%), sodium hydroxide (NaOH) SRL (98%), trisodium citrate dihydrate ($(\text{C}_6\text{H}_9\text{Na}_3\text{O}_9)$ SRL (99%), chloroform (CHCl_3) MERCK (99%), regioregular poly-(3-hexyl thiophene)-2,5 dyl (P3HT) Sigma Aldrich (99.99%) and poly(3,4-ethylene dioxythiophene) doped with polystyrenesulfonic acid (PEDOT:PSS) Sigma Aldrich (99.99%) were used for casting of different layers towards development of solar cell structures.

2.2. Synthesis of TGA capped CdSe nanoparticles

CdSe nanoparticles were synthesised with the following procedure: Cadmium chloride (1 mM) was dissolved in the deionised water and the ligand thioglycolic acid (5 mM) was added with it. A white turbidity of the solution arises which confirms the formation of cadmium thiolate complex. This turbidity was eliminated when the pH of the solution was adjusted into 10.5 using 0.1 M NaOH solution. Then trisodium citrate dihydrate was added into the solution. The entire mixture was taken in the three necked flask and the solution was stirred under the nitrogen atmosphere. With this, sodium selenite

(0.5 mM) and excess of sodium borohydride were added gradually and heated upto 90 °C. The appearance of yellow coloured solution which turned into red orange colour on prolonged refluxing indicates the formation of CdSe nanoparticles. The entire solution was refluxed under the nitrogen atmosphere to get the desired size.

2.3. Phase transfer of the CdSe nanoparticles

Aqueous synthesised CdSe nanoparticles were transformed into organic phase using Gaponik's method [18]. Briefly, 1-dodecanethiol was mixed with equal amount of the aqueous CdSe nanoparticles in solution. A measured quantity of acetone was added and the entire mixture was shaken well with mild heating. The transformation of the CdSe nanoparticles from aqueous phase to organic phase was observed after some time due to partial ligand exchange of the thioglycolic acid by 1-dodecanethiol. The organic phase was separated and precipitated with the addition of methanol and the resultant precipitate was redispersed in chloroform for further studies. The schematic diagram of this phase transfer process is given in Fig. 1. The particles were found to be stable in the organic phase. As prepared 1-DDT capped nanoparticles were mixed with chloroform and P3HT polymer. The entire solution was stirred for 12 h for complete mixing of P3HT and CdSe nanoparticles.

The ITO coated glass substrate was pre-treated with various solvents including acetone, isopropanol, methanol and dried in vacuum. Finally, aqueous dispersion of PEDOT:PSS was applied on the ITO layer for 1000 rpm through spin coating. Then the substrate was allowed to anneal at 80 °C for 15 min. The prepared CdSe/P3HT blend in chloroform was then coated on the substrate at 1500 rpm. The substrate was again heated at 100 °C for 10 min. The final structure ITO/PEDOT:PSS/CdSe–P3HT was analysed for further characterisation.

2.4. Characterisation instruments

UV–visible absorption spectra of the particles were analysed with ELICO SL-159 UV–Visible conventional spectrophotometer in the range of 200–800 nm. Photoluminescence spectra were recorded using JASCO FP-6300 spectrofluorometer at the excitation wavelength 400 nm. HRTEM images were observed with an electron microscope (Tecnai G2 model T-30 s-twin) using an accelerating voltage of 300 kV. SEM images were recorded using Carl Zeiss MA15/EVO 18 Scanning Electron Microscope. AFM

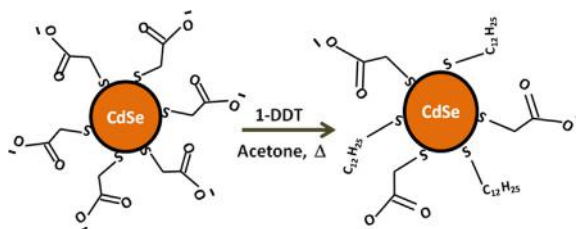
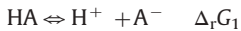


Fig. 1. Phase transfer process of the CdSe nanoparticles.

analysis of the samples was carried out using Park XE-100 Atomic Force Microscope through non-contact mode.

3. Results and discussion

Absorption spectra of the CdSe nanoparticles prepared in water as well as the phase transferred CdSe nanoparticles using 1-DDT is shown in Fig. 2. The spectra clearly show the effect of phase transfer of the nanoparticles. The size distribution of the particles in water and 1-DDT is uniform. The slight difference that occurred between the absorption spectra of the two cases may be due to the change of the medium. The absorption onset of the two cases is approximately about 550 nm. Since the dissociation constant of the 1-dodecanethiol (51 kJ/mol) is much larger than the thioglycolic acid, the Gibbs free energy of the entire phase transfer process can be predicted using the relations [23,24]:



The breaking of the bond between the nanoparticles and TGA ligand from the surface can be interpreted through the following relationship:

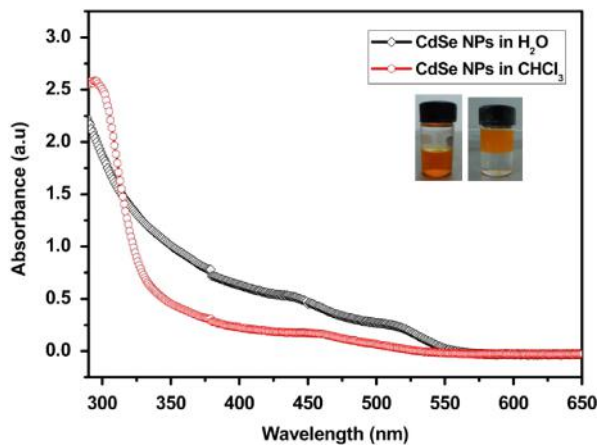
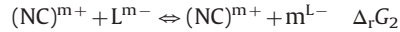
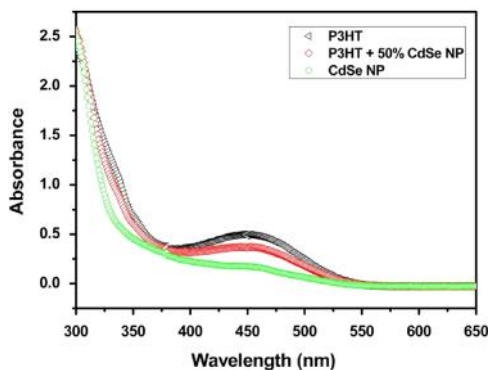
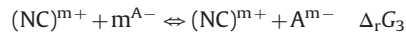


Fig. 2. Absorption spectra of the CdSe nanoparticles in water and Chloroform.



The absorption of 1-dodecanethiol on the surface of the nanoparticles can be understood by the following relation



Hence, the total Gibbs free energy of the ligand exchange process can be

$$\Delta_r G_1 + \Delta_r G_2 + \Delta_r G_3$$

In the case of the CdSe nanoparticles, the value of the $\Delta_r G_1 + \Delta_r G_2 + \Delta_r G_3$ is smaller than zero due to the spontaneous process of ligand exchange. i.e. $\Delta_r G_1 + \Delta_r G_2 + \Delta_r G_3 < 0$.

The absorption spectra of the nanocomposites indicate the sum of the absorption of the individual constituents hence; this confirms the successful coupling of the nanoparticles and polymer [25]. The absorption spectra of CdSe NPs and its blend with the polymer P3HT are shown in Fig. 3. The absorption maximum that corresponds to P3HT polymer was at 450 nm. The maximum intensity of absorption corresponding to the polymer decreases with the addition of the nanoparticles to the polymer [Fig. 3(b)]. The absorption spectrum of the combined blends of polymer and 50% in volume of the CdSe nanoparticles indicates that the data has the combined absorption of its individual constituents. The absorption maximum of the blend of the nanoparticles and polymer lies between 400 and 550 cm^{-1} . The TEM image of the synthesised CdSe nanoparticles is shown in Fig. 4(a). The image reveals that the particles are spherical in nature and distributed in solution without agglomeration. The size distribution histogram of the particles in the solution is given in Fig. 4(b). The average size of the particles was found to be 1.5 nm. Selective Area Electron Diffraction pattern (SAED) of the particles confirms the crystalline nature. Photoluminescence analysis is one of the excellent method to study the identification of the charge transfer process at the donor–acceptor interface of the organic and hybrid solar cells [26]. The emission spectra of P3HT polymer with various volume additions of the CdSe nanoparticles are shown in Fig. 5. Quenching of pure P3HT emission with the

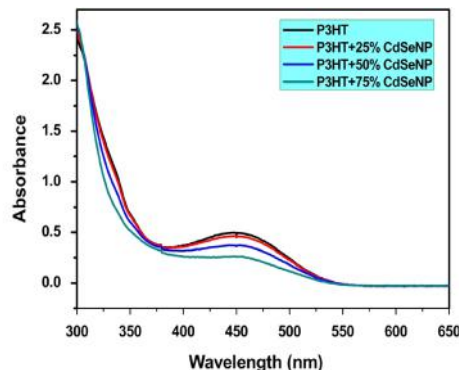


Fig. 3. (a) Absorption spectra of the CdSe, P3HT and CdSe–P3HT blend. (b) The variation of the absorption of the polymer with respect to addition of the nanoparticles in various volumes.

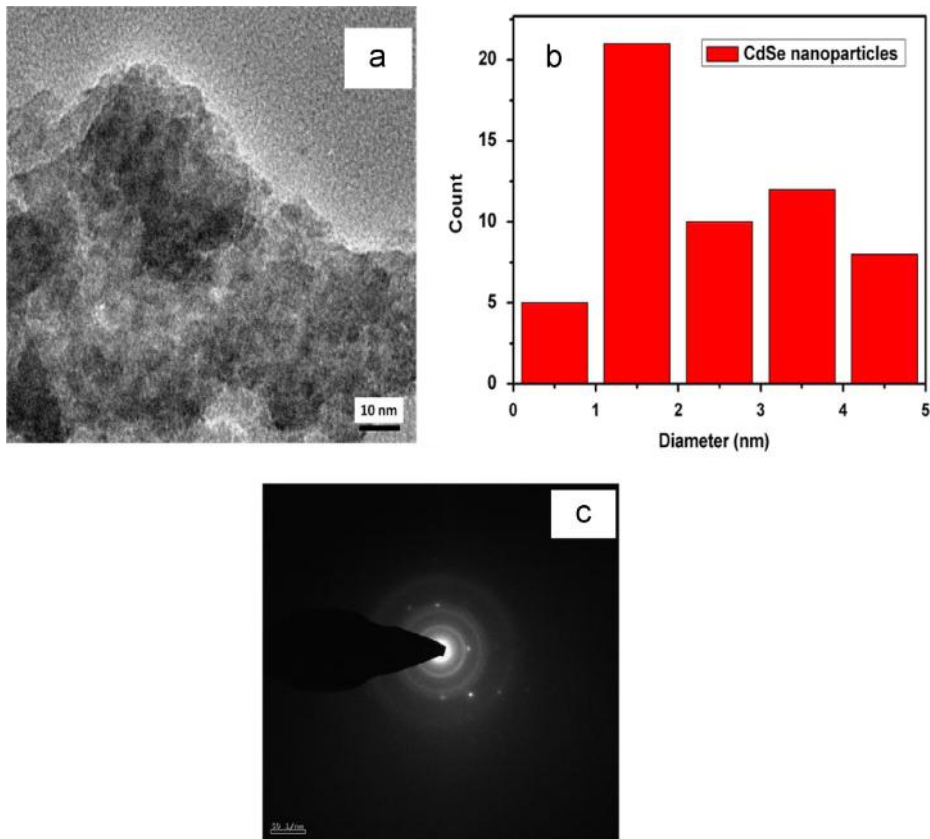


Fig. 4. (a) TEM image of the synthesised CdSe nanoparticles, (b) size histogram of CdSe nanoparticles and (c) SAED pattern of the particles.

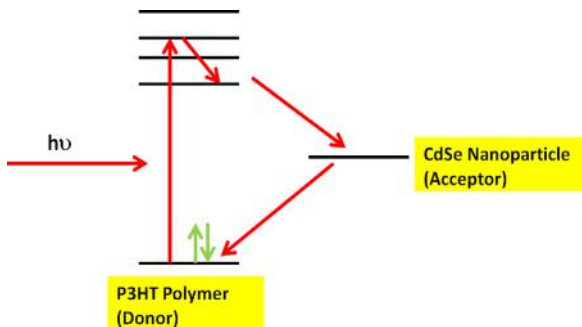


Fig. 5. Mechanism of photoluminescence quenching of CdSeNP–P3HT polymer blend.

addition of the nanoparticles was observed in the spectra. The emission intensity for P3HT was maximum and decreases with increasing content of volume fraction of nanoparticles. It clearly reveals that the recombination of the polymer system has been suppressed by the nanoparticles by splitting the charges at the interface. This charge separated state produce holes in the polymer and the electrons in the CdSe nanoparticles. The donor–acceptor contact area can be increased with the addition of the nanoparticles in P3HT. Minimum quenching for 75% volume of CdSe nanoparticles in P3HT indicates that the particles are effectively blended and confirms the efficient

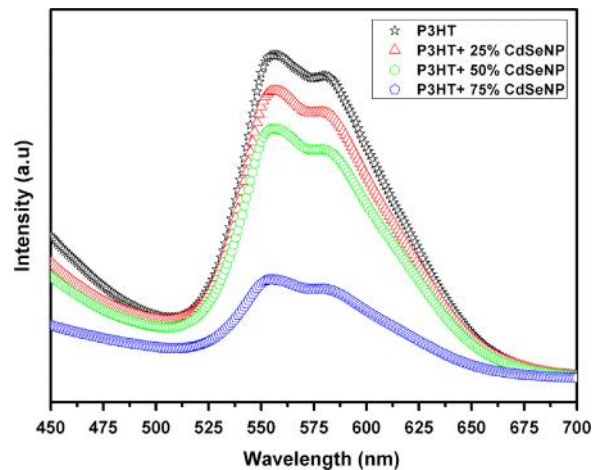


Fig. 6. Photoluminescence spectra of CdSe/P3HT blends in various volume ratios in CHCl_3 .

charge separation. The schematic diagram of these quenching phenomena is illustrated in Fig. 6. In hybrid solar cell structure, the morphology plays an important role in the charge transport and separation. SEM images of the CdSe and P3HT blends in the 50:50 volume percentage mixed in chloroform are shown in Fig. 7(a,b). The images clearly reveal that the nanoparticles (as white spots) are distributed as

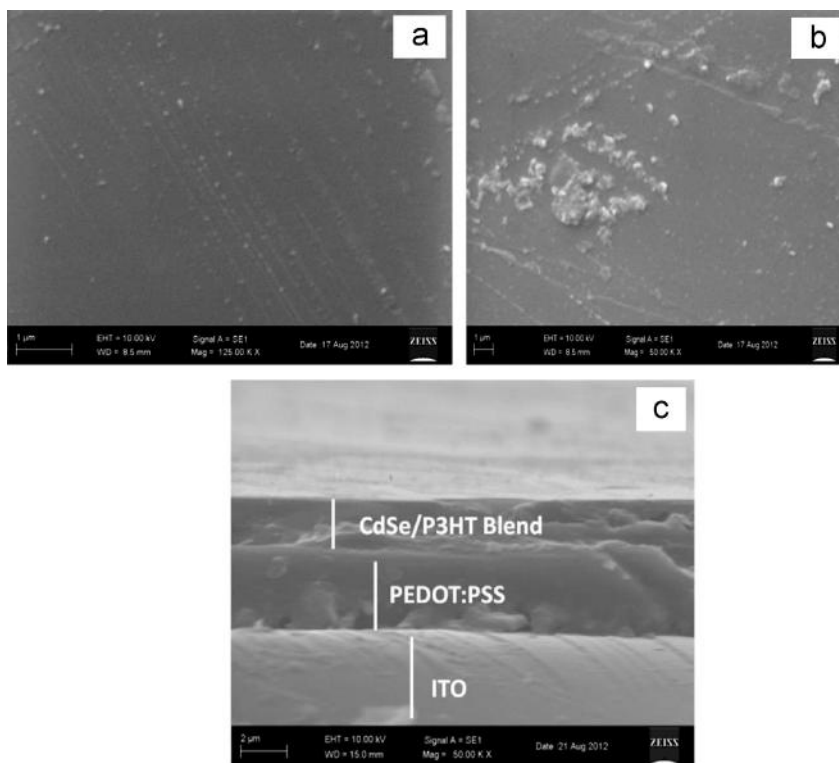


Fig. 7. (a,b) SEM images of CdSe (50% volume) – P3HT blends and (c) cross section image of the ITO/PEDOT:PSS/CdSe–P3HT blend.

bigger in size in the polymer matrix (dark portion). Some aggregations of the nanoparticles were also found on the surface. This aggregation of the nanoparticles may be due to the phase separation and increasing Van der Waal's force of attraction between the particles due to the improvement of the contact area of particles [27]. Since, optimisation of the phase separation phenomena is a major issue in the hybrid solar cells, further studies like effect of solvent, effect of annealing are needed. The cross sectional image of the ITO/PEDOT:PSS/CdSe–P3HT blends are shown in Fig. 7(c). The images clearly indicate that the layers have uniform surface in the substrate and the thickness of the CdSe–P3HT active layer was about 100 nm. Schematic electronic interaction of the CdSe nanoparticles with the polymer is depicted in Fig. 8. A nanoscale phase separation of donor and acceptor materials in the active layer is required to achieve the efficient exciton dissociation and charge transport process. The tapping mode topography AFM images of the CdSe nanoparticles blended with P3HT polymer in the ratio 50:50 in volume level is as shown in Fig. 9. The high level density of the roughness of the films observed for this ratio indicates the effective phase separation of the nanoparticles in the surface. The roughness of the hybrid film increases with increasing the content of nanoparticles [28]. The Root Mean Square (RMS) value of the blended film was determined as 11.9 nm; this value has to be improved with the optimisation of smooth layers.

4. Conclusion

Cadmium selenide (CdSe) semiconductor nanoparticles were synthesised in aqueous medium and phase transferred

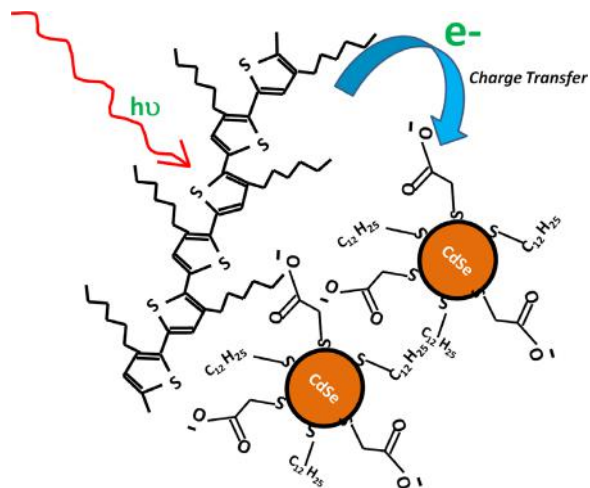


Fig. 8. Schematic diagram of interaction of CdSe nanoparticles with P3HT polymer.

into organic medium using 1-dodecanethiol. The UV–visible and photoluminescence results indicate effective blending of nanoparticles with the polymer. Luminescent quenching in P3HT with the addition of the nanoparticles confirms the effective charge transfer process at the polymer–nanoparticle interface. The morphology of the blends reveals the distribution of the nanoparticles in polymer. Detailed analysis of charge transfer and efficiency of PV process for the hybrid structure and the effect of ligand chain, solvent and annealing process are in progress.

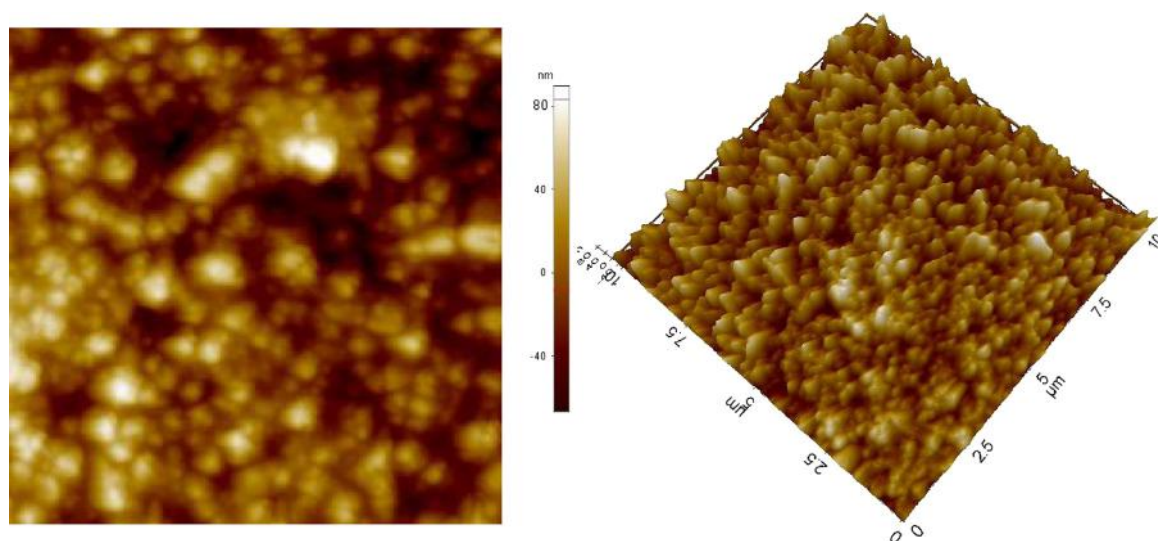


Fig. 9. AFM-TM (a) phase and (b) topography images of the CdSeNP-P3HT blends of the volume ratio 50:50 in chloroform. RMS=11.9 nm and the scan area is $10\ \mu\text{m} \times 10\ \mu\text{m}$.

Acknowledgements

The authors S. Ananthakumar and J. Ramkumar acknowledge Ministry of New and Renewable Energy (MNRE), India for providing Fellowship under National Renewable Energy Fellowship Scheme (NREF) for their doctoral studies. The authors sincerely thank UGC (F. No. 42-885/2013 (SR)) Government of India for funding the part of the investigation.

References

- [1] A. Nozik, *Physica E* 14 (2002) 115.
- [2] J.M. Luther, M. Law, Q. Song, C.L. Perkins, M.C. Beard, A. Nozik, *ACS Nano* 2 (2008) 271.
- [3] A.P. Alivisatos, *Science* 271 (1996) 933.
- [4] W. Huynh, J. Ditter, A.P. Alivisatos, *Science* 295 (2002) 2425.
- [5] S. Kumar, T. Naan, *J. Mater. Res.* 19 (7) (2004) 1990–1994.
- [6] Z. Fan, H. Zhang, W. Yu, Z. Xing, H. Wei, Q. Dong, W. Tian, B. Yang, *Appl. Mater. Interfaces* 3 (2011) 2919–2923.
- [7] L. Wang, Y. Liu, X. Jiang, D.H. Qin, Y. Cao, *J. Phys. Chem. C* 111 (2007) 9538–9542.
- [8] L.W. Ji, W.S. Shih, T.H. Fang, C.Z. Wu, S.M. Peng, T.H. Meen, *J. Mater. Sci.* 45 (2010) 3266–3269.
- [9] T.W. Zeng, Y.Y. Lin, H.H. Lo, C.W. Chen, C.H. Chen, S.C. Liou, H.Y. Huang, W.F. Su, *Nanotechnology* 17 (2006) 5387–5392.
- [10] J. Yang, A. Tang, R. Zhou, J. Xue, *Sol. Energy Mater. Sol. Cells* 95 (2011) 476–482.
- [11] I. Zarazua, E.D. Rosa, T.L. Luke, J.R. Gomez, S. Ruiz, C.A. Chavez, J.Z. Zhang, *J. Phys. Chem. C* 115 (2011) 23209–23220.
- [12] M. Brinkmann, D. Aldakov, F. Chandezon, *Adv. Mater.* 19 (2007) 3819–3823.
- [13] J. Albero, E.M. Ferrero, J. Ajuria, C. Waldauf, R. Pacios, E. Palomares, *Phys. Chem. Chem. Phys.* 11 (2009) 9644–9647.
- [14] D. Celik, M. Krueger, C. Veit, H.F. Schleiermacher, B. Zimmermann, S. Allard, I. Dumsch, F. Rauscher, P. Niyamakom, *Sol. Energy Mater. Sol. Cells* 98 (2012) 433–440.
- [15] D. Dorokhin, N. Tomczak, M. Han, D.N. Reinhoudt, A.H. Velders, G.J. Vancso, *ACS Nano* 3 (2009) 661–667.
- [16] D.A.G. Navarro, D.F. Watson, D.S. Aga, S. Banerjee, *Environ. Sci. Technol.* 43 (2009) 677–682.
- [17] B. Qin, Z. Zhao, R. Song, S. Shanbhag, Z. Tang, *Angew. Chem. Int. Ed.* 47 (2008) 9875–9878.
- [18] N. Gaponik, D.V. Talapin, A.L. Rogach, A. Eychmuller, H. Weller, *Nano Lett.* 2 (8) (2002) 803–806.
- [19] D.S. Koktysh, N. Gaponik, M. Reufer, J. Crewett, U. Scherf, A. Eychmuller, J.M. Lupton, A.L. Rogach, *Feldmaan, Chem. Phys. Chem.* 5 (2004) 1435–1438.
- [20] S. Gunes, H. Neugebauer, N.S. Sariciftci, J. Roither, M. Kovalenko, G. Pillwein, W. Heiss, *Adv. Funct. Mater.* 16 (2006) 1095–1099.
- [21] C. Yan, Z. Deng, F. Tang, L. Li, D. Chen, J. Ren, *Cryst. Eng. Commun.* 14 (2012) 3257–3263.
- [22] J. Ouyang, Y. Xia, *Sol. Energy Mater. Sol. Cells* 93 (2009) 1592.
- [23] K. Zhao, J. Dai, J. Zhuang, J. Li, W. Yang, *Colloids Surf. A: Physicochem. Eng. Asp.* 296 (2007) 154–157.
- [24] J. Aldana, N. Lavelle, Y. Wang, X. Peng, *J. Am. Chem. Soc.* 127 (2005) 2496–2504.
- [25] L. Zhao, X. Pang, R. Adhikary, J.W. Petrich, Z. Lin, *Angew. Chem. Int. Ed.* 50 (2011) 3958–3962.
- [26] M.D. Heinemann, K.V. Maydell, F. Zutz, J. Kolny Olesiak, H. Borchert, I. Riedel, J. Parisi, *Adv. Funct. Mater.* 19 (2009) 3788–3795.
- [27] N.T.N. Truong, W.K. Kim, C. Park, *Sol. Energy Mater. Sol. Cells* 95 (2011) 167–170.
- [28] W.U. Huynh, J.J. Dittmer, W.C. Libby, G.L. Whiting, A.P. Alivisatos, *Adv. Funct. Mater.* 13 (2003) 73–79.



Facile synthesis and transformation of Te nanorods to CdTe nanoparticles



S. Ananthakumar, J. Ramkumar, S. Moorthy Babu*

Crystal Growth Centre, Anna University, Chennai 600025, India

ARTICLE INFO

Available online 25 June 2014

keywords:

CdTe nanoparticles
Tellurium nanorods
Thioglycolic acid

ABSTRACT

Luminescent cadmium telluride nanoparticles were synthesized from the reaction intermediate tellurium nanorods as tellurium source at 100 °C through colloidal approach. Oxyanion source of tellurium, (i.e.) potassium tellurite (K_2TeO_3) was used as precursor to synthesize the tellurium nanorods under the low temperature process without any surfactant in various volumes of water. Thioglycolic acid (TGA) was employed as capping agent for the synthesis of CdTe nanoparticles. Absorption and emission spectra of the prepared nanoparticles clearly indicate the size dependent nature of the particles. SEM and EDX analyses of the nanorods reveal the shape of the synthesized nanorods and the presence of elemental tellurium without any impurities. XRD analysis of the prepared samples confirms the existence of trigonal phase of tellurium nanorods (t-Te) and the formation of CdTe particles with cubic zincblende structure. The size distribution of the prepared CdTe nanoparticles was analyzed through TEM analysis. It was found that considerable influence of solvent on morphology of the synthesized tellurium nanorods. The synthesis mechanism of one dimensional structure as seeds for zero dimensional nanoparticles was analyzed.

© 2014 Elsevier Ltd. All rights reserved.

1. Introduction

Fluorescent semiconductor nanoparticles are widely used in many fields such as optoelectronics, bio-imaging, finger print detection and LED device applications due to their size tunable nature [1,2]. Enhanced light harvesting of semiconductor nanoparticles sensitized photo-electrodes was also widely studied for solar cells [3,4]. The quantum confinement effect makes these nanoparticles towards engineering for such applications. Cadmium telluride (CdTe) because of the direct bandgap has attracted considerable attention in many device applications. Numerous attempts were made to synthesize CdTe nanoparticles with a suitable method. After the successful synthesis of

semiconductor nanoparticles in an aqueous system, lot of interest was focussed on the synthesis of CdTe nanoparticles in aqueous medium due to the usage of simple precursors like K_2TeO_3 [5], and simple experimental arrangements. Moreover, the aqueous based approach of synthesizing CdTe nanocrystals was best proven for the active layer formation in hybrid solar cells with the water soluble semiconducting polymers [6]. The optical properties of the aqueous synthesized CdTe nanoparticles have shown mostly similar kind of phenomena as like organometallic based one. The enhancement of the photoluminescence was observed when tellurium nanorods are used instead of bulk tellurium powder as source in the case of CdTe nanoparticles synthesized through a hydrothermal method at higher temperature [7]. The nano-tellurium has the ability to form Te^{2-} reactive species much easier than the bulk Te powder in alkaline solution. Moreover, Tellurium, a p-type narrow bandgap semiconductor ($E_g=0.35$ eV), is

* Corresponding author. Tel.: +91 44 22358333; fax: +91 44 2235 2774.
E-mail addresses: babu@annauniv.edu,
babusm@yahoo.com (S. Moorthy Babu).

used for many applications including thermoelectrics, non-linear infra red optics, photodetectors, photovoltaics, gas-sensing materials, data-storage devices and bio-labels [8]. Further, nano-tellurium is used as attractive template for the synthesis of metal chalcogenide nanoparticles [9–11]. Hence, synthesis of tellurium nanostructures received considerable interest and was reported using many methods including solvothermal, ultrasonic induced growth, and surfactant assisted method, hydrothermal methods with Te powder or TeO_2 as source [12–15]. Mo et al. [16] have reported the insitu synthesis and formation of Te nanotubes and nanobelts through Na_2TeO_3 under alkaline conditions at high temperature. Further, since the alkali metal tellurites (X_2TeO_3 where $\text{X}=\text{K}, \text{Na}$) are water soluble in nature, the formation of tellurium nanostructures in water with the surfactant has also been widely studied [17–19]. The interesting formation of In_2Te_3 nanosheets from tellurium nanorods in the presence of alkaline solvent was also reported recently [20]. Synthesizing trigonal nanotellurium structures using these methods are the desired one for optoelectronic device applications. Synthesis of one dimensional nanostructure was carried out widely using wet chemical methods. Recently, the aqueous synthesis of ZnSe nanoparticles through the intermediate nanoselenium has been reported [21]. Present work, highlights the aqueous synthesis of luminescent CdTe nanoparticles capped by a short chain thiol ligand (thioglycolic acid) using the tellurium nanorods as tellurium source. The tellurium nanorods were obtained by reducing the oxyanion source of tellurium, (i.e.) potassium tellurite (K_2TeO_3) in aqueous medium at low temperature using a strong reducing agent in the absence of surfactant. The proposed synthesis process is simple and reproducible one compared with other methods.

2. Experimental details

2.1. Synthesis of tellurium nanorods

Precursors in the form of cadmium chloride (CdCl_2) SRL (97%), potassium tellurite (K_2TeO_3) CDH (99%), thioglycolic acid ($\text{C}_2\text{H}_4\text{O}_2\text{S}$) SPECTROCHEM (95%), sodium borohydride (NaBH_4) MERCK (95%), sodium hydroxide (NaOH) SRL (98%), and trisodium citrate dihydrate ($\text{C}_6\text{H}_9\text{Na}_3\text{O}_9$) SRL (99%), were used for the synthesis of tellurium nanorods as well as CdTe nanoparticles.

Synthesis of tellurium nanostructures was performed using the method similar to the Gautham and Rao [12] without utilizing any surfactants. Briefly, potassium tellurite (1 mM) was taken in a three necked flask with 100 ml of water, then, excessive amount of the sodium borohydride (ratio1:10) was added into the solution. The mixture was immediately turned to black and the resultant solution was refluxed strongly at the temperature of 60°C under the nitrogen atmosphere until the solution colour turned into light pink. Then, the solution was kept under dark for two days without any disturbance. The resultant black precipitate was filtered off and washed with water three times. The final precipitate was dried in vacuum. The experiment was repeated for the 50 ml, 25 ml volume of the water by keeping the ratio of potassium tellurite and sodium borohydride as constant.

2.2. Synthesis of CdTe nanoparticles

Cadmium chloride (1 mM) was dissolved in 100 ml water and thioglycolic acid (5 mM) was added in drop wise and the resultant mixture was stirred. The resultant turbidity appearance of the mixture indicates the formation of the cadmium-TGA complex which turned into clear transparent one, when pH was maintained as 10.5 using 1 M NaOH solution. Then tri sodium citrate dihydrate was added with this mixture to avoid the formation of cadmium tellurite (CdTeO_3) in the solution [22]. The entire solution was purged with nitrogen in a three necked flask. Then the tellurium nanorods were added simultaneously as tellurium source in the presence of excessive sodium borohydride. The molar ratio of Cd^{2+} : Te^{2-} : TGA for this entire synthesis process is 1:0.5:5. Now, the mixture was strongly heated to 100°C . The colour of the initial solution was observed as yellow and then converted to orange after prolonged refluxing. Aliquot samples were taken at different time intervals and the size dependency was checked through absorption and emission spectra. The synthesized particles were precipitated by adding the non-solvent iso-propanol and centrifuged. The resultant precipitate was washed twice using ethanol to remove the excess of surface ligand and by-products and then dried in vacuum for further analysis.

2.3. Characterization

Absorption spectra were analyzed using a ELICO SL-159 UV-visible conventional spectrophotometer in the range of 200–800 nm. The samples were taken as liquid in quartz cuvette and diluted using water for the analysis. Fluorescence analyses were carried out for the samples using a JASCO FP-6300 spectrofluorometer at the excitation wavelength 420 nm. The excitation was done using xenon lamp source. The samples were used as liquid form in quartz cuvette. SEM images were recorded using the Carl Zeiss MA15/EVO 18 Scanning Electron Microscope. In order to avoid the charging effect, gold/palladium alloy was coated on samples for SEM analysis. XRD patterns were taken using a powder X-ray diffractometer (SEI FERT)

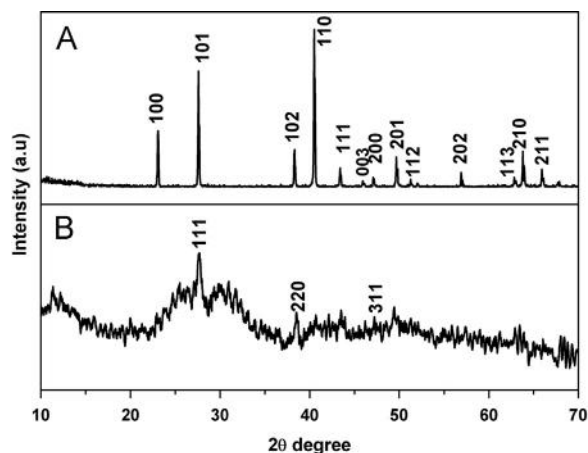


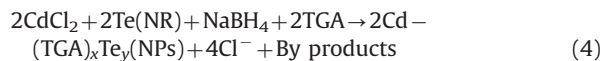
Fig. 1. XRD pattern of (a) Te nanorods and (b) CdTe nanoparticles.

JSO DEBYEFLEX 2002 model with $\text{CuK}\alpha_1$ ($\lambda=0.154$ nm) radiation. The accelerating voltage and the applied current were 40 kV and 30 mA respectively. TEM images were observed with an electron microscope (Tecnai G2 model T-30 s-twin) using an accelerating voltage of 300 kV. The colloidal nanoparticles solution was allowed to dry on the copper grid before analysis.

3. Results and discussion

3.1. Structural analysis

Powder XRD pattern of Te nanorods and CdTe nanoparticles are as shown in Fig. 1. Fig. 1(a) shows the trigonal phase of tellurium (t-Te) nanorods [JCPDS no: 36-1452] and high intensity of the (100), (110) and (200) peaks denotes the preferential growth of the one dimensional tellurium nanostructures along the (001) direction under the prolonged ageing time [23]. Fig. 1(b) depicts the XRD pattern of the as synthesized CdTe nanoparticles. The broad diffractive peaks of CdTe nanoparticles confirm the nanodimension of the particles. The characteristic peaks of the particles (111), (220), (311) indicate cubic zinblende structure [JCPDS no:65-8367]. The size of the particles was calculated using the Scherrer formula, $\tau=0.9 \lambda/\beta \cos\theta$ where τ =shape factor; λ =X-ray wavelength used for the measurement; β =line width (FWHM) in radians, and θ =Bragg angle. Using the above formula, the crystallite size of the CdTe nanoparticles was calculated based on the peak due to [111] as about 1.9 nm which is approximately consistent with the TEM analysis. There were no impurity peaks observed in both cases. Fig. 2 presents the schematic diagram for the formation of CdTe nanoparticles from the tellurium nanorods. The overall reaction route for the formation of t-tellurium nanorods and the conversion of tellurium nanorods to cadmium telluride nanoparticles can be summarized as:



3.2. Morphological analysis

The SEM images of the as prepared nanorods are as shown in Fig. 3. All the rods are uniform in shape and have diameter around 100 nm and length around 1 μm approximately. Due to strong anisotropic crystal structure exists in tellurium, the nanorod like morphology is favourable under the reducing conditions [24]. Initially when the tellurite source was heated strongly with reducing agent, it forms the t-Te sphere like particles which makes the free tellurium atoms in the solution. This further transfers onto the surface of the particles which direct the intrinsic tendency and lead to these nanorods because of this anisotropy [25]. When tellurite source was heated with reducing agent NaBH_4 it forms the pink coloured solution under the nitrogen atmosphere and when it was exposed to air, an instantaneous and strong oxidation of Te^{2-} ions happen with a black coloured product of nano-tellurium on the surface of the solution. Compared with selenium it was observed that this effect was faster in tellurium with sodium borohydride. This may be due to high negative value of the reduction potential of telluride (Te^{2-}) ions than selenide (Se^{2-}) in solution [26]. The intensity of the black coloured product was much higher after it was allowed for ageing for a day. Clear colourless solution was observed after the formation of black coloured product on top. Various ratios of water and NaBH_4 with 0.1 M of K_2TeO_3 were done for the synthesis of tellurium nanorods. There was no dimensional change observed in all cases. The increasing diameter of the nanorods were observed when the water content of the synthesis medium got reduced. When the water content was 100, 50 ml, very fine nanorods were obtained. For 100 ml water, the diameter of the nanorods was around 60–100 nm (Fig. 3(a and b)) and it was 300–500 nm for the 50 ml water (Fig. 3(c-e)). When the water content was reduced

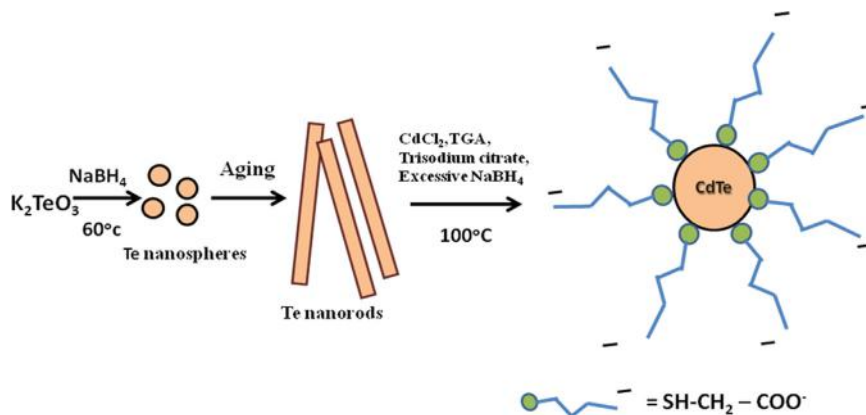


Fig. 2. Schematic representation of formation of CdTe nanoparticles from tellurium nanorods.

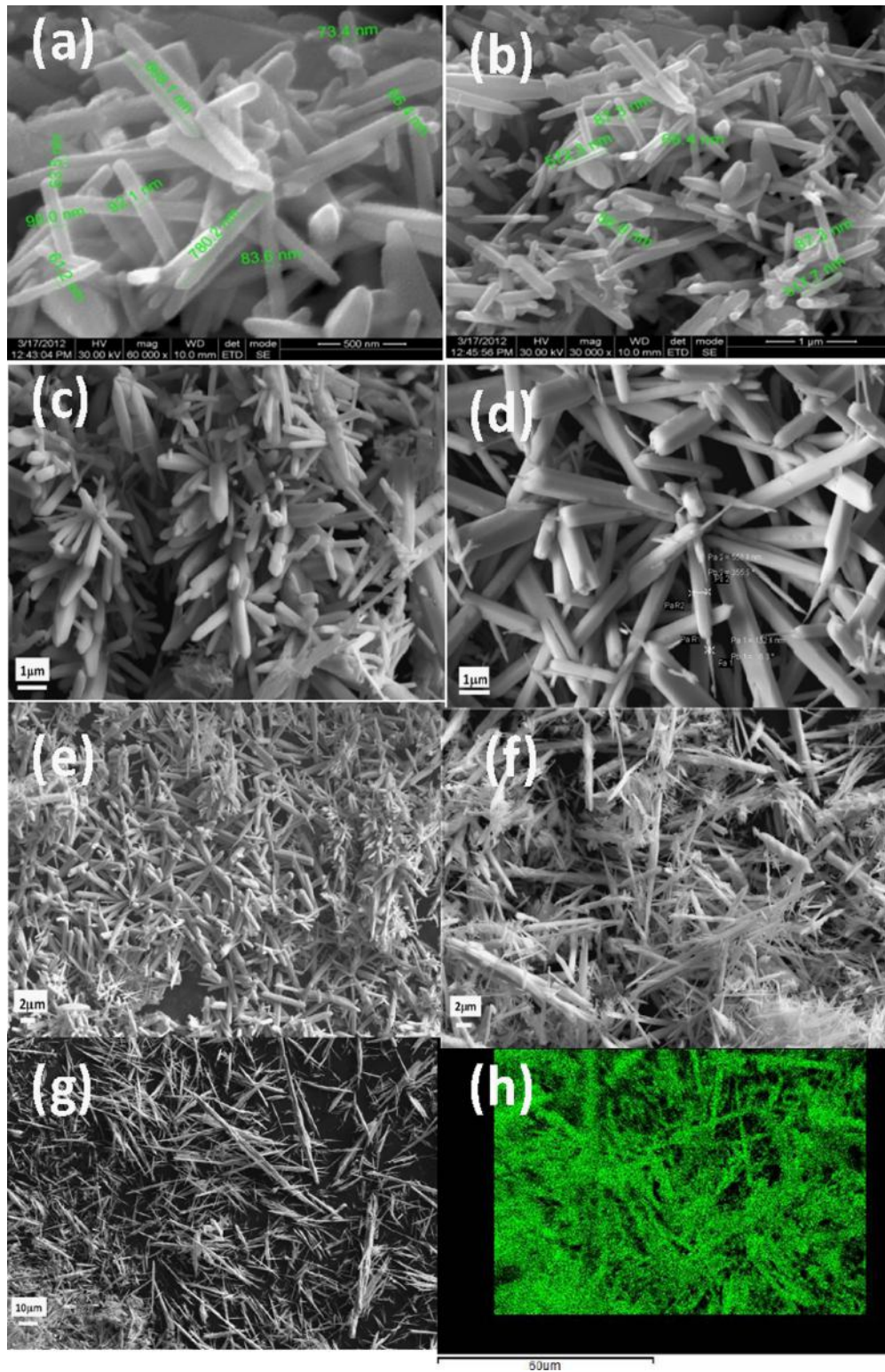


Fig. 3. SEM images of the tellurium nanorods prepared under 10 mM of NaBH_4 with 0.1 M K_2TeO_3 in (a, b) 100 ml water (c–e) 50 ml water (f, g) 25 ml water and the EDS mapping of obtained Tellurium (Te) nanorods (h).

to 25 ml, irregular nano-needle like morphology was obtained instead of nanorods (Fig. 3(f and g), which clearly indicates the influence of solvent (water) on the structural

evolution of the nanorods. Elemental distribution from EDS mapping analysis of tellurium nanorods in Fig. 3(h) confirms the well distribution of tellurium. When these

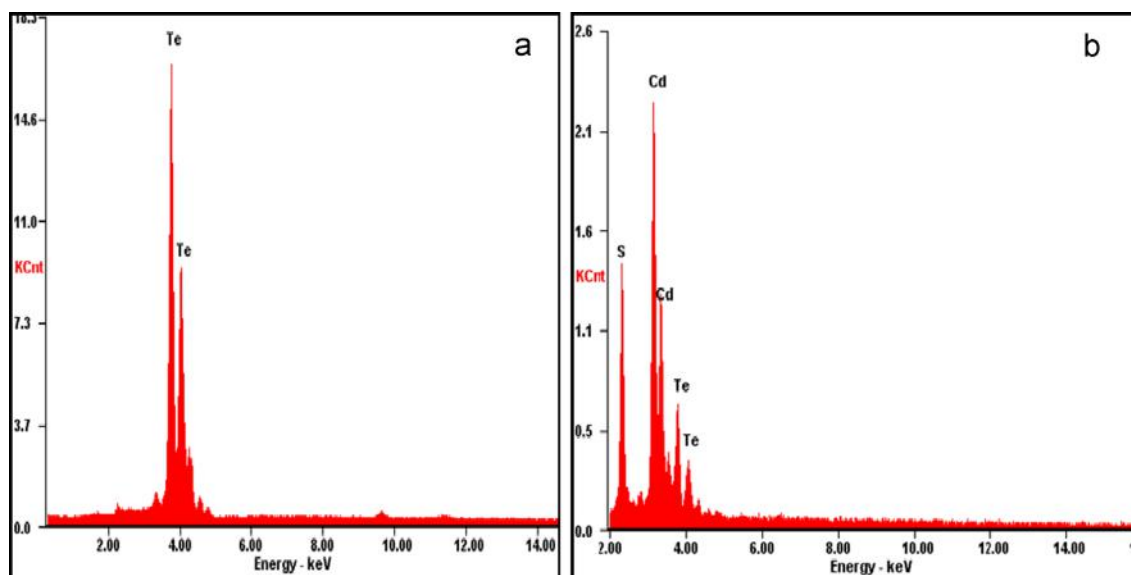


Fig. 4. EDX spectra of the (a) Te nanorods and (b) CdTe nanoparticles.

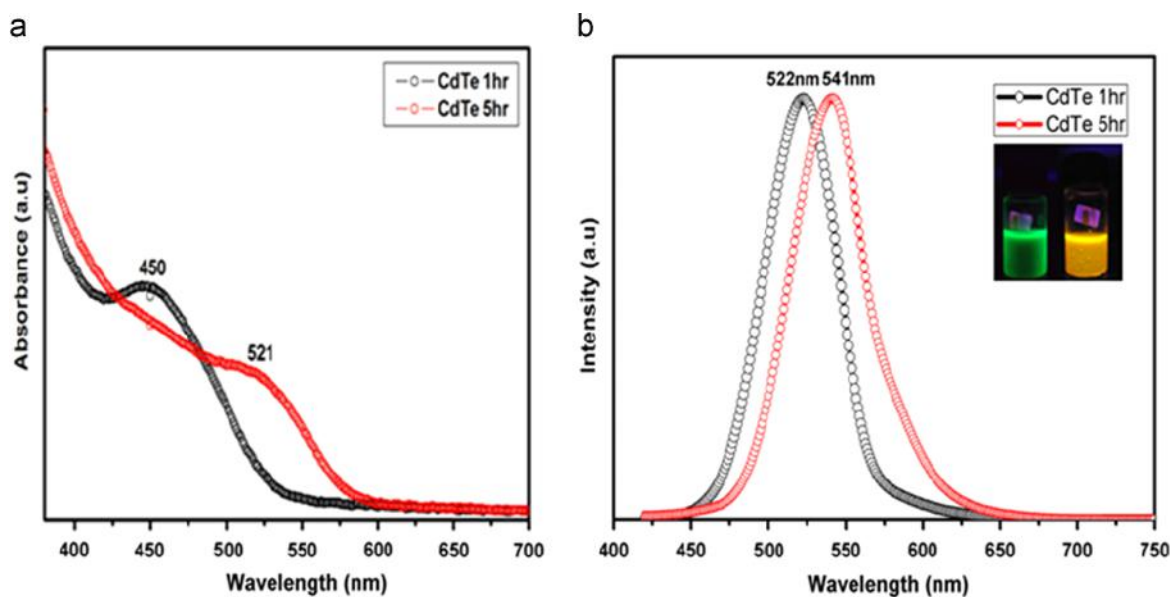


Fig. 5. (a) Absorption and (b) emission spectra of the synthesized CdTe nanoparticles at different refluxing times ($\lambda_{\text{ex}}=420$ nm). Inset shows the fluorescence image of the particles under UV light (365 nm).

nanorods are used as tellurium source in the presence of the reducing agent, acceleration of the reaction was observed with cadmium-TGA complex and forms the spherical cadmium telluride nanoparticles. The overall formation process of CdTe nanoparticles from tellurium nanorods is schematically shown in Fig. 2. Moreover, the Te^{2-} which forms as insitu reduction reacts very efficiently to bind with Cd^{2+} ion and form the CdTe particles. The excessive amount of the reducing agent sodium borohydride protects the Te^{2-} ions in solution very effectively by making the inert atmosphere around it [22] and CdTe nanoparticles with very good luminescence were obtained. These particles are well capped by the thioglycolic acid

ligand through the sulphur atom on the surface and make it as negatively charged one due to the carboxylate end.

3.3. Elemental analysis

The energy dispersive X-ray (EDX) spectra are shown in Fig. 4. Fig. 4(a) confirms the composition of the tellurium nanorods as pure elemental tellurium without any impurities. Fig. 4(b) presents the EDX spectrum of CdTe nanoparticles with Cd, Te along with sulphur. The presence of sulphur in the spectrum may be due to the incorporation of the sulphur from the capping agent thioglycolic acid (TGA). The inclusion of the sulphur was a common

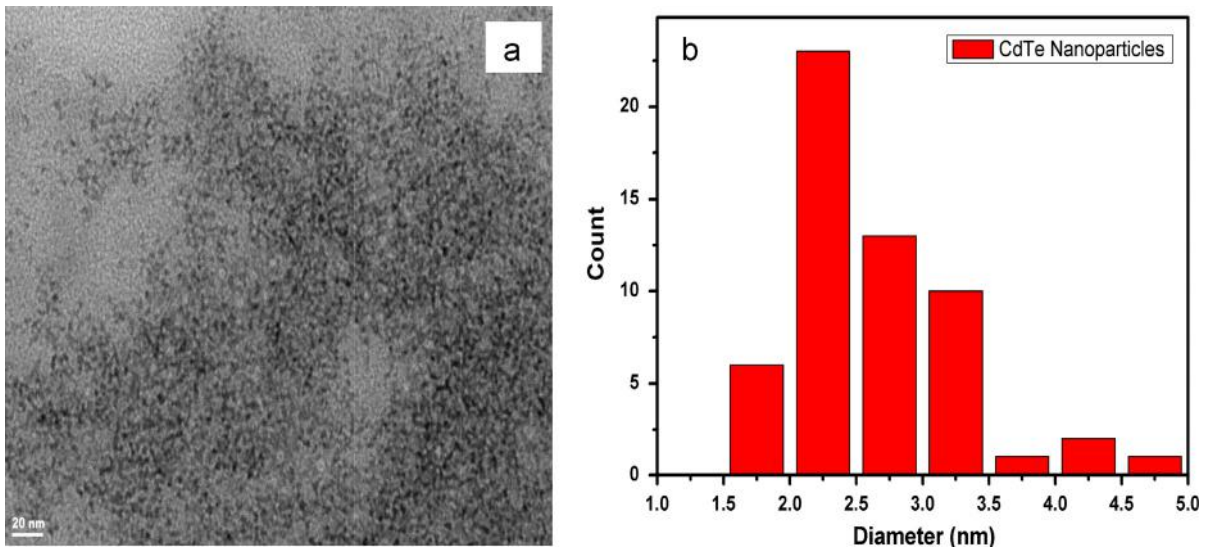


Fig. 6. (a) TEM image of the synthesized CdTe nanoparticles at 1 h and (b) size histogram of the particles.

phenomenon observed when the nanoparticles are refluxed at high temperature.

3.4. Optical analysis

UV–visible spectra of the synthesized CdTe nanoparticles are shown in Fig. 5(a). The spectra clearly indicate that the prepared samples possess very good size dependent properties. The absorption edge of the two samples increases from 450 to 521 nm. The first excitonic peak in the absorption spectra of the two samples which were refluxed at two different time intervals represents the red-shift of the particles for the tunable bandgap properties. Due to the Ostwald ripening in solution, the smaller particles are exploited by the bigger one and growth occurred. The optical bandgap of the synthesized particles were calculated from the wavelength of the absorption spectrum edge using the formula $E_g = hc/\lambda$ where h = Plank's constant; c = velocity of light and λ = wavelength of the absorption peak edge. The obtained bandgap is 2.76 eV and 2.38 eV for 1 h and 5 h refluxed samples, respectively. The resultant bandgap for both samples is very large one compared with the bulk CdTe ($E_g = 1.5$ eV). This clearly confirms the presence of strong quantum confinement in the particles due to size reduction. The size dependent bandgap energy shift of the particles calculated based on the strong confinement model of a spherical quantum dot using the following relation [27]:

$$\Delta E = E - E_g + E^*R_y$$

$$= \frac{\hbar^2 \pi^2}{2\mu R^2} - \frac{1.786e^2}{\epsilon R} + 0.752E^*R_y$$

where $E_g = 1.606$ eV is the band-gap energy, R is the radius of the dot, $\mu = 0.0774m_0$ is the reduced mass of an electron mass $m^*e = 0.096m_0$ and a hole mass $m^*h = 0.4m_0$, $\epsilon = 7.1$ is the dielectric constant and $E^*R_y = 10$ meV is Rydberg energy. The calculated energy shift for the 1 h refluxing sample was

found to be about 0.75 eV. The fluorescence spectra of the CdTe nanoparticles are shown in Fig. 5(b). The emission wavelength was observed as gradually red-shifted and increased from 522 to 541 nm for 1 h and 5 h refluxed particles. The increasing wavelength resulting from the increasing refluxing time clearly indicates that the size of the particles increases with the refluxing time. There was no trap state emission, which clearly explores that the particles are effectively passivated by the ligand thioglycolic acid.

3.5. TEM analysis

The TEM image of the 1 h refluxed particles is shown in Fig. 6(a). The particles are spherical in shape with crystal-line structure and also have a good monodispersability. The average size of the particles was found to be 2.25 nm through size distribution histogram (Fig. 6(b)). The capping ligand thioglycolic acid makes the electrostatic interaction on the surface of the CdTe nanoparticles and stabilizes the resultant nanoparticles.

4. Conclusion

Highly luminescent CdTe nanoparticles were synthesized successfully using Te nanorods obtained from potassium tellurite as the tellurium source through simple wet chemical approach. The prepared nano-particles possess high crystallinity and good optical properties. The sizes of the particles were found consistent for TEM and XRD analyses. The one dimensional structure of tellurium motivates the zero dimensional growth of the CdTe nanoparticles. The synthesized nanoparticles were spherical in shape and have very good fluorescence. These nanoparticles with water soluble semiconducting polymers can be used in hybrid solar cells as active layer and also for bio labelling with a coating of biocompatible layer around it.

Acknowledgements

The authors sincerely thank UGC- (F.No. 42-885/2013 (SR)), Govt. of India for funding the research. S. Ananthakumar and J. Ramkumar sincerely thanks Ministry of New and Renewable Energy (MNRE), Govt. of India for providing fellowship under National Renewable Energy Fellowship (NREF) (Grant no. NREF/TU/2011/11) scheme for the doctoral studies.

References

- [1] N. Gaponik, D.V. Talapin, A.L. Rogach, K. Hoppe, E.V. Shevchenko, A. Kornowski, A. Eychmuller, H. Weller, *J. Phys. Chem. B* 106 (2002) 7177–7185.
- [2] J. Liu, Z. Shi, Y. Yu, R. Yang, S. Zuo, *J. Colloid Interface Sci.* 342 (2010) 278–282.
- [3] M.K. Son, H. Seo, I. Shin, J.K. Kim, J. Choi, K. Prabakar, H.J. Kim, *Curr. Appl. Phys.* 11 (2011) S154–S157.
- [4] X.F. Gao, H.B. Li, W.T. Sun, Q. Chen, F.Q. Tang, L.M. Peng, *J. Phys. Chem. C* 113 (2009) 7531–7753.
- [5] M.S. Abd El-Sadek, J.R. Kumar, S.M. Babu, *Curr. Appl. Phys.* 10 (2010) 317–322.
- [6] Z. Fan, H. Zhang, W. Yu, Z. Xing, H. Wei, Q. Dong, W. Tian, B. Yang, *Appl. Mater. Interfaces* 3 (2011) 2919–2923.
- [7] R. Zheng, S. Guo, S. Dong, *Inorg. Chem.* 46 (2007) 6920–6923.
- [8] L. Yang, Z.G. Chen, G. Han, L. Cheng, H. Xu, J. Zou, *Cryst. Growth Des.* 13 (2013) 4796–4802.
- [9] X. Chen, T.J. Zhu, X.B. Zhao, *J. Cryst. Growth* 311 (2009) 3179–3183.
- [10] G.D. Lilly, Y. Chen, X. Pan, N.A. Kotov, *J. Phys. Chem. C* 114 (2010) 2428–2433.
- [11] H. Fan, Y. Zhang, M. Zhang, X. Wang, Y. Qian, *Cryst. Growth Des.* 8 (2008) 2838–2841.
- [12] U.K. Gautam, C.N.R. Rao, *J. Mater. Chem.* 14 (2004) 2530–2535.
- [13] B. Zhou, J.R. Zhang, L. Zhao, J.M. Zhu, J.J. Zhu, *Ultrason. Sonochem.* 13 (2006) 352–359.
- [14] J. Li, J. Zhang, Y. Qian, *Solid State Sci.* 10 (2008) 1549–1555.
- [15] G. Xi, Y. Peng, W. Yu, Y. Qian, *Cryst. Growth Des.* 5 (1) (2005) 325–328.
- [16] M. Mo, J. Zeng, X. Liu, W. Yu, S. Zhang, Y. Qian, *Adv. Mater.* 14 (22) (2002) 1658–1662.
- [17] X. Wu, Y. Wang, S. Zhou, X.Y. Yuan, T. Gao, K. Wang, S. Lou, Y. Liu, X. Shi, *Cryst. Growth Des.* 13 (2013) 136–142.
- [18] H. Gong, X. Hao, Y. Wu, B. Cao, H. Xu, X. Xu, *J. Solid State Chem.* 184 (2011) 3269–3272.
- [19] G. Li, X. Cui, C. Tan, N. Lin, *RSC Adv.* 4 (2014) 954.
- [20] M. Safdar, Z. Wang, M. Mirza, F.K. Butt, Y. Wang, L. Sun, J. He, *J. Mater. Chem. A* 1 (2013) 1427–1432.
- [21] H. Qin, W. Jian, Y. Zhang, T. Kim, Z. Jiang, D. Jiang, D. Sun, *Mater. Lett.* 67 (2012) 28–31.
- [22] H. Bao, E. Wang, S. Dong, *Small* 2 (4) (2006) 476–480.
- [23] B. Mayers, B. Gates, Y. Yin, Y.N. Xia, *Adv. Mater.* 13 (2001) 1380–1384.
- [24] G. Xi, Y. Peng, W. Yu, Y. Qian, *Cryst. Growth Des.* 5 (1) (2005) 325–328.
- [25] Z. Tang, Y. Wang, K. Sun, N.A. Kotov, *Adv. Mater.* 17 (3) (2005) 358–363.
- [26] W. Lu, Y. Ding, Y. Chen, Y. Chen, Z.L. Wang, J. Fang, *J. Am. Chem. Soc.* 127 (2005) 10112–10116.
- [27] Y. Masumoto, K. Sonobe, *Phys. Rev. B* 56 (15) (1997) 9734–9737.

Size-independent peak shift between normal and upconversion photoluminescence in MPA-capped CdTe nanoparticles

S ANANTHAKUMAR¹, J JAYABALAN^{2,*}, ASHA SINGH²,
SALAHUDDIN KHAN², SUBHASH PRAJAPATI², S MOORTHY BABU¹
and RAMA CHARI²

¹Crystal Growth Centre, Anna University, Chennai 600 025, India

²Laser Physics Applications Section, Raja Ramanna Centre for Advanced Technology,
Indore 452 013, India

*Corresponding author. E-mail: jjaya@rrcat.gov.in

DOI: 10.1007/s12043-014-0689-6; **ePublication:** 12 February 2014

Abstract. In this article, we report size-dependent measurement of the shift in peak of upconversion photoluminescence spectra compared to that of normal photoluminescence using a 800 nm femtosecond laser and its second harmonic. It has been shown that the upconversion photoluminescence is always red-shifted compared to that of normal PL in all the samples. By measuring the power-dependent upconversion photoluminescence (UCPL), it has been shown that the origin of UCPL from MPA-capped CdTe nanoparticles is mainly of two-photon absorption

Keywords. Upconversion photoluminescence; CdTe nanoparticles; femtosecond laser.

PACS Nos 64.70.pv; 76.67.Bf; 78.47.J–; 78.67.Hc; 82.53.Mj

1. Introduction

Unlike bulk semiconductors, the light absorbing and emitting properties of semiconductor nanoparticles can be tuned in a wide spectral range by varying their sizes [1]. Such tunability in the optical properties make semiconductor nanoparticles a potential candidate for applications as emitters (light emitting diodes and lasers), light harvesters (photodiodes and solar cells) and as biological labels [2–5]. In addition to their linear optical properties, semiconductor nanoparticles have large nonlinearities making them efficient nonlinear absorbers of light. Similar to the case of linear absorption, the light absorbed by the semiconductor nanoparticles through the nonlinear process is also emitted as photoluminescence [5,6]. Thus, in the case of upconversion photoluminescence (UCPL) the emitted photon has larger energy than the input photon. For the past few years, studies

are being carried out on the UCPL in semiconductor nanoparticles like CdTe, CdSe and CdS [5–7]. The UCPL peak wavelength has been found to be red-shifted compared to that of normal PL [5,6]. The origin of such difference between the peak wavelength of UCPL and normal PL is still under study. In this article, we report a comparative study of the UCPL emission (when excited at 800 nm) with that of the normal PL emission (when excited at 400 nm) for different sizes of MPA-capped CdTe nanoparticles. We show that the UCPL in MPA-capped CdTe nanoparticles is induced by two-photon absorption. The origin of shift between the UCPL and PL is also discussed.

The MPA-capped CdTe nanoparticles were prepared by the following procedure. Cadmium chloride (CdCl_2) (1 mM) was dissolved in 150 ml water and 3-mercaptopropionic acid ($\text{C}_3\text{H}_6\text{O}_2\text{S}$) (5 mM) was added with it in drops, under vigorous stirring condition. The white turbid coloured solution immediately turned into a clear solution when the pH of the solution was adjusted to 11.2 by 1 M sodium hydroxide (NaOH). Following this, a measured amount of sodium citrate tribasic dihydrate ($\text{C}_6\text{H}_5\text{Na}_3\text{O}_7 \cdot 2\text{H}_2\text{O}$) was added to the solution. The entire solution was kept under nitrogen atmosphere in a three-necked flask system. Then, potassium tellurite (K_2TeO_3) (0.5 mM) solution reduced by excessive sodium borohydride (NaBH_4) was injected into it and the entire solution was heated to 100°C . The immediate appearance of yellow colour indicated the formation of CdTe cores in the solution. The colour of the solution was changed after strong refluxing. Aliquots of the samples were taken at different time intervals to study the properties of the prepared CdTe nanoparticles.

Figure 1 shows the linear absorption spectra of the MPA-capped CdTe nanoparticles prepared at different reflux times (3 h, 5 h, 12 h and 18 h). The average sizes of the nanoparticles can be estimated from the measured linear absorption coefficients by considering the size-dependent quantum confinement effects. We estimate the average size of nanoparticles to be 2.4 nm, 3.0 nm, 3.3 nm and 3.7 nm for the samples CdTe-530, CdTe-561, CdTe-603 and CdTe-646, respectively.

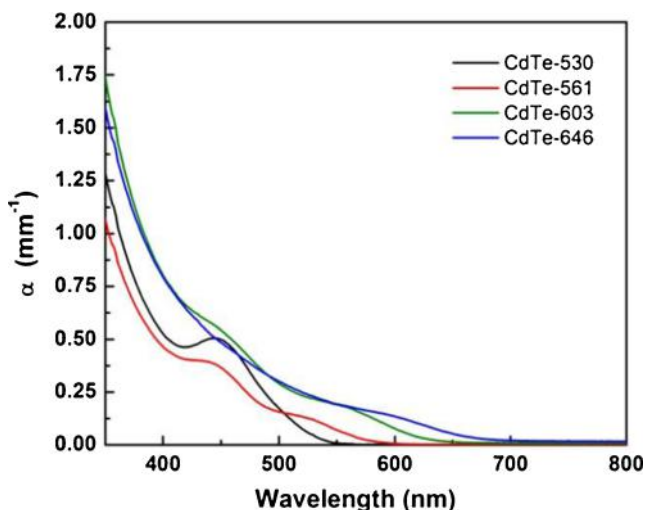


Figure 1. The wavelength dependence of the linear absorption coefficient of MPA-capped CdTe nanoparticles prepared at different reflux times.

Size-independent peak shift

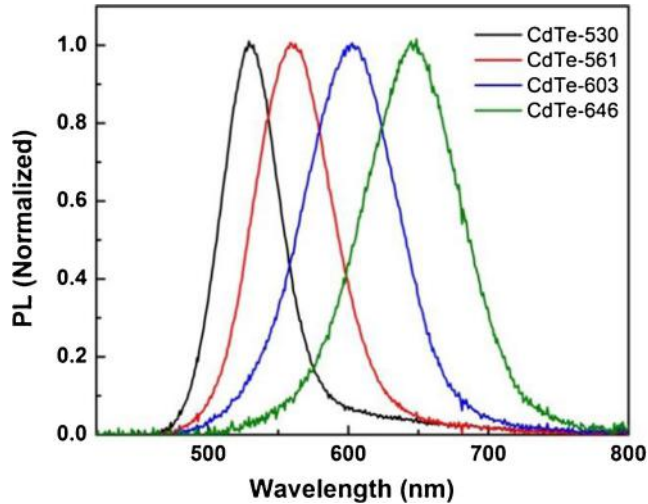


Figure 2. The photoluminescence spectra of CdTe nanoparticles of different sizes. The wavelength of the pump laser is 400 nm.

CdTe-561, CdTe-603 and CdTe-646 respectively [8,9]. Note that in all the cases the sample has very low absorption at 800 nm and very large absorption at 400 nm.

Figure 2 shows the measured photoluminescence spectra of the CdTe nanoparticles when excited at ~ 400 nm. The 400 nm pump was generated from 100 fs, 800 nm wavelength, Ti-sapphire laser operating at 82 MHz by second harmonic generation. Note that as the size of the particles increase, the peak wavelength of the PL red-shifts, which is consistent with earlier reports [1]. In figure 3, we show the UCPL of the samples when

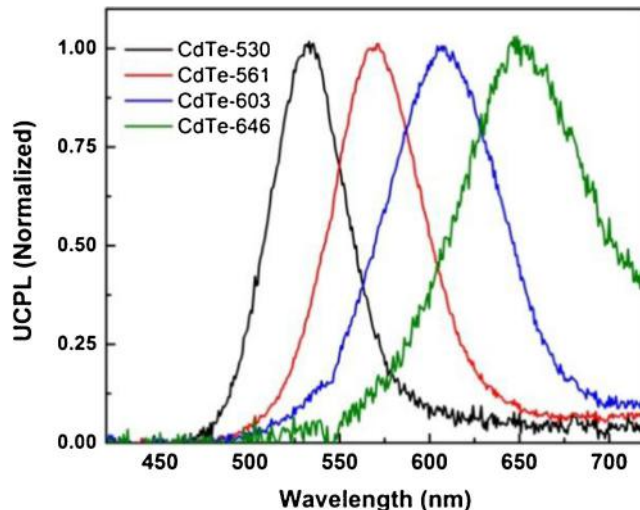


Figure 3. The UCPL spectra of CdTe nanoparticles of different sizes excited at 800 nm.

excited directly by the femtosecond laser at 800 nm wavelength. Similar to the above-mentioned normal PL, the peak wavelength of UCPL red-shifts with the increase in size of the particles. Before discussing the origin of shift in the PL peaks, we look at the input power dependence of PL emission in both of these cases.

In the case of CdTe nanoparticles, the output power of upconversion photoluminescence has been reported to depend linearly on the input power while in some other cases quadratic dependence has also been observed [5,10,11]. In order to understand the origin of the UCPL in our case, we have measured the pump energy dependence of UCPL emission. Figure 4 shows the input power dependence of UCPL when pumped at 800 nm for the sample CdTe-530 at its peak emission, 533 nm. Clearly, the increase in UCPL is not linear with the input intensity. By fitting a simple power-dependent function, I^p , to the variation of output UCPL with the input power (I), we find the value of p to be 1.8. For comparison, we have also measured the power dependence of PL emission when pumped at 400 nm and is shown in figure 5. The linear dependence of the peak PL emission on pump power shows that it is originating from linear absorption. Thus, we attribute the origin of UCPL in the present case to two-photon absorption.

In figure 6 we plot the photoluminescence peak wavelengths of the normal PL and UCPL (obtained from figures 2 and 3). The peak wavelength of UCPL is always red-shifted compared to that of the normal PL. This result shows that the direction of the peak shift is independent of the size of the CdTe nanoparticles. As mentioned before, the difference between the peak wavelength of normal PL and UCPL is attributed to several different processes involving electronic surface states, hole surface states, phonons, size and trap states dependence of two-photon absorption coefficients in CdTe nanoparticles. In the present case, since the origin of UCPL is two-photon absorption, we attribute the shift observed in the UCPL compared to PL to the size dependence of two-photon absorption coefficient of CdTe nanoparticles. It has been shown that the TPA coefficient of CdTe

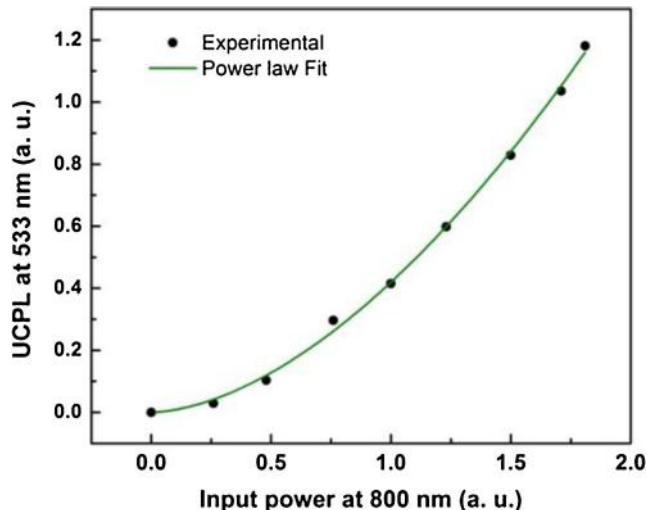


Figure 4. 800 nm pump power dependence of UCPL peak emission for the sample CdTe-530.

Size-independent peak shift

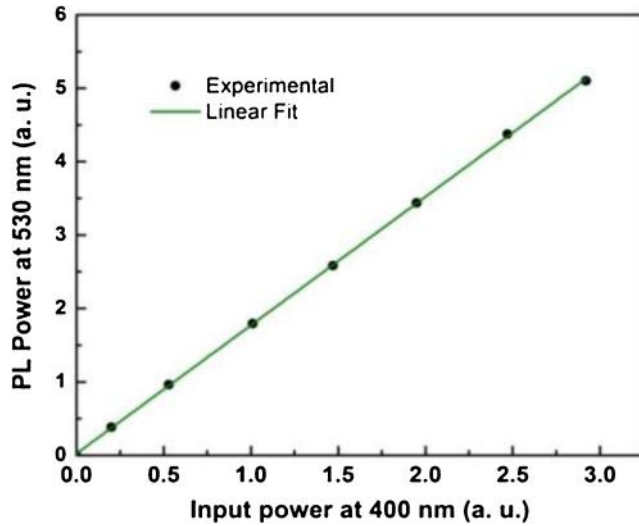


Figure 5. 400 nm pump power dependence of PL peak emission for the sample CdTe-530.

nanoparticles depends strongly on the size of the nanoparticles and increases with increase in particle size [12]. Thus, in a given distribution of size of the nanoparticles around an average value, the larger particles will have a higher two-photon absorption leading to a red-shifted UCPL emission. However, since the variation in the peak shift with the size of the particle is not uniform, we believe a contribution from trap states dependent TPA may also play a role in the observed peak shift.

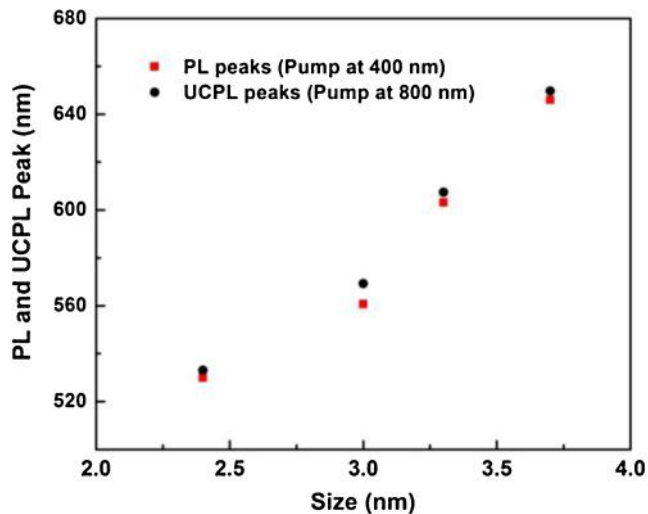


Figure 6. The variation of peak wavelengths of the normal PL and UCPL with size of the CdTe particles.

2. Conclusion

We have measured upconversion photoluminescence from MPA-capped CdTe nanoparticles of different sizes. It has been shown that the UCPL is always red-shifted compared to that of normal PL in all the samples. By measuring the power-dependent UCPL, it has been shown that the origin of UCPL from MPA-capped CdTe nanoparticles is mainly of two-photon absorption.

Acknowledgements

The authors acknowledge the support and encouragement of Dr H S Rawat, Head, LPAS during the course of this work. The authors sincerely thank UGC, Govt. of India (F. No. 42-885/2013 (SR)) for funding the research. One of the authors S. Ananthakumar acknowledges Ministry of New and Renewable Energy (MNRE), Govt. of India for providing fellowship under National Renewable Energy Fellowship (NREF) Scheme.

References

- [1] Z Yuan, A Zhang, Y Cao, J Yang, Y Zhu and P Yang, *J. Fluoresc.* **22**, 121 (2012)
- [2] W Chen, D Grouquist and J J Roark, *Nanosci. Nanotechnol.* **2**, 47 (2002)
- [3] J H Bang and P V Kamat, *ACS Nano.* **3**, 1467 (2009)
- [4] D H Kim and J U Kang, Microscopy: Science, technology, applications and education, in: *Review: Upconversion microscopy for biological applications* edited by A Méndez-Vilas and J Díaz (Formatex Research Center, Spain, 2010) Vol. 3, p. 571
- [5] A G Joly, W Chen, D E McCready, J Malm and J Bovin, *Phys. Rev. B* **71**, 165304 (2005)
- [6] W Chen, A G Joly and D E McCready, *J. Chem. Phys.* **122**, 224708 (2005)
- [7] J W M Chon, M Gu, C Bullen and P Mulvaney, *Appl. Phys. Lett.* **84**, 4472 (2004)
- [8] A I Ekimov, A I Efros and A A Onushchenko, *Solid State Commun.* **56**, 921 (1985)
- [9] W W Yu, L Qu, W Guo and X Peng, *Chem. Mater.* **15**, 2854 (2003)
- [10] X Wang, W Yu, J Zhang, J Aldana, X Peng and M Xiao, *Phys. Rev. B* **68**, 125318 (2003)
- [11] Y P Rakovich, S A Filonovich, M J Gomes, J F Donegan, D V Talapin, A L Rogach and A Eychmuller, *Phys. Status Solidi B* **229**, 449 (2002)
- [12] Y Qu and W Ji, *J. Opt. Soc. Am. B* **26**, 1897 (2009)



Effect of co-sensitization of CdSe nanoparticles with N3 dye on TiO₂ nanotubes

S. Ananthakumar, J. Ramkumar, S. Moorthy Babu*

Crystal Growth Centre, Anna University, Chennai 600025, India

Available online 24 February 2014

Communicated by: Associate Editor Smagul Zh. Karazhanov

Abstract

Cadmium selenide (CdSe) nanoparticles were synthesized in aqueous medium using mercaptopropionic acid (MPA) as the stabilizer at the temperature 100 °C. Air stable sodium selenite (Na₂SeO₃) was used as the selenium source. The synthesized particles were used to co-sensitize the TiO₂ nanotubes with N3 dye. Ex-situ linker assisted method was used to sensitize the nanotubes by CdSe nanoparticles. Electrochemical anodization technique was employed to prepare TiO₂ nanotubes in the presence of hydrogen fluoride (HF) as electrolyte. A solar cell was fabricated using co-sensitized TiO₂ nanotubes by N3 dye/CdSe nanoparticles as the anode and platinum coated fluorine doped tin oxide (FTO) electrode as the cathode. Polysulphide (S²⁻/S_x²⁻) mixture was used as the electrolyte. UV–Visible, SEM, AFM and TEM analysis were used to characterize the synthesized particles and TiO₂ nanotubes.

© 2014 Elsevier Ltd. All rights reserved.

Keywords: CdSe nanoparticles; TiO₂ nanotubes; Co-sensitization

1. Introduction

Semiconductor nanoparticles are widely used in the photovoltaic applications due to their size dependent optical properties and their tunable spectrum in visible to IR. Among others, II–VI group semiconductor nanoparticles are widely used in such applications (Debnath et al., 2011). Cadmium selenide (CdSe) is focused much in recent years for third generation photovoltaics due to its low band gap (1.74 eV in bulk form). Various ligands were employed including thiol for the synthesis of CdSe nanoparticles in aqueous medium. When short chain ligands are employed as the stabilizer for the nanoparticles, it was observed that the efficiency of the solar cells fabricated using these

particles are much improved than the bulky ligands (Moule et al., 2012). Titanium di-oxide, a wide band gap semiconductor was also utilized for solar cells and the extended large absorption is possible with the sensitization of ruthenium dyes. The mesoporous structure of the titanium dioxide nanoparticles facilitates this sensitization where the carboxylate group of the dye molecules anchors on the surface. Semiconductor nanoparticles are considered superior than organic dyes due to their high photochemical stability, efficient transfer of electron to conduction band of the TiO₂ and multiple exciton generation (MEG) etc. (Tvrđy and Kamat, 2009). In recent years, one dimensional semiconductor nanostructures are more studied due to their advantages than zero dimension structures. Due to the reduced recombination rate, titanium di-oxide nanotubes are very much considered for solar cells, fuel cells (Gan et al., 2011), sensors (Lu et al., 2008) and photo-catalytic reactions (Shankar et al., 2009) than TiO₂ nanoparticles.

* Corresponding author. Tel.: +91 44 22358333; fax: +91 44 2235 2774.
E-mail addresses: smoorthybabu@gmail.com, babu@annauniv.edu (S. Moorthy Babu).

Eventhough several methods like sol–gel (Jung et al., 2002), hydrothermal (Kasuga et al., 1998) were followed to synthesize TiO_2 nanotubes, anodization method is the most desirable one due to its tunable pore diameter that depends on reaction conditions (Li et al., 2010; Wang et al., 2009). Several studies were made in order to get fine tubular structures with even preferred crystallographic orientation for solar cells (Lee et al., 2012). When ruthenium based dyes such as N719, N3 sensitize the TiO_2 nanotubes through its carboxylate groups, the considerable power conversion efficiency was observed (Stergiopoulos et al., 2008; Chen et al., 2008). Alternatively, the TiO_2 nanotube membranes on transparent conducting glass gives 6.1% efficiency (Dubey et al., 2011). There are several strategies including front side and back side illuminated TiO_2 nanotube solar cells were analyzed with ruthenium dyes (Hao et al., 2011). However, the efficiency of dye sensitized TiO_2 nanotube solar cells is still low due to the partial incorporation of dye on the surface of the nanotubes. Efforts have been made to improve the visible light absorption of the TiO_2 by depositing the noble metals like Ag, Au, and Pt etc. The improved photo catalytic activity was also observed when Cu_2O nanoparticles were loaded on TiO_2 nanotubes (Huang et al., 2010a,b). Semiconductor nanoparticles sensitized TiO_2 NTs were widely utilized for various applications (Bai et al., 2010; Song et al., 2012). When a semiconductor nanoparticles like CdS sensitize TiO_2 nanotubes, the internal photon conversion efficiency (IPCE) value increase nearly two times (Baker and Kamat, 2009). The co-sensitization of CdS/CdSe quantum dot systems was also used to obtain the improved efficiency (Huang et al., 2010a,b; Guan et al., 2011). When semiconductor nanoparticles with short thiol ligand like mercaptopropionic acid (MPA) was coupled with TiO_2 , enhanced absorption was observed. But due to the fast recombination rate and charge transfer limitations at the interface, very poor conversion efficiency was observed. Quantum dots coupled with molecular dyes were also much studied for energy transfer studies. When quantum dots with molecular dyes hybrid were used as the sensitizer for the solar cells, there are several advantages including extending the absorption spectrum, reducing the internal charge recombination and the improved charge extraction (Gimenez et al., 2011). Hybrid structures like, P3HT/CdS/ TiO_2 NT was also used as a photo anode for solar cell, which resulted in improved photo conversion efficiency (Hao et al., 2012). The heterojunction type PCBM: P3HT: TiO_2 NT also provide excellent pathway for the charge separation through the infiltration process of the polymer blends into the TiO_2 nanotubes which results the power conversion efficiency up to 4.1% (Mor et al., 2007). Similar kind of observation was also observed with ZnO nanorod template based growth of TiO_2 nanotubes with the infiltration of P3HT:PCBM blend (Yodyingyoung et al., 2010). Hence, hybrid structures have received much interest for solar cell applications. CdSe nanoparticles alone were also used to sensitize TiO_2 nanotubes effectively for the solar

cell applications (Guijarro et al., 2009; Shen et al., 2010). It was observed that the interaction of thiol capped CdSe nanoparticles with N3 dye had increased the effect of injection from nanoparticles towards acceptors by nearly two orders of magnitude (Sero et al., 2010). The extraction of holes from CdSe nanoparticles with the help of dye was also confirmed by the surface photo voltage spectroscopy (Sero et al., 2008). Moreover, the co-sensitization process in plastic dye-sensitized solar cells (Lee et al., 2011) has proved the remarkable improvement in the active spectra and the photocurrent. In case of the co-sensitization of PbS nanoparticles with N719 dye on TiO_2 nanotubes, a considerable enhancement of the efficiency (from 5.95% to 6.35%) was observed (Liu and John, 2010). Here, in the present work, colloidal cadmium selenide (CdSe) nanoparticles were synthesized in aqueous medium in the presence of mercaptopropionic acid (MPA) as the stabilizer. The prepared particles were allowed to sensitize the titanium di-oxide (TiO_2) nanotubes along with the N3 dye. The CdSe nanoparticles/N3 dye co-sensitized TiO_2 nanotubes were used to fabricate the solar cell as the working electrode with the platinum coated fluorine doped tin oxide (FTO) as the counter electrode.

2. Experiment

2.1. Chemicals

Cadmium chloride (CdCl_2), sodium selenite (Na_2SeO_3), trisodium citrate dihydrate ($\text{Na}_3\text{C}_6\text{H}_5\text{O}_7$), mercaptopropionic acid (MPA), sodium borohydride (NaBH_4), sodium hydroxide (NaOH), titanium foil, hydrogen fluoride (HF), ethylene glycol ($\text{C}_2\text{H}_6\text{O}_2$), N3 dye, tertiary butyl alcohol ($\text{C}_4\text{H}_{10}\text{O}$), acetonitrile (CH_3CN) were used for the synthesis of nanoparticles.

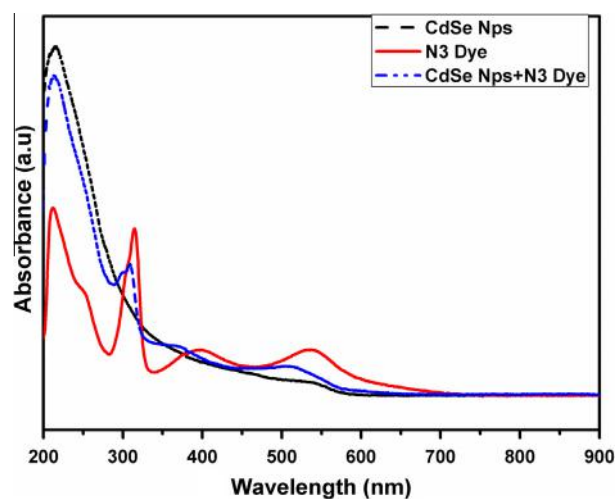


Fig. 1. Absorption spectra of the as synthesized CdSe nanoparticles, N3 dye and CdSe nanoparticles with N3 dye in water/tertiary butyl alcohol/acetonitrile trisolvant mixture.

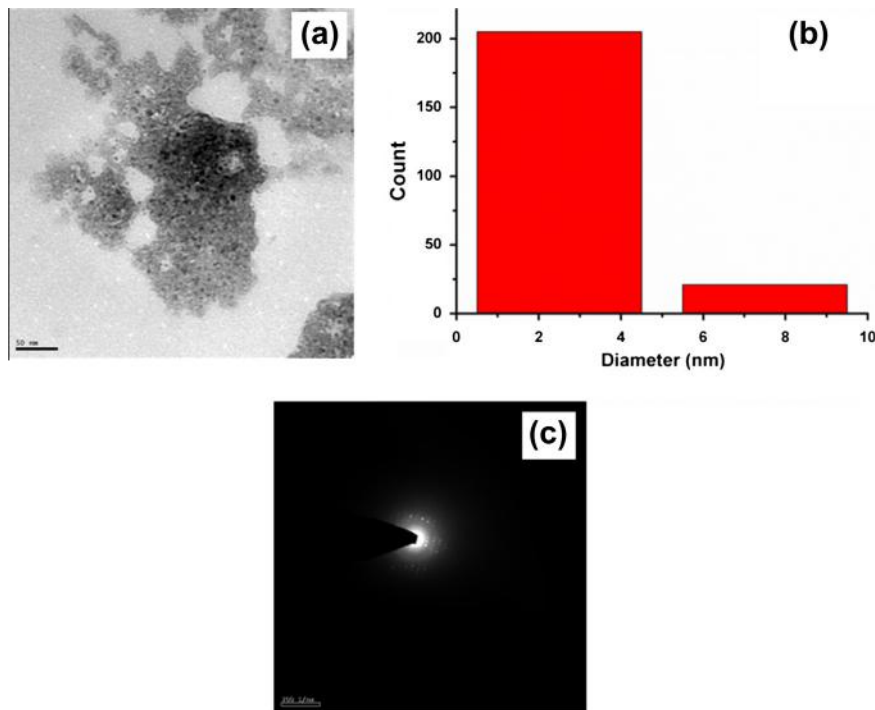


Fig. 2. TEM image of the synthesized CdSe nanoparticles (a) size histogram of the CdSe nanoparticles (b) and SAED pattern of the synthesized CdSe nanoparticles (c).

2.2. Synthesis of CdSe nanoparticles

Synthesis of CdSe nanoparticles in aqueous medium was carried out using the following procedure. In briefly, Cadmium chloride (CdCl_2) and mercaptopropionic acid (MPA) were mixed together in water in three necked flask and pH of the solution was adjusted till 11.2 by 1 M NaOH. With this, trisodium citrate dihydrate, sodium selenite and sodium borohydride were added successively under nitrogen atmosphere. The entire mixture was stirred together and heated strongly to 100 °C in an oil bath. The appearance of pale yellow color of the solution indicates the formation of cadmium selenide nanoparticles in the solution (Guar and Tripathi, 2014). The entire solution was further allowed into reflux for two hours and finally cooled to room temperature. This solution was used to sensitize the TiO_2 nanotubes.

2.3. Formation of TiO_2 nanotubes

TiO_2 nanotubes were prepared through electrochemical anodization method. The titanium foil was taken as the anode and graphite counter electrode using the ethylene glycol as the solvent with 1% of hydrogen fluoride (HF). When voltage is at 40 V for five hours, TiO_2 nanotubes were formed. The foil was taken out and cleaned by the distilled water twice to remove the excess fluoride ions on the surface. Then the foil was heated to 500 °C for 1 h to increase the crystallinity.

2.4. Sensitization of TiO_2 nanotubes and fabrication of solar cell

The synthesized CdSe nanoparticles in water were taken in a beaker and with this the anodized TiO_2 nanotube array was allowed to sensitize for about 24 h. Further, the CdSe sensitized TiO_2 nanotubes were allowed into the appropriate amount of the N3 dye which was dissolved in tertiary butyl alcohol and acetonitrile. The sensitization time followed here was about 24 h. Then the anodized foil was heated at 100 °C for an hour to liberate the solvent on the TiO_2 foil. The solar cell was made using the CdSe nanoparticles co-sensitized electrode as the anode and platinum coated FTO electrode as the cathode. The electrolyte used here was a polysulphide mixture ($\text{S}^{2-}/\text{S}_x^{2-}$).

3. Characterization

Absorption spectra were analyzed through the ELICO SL-159 UV–Visible conventional spectrophotometer in the range of 200–800 nm. TEM images were observed with an electron microscope (Tecnai G2 model T-30 s-twin) using an accelerating voltage of 300 kV. SEM images were recorded using the Carl Zeiss MA15/EVO 18 Scanning Electron Microscope. AFM analysis of the samples was done using Park XE-100 Atomic Force Microscope through non-contact mode.

The UV–Visible absorption spectra of as synthesized CdSe nanoparticles, N3 dye and CdSe nanoparticles with

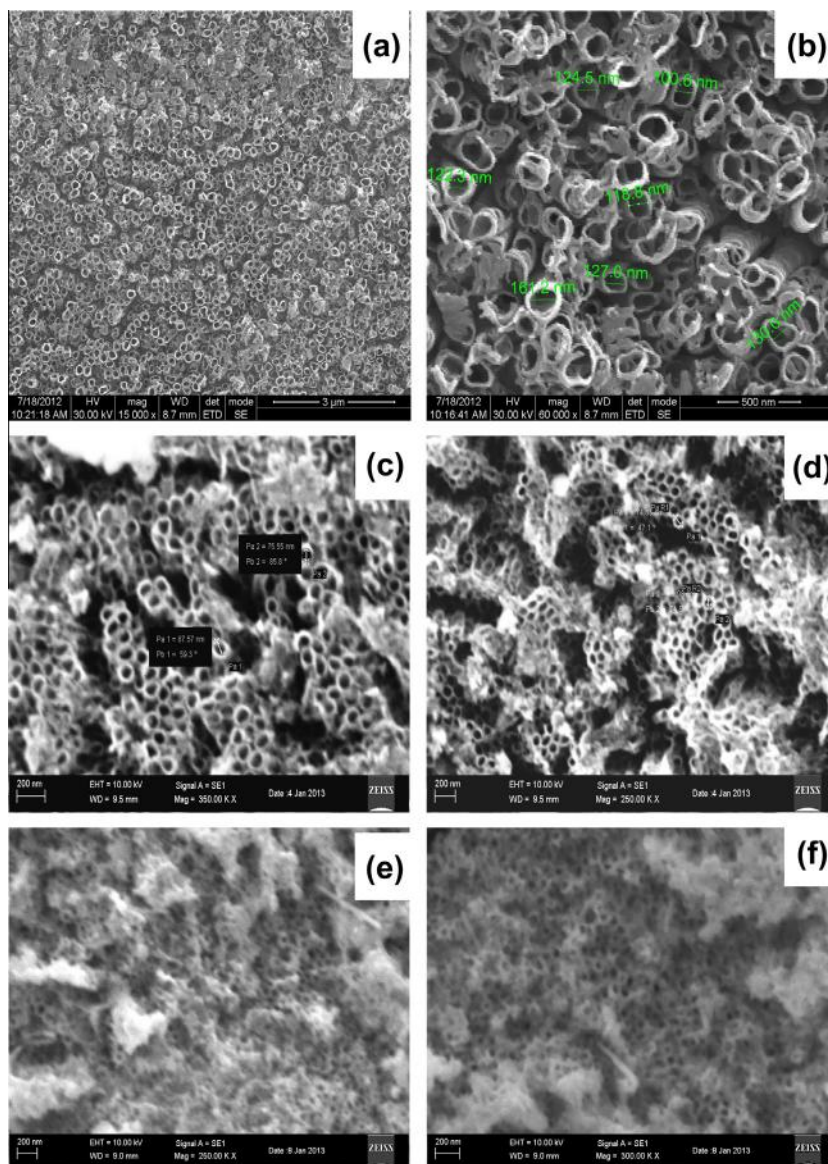


Fig. 3. Surface morphology of as-anodized TiO_2 nanotubes at 40 V on 15 h (a and b) and (c and d) 10 h and the CdSe nanoparticles/N3 dye sensitized nanotubes (e and f).

the N3 dye is shown in Fig. 1. The first excitonic shift of the CdSe nanoparticles were found at 425 nm. The absorption edge of nanoparticles was at 500 nm. The bands of the dye emerges at 314, 400 and 537 nm are due to the $\pi-\pi^*$ transitions of the bipyridine ligand (Fantacci et al., 2003). When CdSe nanoparticles were mixed with the N3 dye, absorption enhancement of the hybrid was observed and compared with the pure nanoparticles. The collective absorption spectrum of CdSe nanoparticles with N3 dye clearly indicates the interaction of nanoparticles with the dye. TEM image and SAED pattern of the synthesized CdSe nanoparticles are shown in Fig. 2. The particles show agglomerated nature which indicates the common behavior of the aqueous medium synthesized particles (Silva et al., 2012). The size of the particles were calculated through particle size histogram and found approximately around

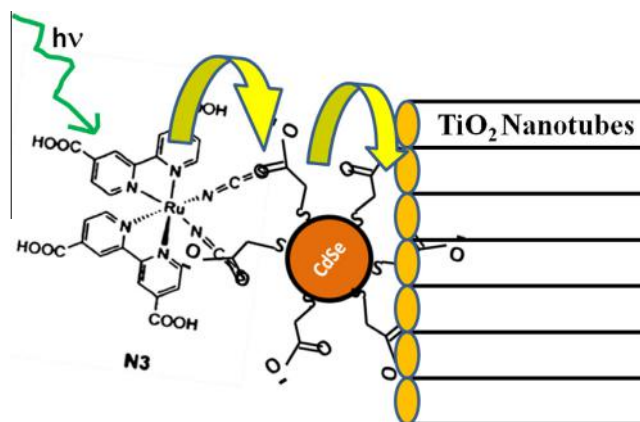


Fig. 4. Schematic diagram of the co-sensitization of CdSe nanoparticles with N3 dye on TiO_2 nanotubes.

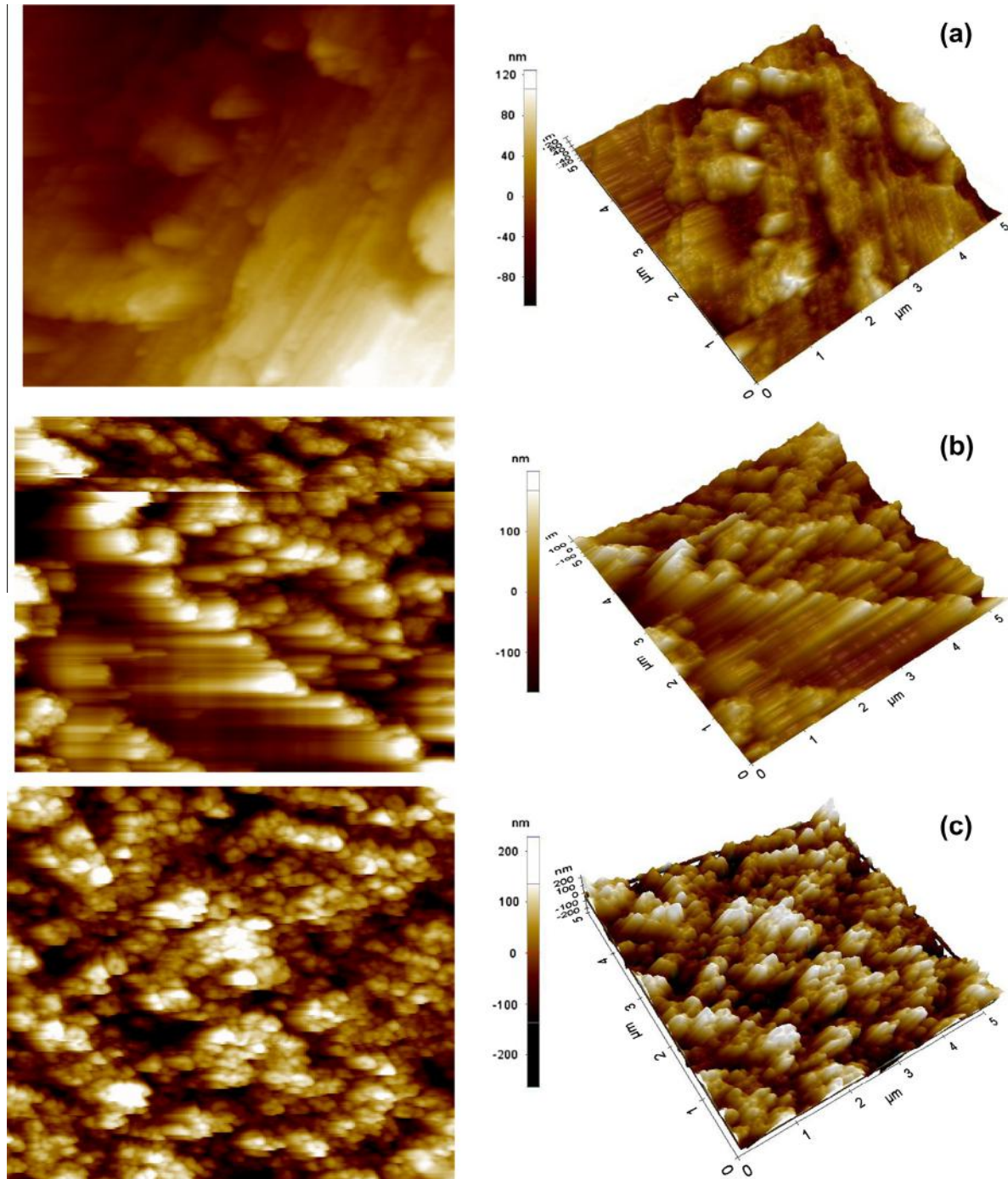


Fig. 5. AFM images of the (a) Ti foil, (b) as anodized Ti foil and (c) TiO_2 nanotubes after the co-sensitization of CdSe nanoparticles with N3 Dye.

1–4 nm. The SAED pattern of the particles (Fig. 2(c)) also confirms the crystalline nature of the nanoparticles.

The SEM images of the anodized Ti foil are shown in Fig. 3. It clearly represents the formation of nanotubes structure on the surface of the foil. The tubes were grown as array and they were parallel to each other. The diameter of the tubes was found to be 100–130 nm for the 15 h anodized tubes and it was 60–90 nm for the 10 h anodized samples. Eventhough several electrolytes were employed as the medium for the production of the TiO_2 nanotubes, ethylene glycol was found to be suitable one for the

production of the uniformly oriented TiO_2 nanotubes (Griemes, 2007). Fig. 3(e and f) also reveals the attachment of the CdSe nanoparticles on the surface of the nanotubes through the surface coverage layer formation of the tubes by CdSe nanoparticles.

The carboxylate group present in both MPA and N3dye favors the attachment of the molecule on the surface of the TiO_2 nanotubes. The energy transfer process between the dye to CdSe nanoparticles are normally depends upon the energy level alignment. The functional groups present in the ligand and dye also plays an important role in this

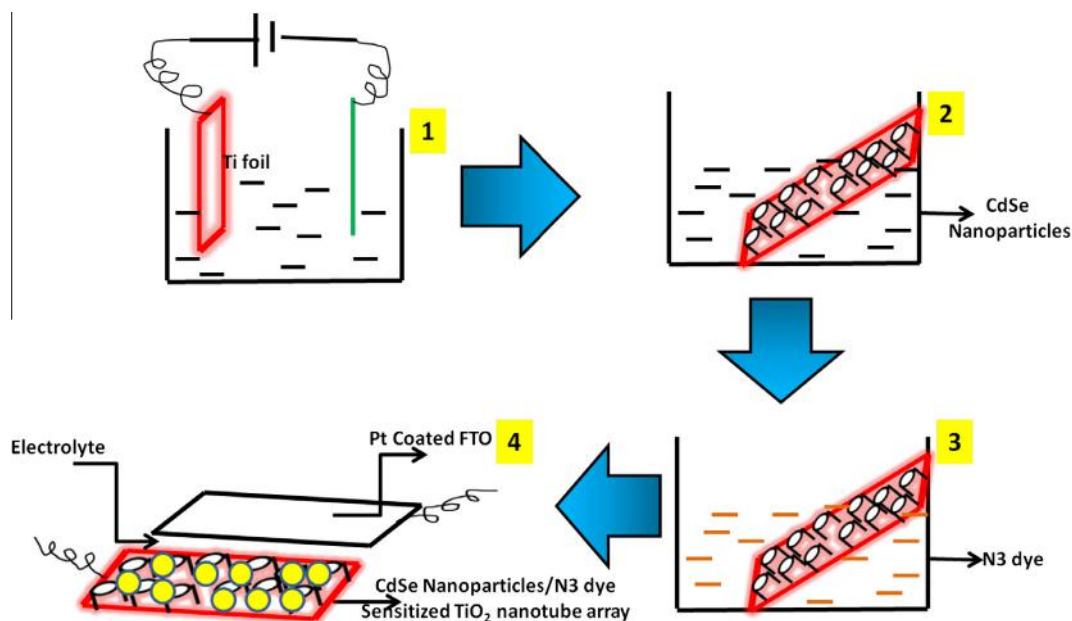


Fig. 6. Schematic representation of (a) anodization process of Ti foil, (b) sensitization of TiO_2 nanotubes by CdSe nanoparticles, (c) sensitization of CdSe nanoparticles sensitized TiO_2 NTs by N3 dye and (d) final structure of the fabricated solar cell device.

mechanism (Gimenez et al., 2011). The schematic diagram (Fig. 4) of the sensitization of N3 dye with CdSe nanoparticles gives the overview of the process.

The morphology and roughness of the tubes were analyzed through AFM technique. The porous nature of the anodized substrate was revealed by the AFM analysis which is shown in Fig. 5. The roughness of the bare Ti foil was 30.7 nm (Fig. 5(a)). It was found that the roughness of the as anodized nanotubes were 50 nm (Fig. 5(b)) while for the nanotubes after sensitization it was around 75 nm (Fig. 5(c)). It also confirms the attachment of the particles through sensitization process. The enhancement in roughness is due to the attachment of the particles along with dyes on the sides of the tube walls through ligand (Guijarro et al., 2009).

A solar cell was fabricated using CdSe nanoparticles co-sensitized TiO_2 nanotubes with N3 dye as the anode and the platinum coated FTO glass substrate as the cathode. For comparison, the CdSe nanoparticles sensitized photoanode based solar cell with similar configuration also was prepared. A polysulphide electrolyte was employed as the electrolyte for the prepared solar cell in order to avoid the corrosion nature of traditional tri-iodide liquid electrolyte by metal chalcogenides (Chakrapani et al., 2011). The schematic diagram of overall steps involved in fabrication of the solar cell is given in Fig. 6. Analysis of the fabricated cell through Keithley 2420 source meter under the illumination of a halogen lamp is in progress.

4. Conclusion

Colloidal cadmium selenide (CdSe) nanoparticles were prepared using water as the solvent at 100 °C. The prepared particles were used to sensitize TiO_2 nanotubes along

with ruthenium dyes. A solar cell was fabricated using this co-sensitized TiO_2 nanotubes and CdSe nanoparticles with N3 dye as the working electrode. The current–voltage (I – V) measurement of the fabricated device is under progress.

Acknowledgments

The authors sincerely thank UGC, Govt. of India (F. No 42-855/2013(SR)) for providing financial support. S.Ananthakumar and J. Ramkumar sincerely thanks Ministry of New and Renewable Energy (MNRE), Govt. of India for providing fellowship under the National Renewable Energy Fellowship (NREF) scheme.

References

- Bai, J., Li, J., Liu, Y., Zhou, B., Cai, W., 2010. A new glass substrate photoelectrocatalytic electrode for efficient visible-light hydrogen production: CdS sensitized TiO_2 nanotube arrays. *Appl. Catal. B: Environ.* 95, 408–413.
- Baker, D.R., Kamat, P.V., 2009. Photosensitization of TiO_2 nanostructures with CdS quantum dots: particulate versus tubular support architectures. *Adv. Funct. Mater.* 19, 805–811.
- Chakrapani, V., Baker, D., Kamat, P.V., 2011. Understanding the role of the sulphide redox couple ($\text{S}^{2-}/\text{S}_n^{2-}$) in quantum dot-sensitized solar cells. *J. Am. Chem. Soc.* 133, 9607–9615.
- Chen, C.C., Chung, H.W., Chen, C.H., Lu, H.P., Lan, C.M., Chen, S.F., Luo, L., Hung, C.S., Diau, E.W.G., 2008. Fabrication and characterization of anodic titanium dioxide nanotube arrays of controlled length for highly efficient dye sensitized solar cells. *J. Phys. Chem. C* 112, 19151–19157.
- Debnath, R., Bakr, O., Sargent, E.H., 2011. Solution-processed colloidal quantum dot photovoltaics – a perspective. *Energy Environ. Sci.* 4, 4870.
- Dubey, M., Shrestha, M., Zhong, Y., Galipeau, D., He, H., 2011. TiO_2 nanotube membranes on transparent conducting glass for high efficiency solar cells. 22, 285201 (1–9).

- Fantucci, S., De Angelis, F., Selloni, A., 2003. Absorption spectrum and solvatochromism of the [Ru(4,4'-COOH-2,2'-bpy)₂(NCS)] molecular dye by time dependent density functional theory. *J. Am. Chem. Soc.* 125, 4381.
- Gan, X.Y., Gan, B.J., Su, L., 2011. Biophotofuel cell anode containing self-organized titanium dioxide nanotube array. *Mater. Sci. Eng. B* 176, 1197–1206.
- Gimenez, S., Rogach, A.L., Lutich, A.A., Gross, D., Poeschi, A., Susa, A.S., Lana-Villareal, T., Bisquert, J., 2011. Energy transfer versus charge separation in hybrid systems of semiconductor quantum dots and Ru-dyes as potential co-sensitizers of TiO₂ based solar cells. *J. Appl. Phys.* 110, 014314.
- Griemes, C.A., 2007. Synthesis and application of highly ordered arrays of TiO₂ nanotubes. *J. Mater. Chem.* 17, 1451–1457.
- Guan, X.F., Huang, S.Q., Zhang, Q.X., Shen, X., Sun, H.C., Li, D.M., Lio, Y.H., Yu, R.C., Meng, Q.B., 2011. Front Side illuminated CdS/CdSe quantum dots co-sensitized solar cells based on TiO₂ nanotube arrays. *Nanotechnology* 22, 465402.
- Guar, K., Tripathi, S.K., 2014. Size tuning of MAA capped CdSe and CdSe/CdS quantum dots and their stability in different pH environments. *Mater. Chem. Phys.* 143, 514–523.
- Guijarro, N., Villarreal, T.L., Sero, I.M., Bisquert, J., Gomez, R., 2009. CdSe quantum dot-sensitized TiO₂ electrodes-effect of quantum dot coverage and mode of attachment. *J. Phys. Chem. C* 113, 4208–4214.
- Hao, P.T., Liou, Y.J., Teng, H., 2011. Electron Transport patterns in TiO₂ nanotube arrays based dye sensitized solar cells under frontside and backside illuminations. *J. Phys. Chem. C* 115, 15018–15024.
- Hao, Y., Cao, Y., Sun, B., Li, Y., Zhang, Y., Xu, D., 2012. A novel semiconductor-sensitized solar cell based on P3HT@CdS@TiO₂ core-shell nanotubes array. *Sol. Energy Mater. Sol. Cells* 101, 107–113.
- Huang, L., Zhang, S., Peng, F., Wang, H., Yu, H., Yang, J., Zhang, S., Zhao, H., 2010a. Electrodeposition preparation of octahedral-Cu₂O-loaded TiO₂ nanotube arrays for visible light-driven photocatalysis. *Scripta Mater.* 63, 159–161.
- Huang, S., Zhang, Q., Huang, X., Guo, X., Deng, M., Li, D., Luo, Y., Shen, Q., Toyoda, T., Meng, Q., 2010b. Fibrous CdS/CdSe quantum dot co-sensitized solar cells based on ordered TiO₂ nanotube arrays. *Nanotechnology* 21, 375201 (1–7).
- Jung, J.H., Kobayashi, H., Van Bommel, K.J.C., Shinkai, S., Shimizu, T., 2002. Creation of novel helical ribbon and double-layered nanotube TiO₂ structures using an organogel template. *Chem. Mater.* 14, 1445.
- Kasuga, T., Hiramatsu, M., Hoson, A., Sekino, T., Niihara, K., 1998. Formation of titanium oxide nanotube. *Langmuir* 14, 3160.
- Lee, K.M., Hsu, Y.C., Ikegami, M., Miyasaka, T., Thomas, K.R.J., Lin, J.T., Ho, K.C., 2011. Co-sensitization promoted light harvesting for plastic dye-sensitized solar cells. *J. Power Sources* 196, 2416–2421.
- Lee, S., Park, I.J., Kim, D.H., Seong, W.M., Kim, D.W., Han, G.S., Kim, J.Y., Jung, H.S., Hong, K.S., 2012. Crystallographically preferred oriented TiO₂ nanotube arrays for efficient photovoltaic energy conversion. *Energy Environ. Sci.* 5, 7989–7995.
- Li, D., Chang, P.C., Chien, C.J., Lu, J.G., 2010. Applications of tunable TiO₂ nanotubes as nanotemplate and photovoltaic device. *Chem. Mater.* 22, 5707–5711.
- Liu, Y., John, W., 2010. Co-sensitization of TiO₂ by PbS quantum dots and N719 in dye-sensitized solar cells. *Thin Solid Films* 518, e54–e56.
- Lu, H.F., Li, F., Liu, G., Chen, Z.G., Wang, D.W., Fang, H.T., Lu, G.Q., Jiang, Z.H., Cheng, H.M., 2008. Amorphous TiO₂ nanotube arrays for low-temperature oxygen sensors. *Nanotechnology* 19, 405504.
- Mor, G.K., Shankar, K., Paulose, M., Varghese, O.K., Grimes, C.A., 2007. High efficiency double heterojunction polymer photovoltaic cells using highly ordered TiO₂ nanotube arrays. *Appl. Phys. Lett.* 91, 152111.
- Moule, A.J., Chang, L., Thambidurai, C., Vidu, R., Stroeve, P., 2012. Hybrid solar cells-basic principles and the role of ligands. *J. Mater. Chem.* 22, 2351.
- Sero, I.M., Dittrich, T., Susa, A.S., Rogach, A.L., Bisquert, J., 2008. Large improvement of electron extraction from CdSe quantum dots into a TiO₂ thin film layer by N3 dye coabsorption. *Thin Solid Films* 516, 6994–6998.
- Sero, I.M., Gross, D., Mittereder, T., Lutih, A.A., Susa, A.S., Dittrich, T., Belaidi, A., Caballero, R., Langa, F., Bisquert, J., Rogach, A.L., 2010. Nanoscale interaction between CdSe or CdTe nanocrystals and molecular dyes fostering or hindering directional charge separation. *Small* 6, 221–225.
- Shankar, K., Basham, J.I., Allam, K.N., Varghese, O.K., Mor, K.G., Feng, X., Paulose, M., Seabold, J.A., Choi, K.S., Griemes, C.A., 2009. Recent advances in the use of TiO₂ nanotube and nanowire arrays for oxidative photo electrochemistry. *J. Phys. Chem. C* 113 (16), 6327–6359.
- Shen, Q., Yamada, A., Tamura, S., Toyoda, T., 2010. CdSe quantum dot-sensitized solar cell employing TiO₂ nanotube working-electrode and Cu₂S counter-electrode. *Appl. Phys. Lett.* 97, 123107.
- Silva, O.F., Carvalho, S.M., Mendonca, R., Macedo, W.A.A., Balzuweit, K., Reiss, P., Schiavon, M.A., 2012. Effect of Surface ligands on the optical properties of aqueous soluble CdTe quantum dots. *Nanoscale Res. Lett.* 7 (536), 1–10.
- Song, Y.Y., Zhuang, Q.L., Li, C.Y., Liu, H.F., Cao, J., Gao, Z.D., 2012. CdS nanocrystals functionalized TiO₂ nanotube arrays: novel electrochemiluminescence platforms for ultrasensitive immunosensors. *Electrochim. Commun.* 16, 44–48.
- Stergiopoulos, T., Ghicov, A., Likodimos, V., Tsoukleris, D.S., Kunze, J., Schmuki, P., Falaras, P., 2008. Dye sensitized solar cells based on thick highly ordered TiO₂ nanotubes produced by controlled anodic oxidation in non-aqueous electrolytic media. *Nanotechnology* 19, 235602.
- Tvrđy, K., Kamat, P.V., 2009. Substrate driven photochemistry of CdSe quantum dot films-charge injection and irreversible transformations on oxide surfaces. *J. Phys. Chem. A* 113, 3765–3772.
- Wang, D., Liu, Y., Yu, B., Zhou, F., Liu, W., 2009. TiO₂ nanotubes with tunable morphology, diameter, and length: synthesis and photoelectrical/catalytic performance. *Chem. Mater.* 21, 1198–1206.
- Yodyingyoung, S., Zhou, X., Zhang, Q., Triampo, D., Juntong, X., Park, K., Limeketkai, K., Guozhong, C., 2010. Enhanced photovoltaic performance of nanostructured hybrid solar cell using highly oriented TiO₂ nanotubes. *J. Phys. Chem. C* 114, 21851–21855.



Effect of ligand exchange in optical and morphological properties of CdTe nanoparticles/P3HT blend

S. Ananthakumar, J. Ramkumar, S. Moorthy Babu*

Crystal Growth Centre, Anna University, Chennai 600 025, India

Available online 4 March 2014

Communicated by: Associate Editor Smagul Zh. Karazhanov

Abstract

Luminescent CdTe nanoparticles were synthesized in aqueous medium at low temperature under the inert atmosphere using water soluble precursors. Potassium tellurite was employed as the tellurium source for the synthesis. As synthesized CdTe nanoparticles were phase transferred into organic medium via partial ligand exchange method through long chain organic ligand 1-dodecanethiol in the presence of acetone. The phase transferred CdTe nanoparticles were blended homogeneously with P3HT polymer in a common solvent (chloroform) for possible application as the active layer in hybrid solar cell structure. The prepared blends were characterised with UV–Vis, Photoluminescence, SEM and AFM analysis. The XRD patterns of the particles in two phases confirm the uniformity of the cubic structure. The size distribution of the synthesized particles was confirmed through TEM analysis. The effective interactions of the donor and acceptor components were confirmed through UV–Visible spectroscopy. The efficient charge transfer processes of the blends were confirmed through photoluminescence analysis of the nanoparticles various volume additions with polymer. The morphological analysis of the blends was carried out using the Scanning Electron Microscopy which reveals the distribution of the nanoparticles in the polymer. AFM analysis of the coated blend film explores the phase separation of the nanoparticles when blended with the polymer in chloroform. Advantages of these nanoparticles for solar cell applications were discussed.

© 2014 Elsevier Ltd. All rights reserved.

Keywords: CdTe nanoparticles; Phase transfer; 1-Dodecanethiol; Hybrid solar cells

1. Introduction

Semiconductor nanoparticles are widely used in various applications due to the presence of quantum confinement effect and size tunable properties (Biju et al., 2008). Among II–VI group semiconductor compounds, CdTe nanoparticles are widely used in many fields due to their high fluorescent quantum yield, size tunability, etc. (Li et al., 2006). A wide range of applications are being reported for the use of CdTe nanoparticles including finger print detection, solar

cells and electroluminescent devices such as Light Emitting Diode (LED)'s (Cheng et al., 2008; Olson et al., 2010; Gallardo et al., 2007; Gaponik et al., 1999; Rogach et al., 2008). In recent years, II–VI semiconductor nanoparticles are used as active layer of hybrid solar cells as acceptor molecules (Kumar and Nann, 2004; Chen et al., 2011; Fan et al., 2011). Due to their high carrier mobility and the possibility of multiple exciton generation semiconductor nanocrystals are much reliable for such applications. Eventhough the organometallic precursor based synthesis of CdTe nanoparticles give high crystalline and monodispersible nanoparticles, the use of very highly toxic tellurium precursors like H_2Te and Al_2Te_3 with cumbersome experimental arrangements (Murray et al., 1996; Yu

* Corresponding author. Tel.: +91 44 22358333; fax: +91 44 2235 2774.
E-mail addresses: babusm@yahoo.com, babu@annauniv.edu (S. Moorthy Babu).

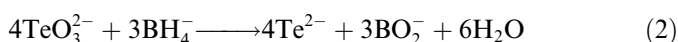
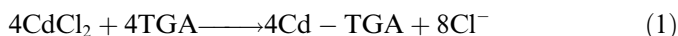
et al., 2003) and also high temperature requirement are major disadvantages. Moreover, in these reactions, usually tri-octyl phosphine oxide (TOPO) and tri-octyl phosphine were used to cap CdTe and as a solvent for the synthesis. Since this TOPO is a strong barrier for the charge conduction, it has to be removed using pyridine treatment to make the charge transport more efficient before blending CdTe with the conducting polymers (Wang et al., 2007; Lokteva et al., 2010; Celik et al., 2012; Moule et al., 2012). The arrival of aqueous based synthetic procedures has eliminated these problems with simple precursors. The aqueous based synthesis of CdTe nanoparticles was normally carried out using simple precursors like CdCl₂, Cd(CH₃COO)₂, NaH₂Te and K₂TeO₃ (Green et al., 2007; Gao et al., 1998; Jiang and Jia, 2007; Abd El-Sadek and Babu, 2010). But, in the application point of view, the utility of these semiconductor nanoparticles are limited when they are synthesized through aqueous medium particularly for photovoltaics. To avoid this, phase transfer chemistry is applied to transfer the nanoparticles from aqueous to organic phase which allows utilisation of these particles for further applications. The phase transfer of CdTe nanoparticles were carried out with various types of ligands including amines, alkanethiol etc. (Qin et al., 2008; Wuister et al., 2003). Gaponik et al. proposed a suitable method using a long chain thiol, 1-dodecanethiol to transfer the CdTe nanoparticles into organic phase and the possibility of applying these particles for the solar cell (Gaponik et al., 2002). Gaponik's method of ligand exchange process using 1-dodecanethiol has successfully been applied for the HgTe and Mn doped ZnS nanoparticles to transfer them from aqueous to organic phase (Kovalenko et al., 2006; Gunes et al., 2006; Zhao et al., 2007). There are no elaborate reports, available for the phase transfer of TGA capped CdTe nanoparticles using this method and then preparation of CdTe–P3HT blends for application in hybrid solar cells. Recently, the high power conversion efficiency of CdSe–P3HT blends was achieved using n-butanethiol (n-BT) ligand using the post treatment of the nanoparticles (Fu et al., 2012). Hence, thiols have emerged as the suitable ligands for the potential applications in hybrid solar cells. In case of the quantum dot sensitized solar cells, thiol group ligands play an important role in charge transport properties (Guijarro et al., 2009; Chen et al., 2009). Moreover, the pyridine treatment can be avoided to remove the ligand from the surface when the nanoparticles are capped by thiol unlike TOPO. In the present work, colloidal synthesis of thioglycolic acid (TGA) capped CdTe nanoparticles were reported in aqueous medium and the prepared particles were transferred to organic medium through efficient phase transfer method using 1-dodecanethiol as partial surface exchange ligand in the presence of acetone. The phase transferred CdTe nanoparticles were blended homogeneously with P3HT in chloroform. The synthesized CdTe nanoparticles and CdTe nanoparticles/P3HT blend were characterised using UV–Vis, Photoluminescence, TEM, XRD, and AFM analysis.

2. Experiment

Precursors in the form of cadmium chloride (CdCl₂), potassium tellurite (K₂TeO₃), thioglycolic acid (C₂H₄O₂S), sodium borohydride (NaBH₄), sodium hydroxide (NaOH), trisodium citrate dihydrate (Na₃C₆H₅O₇), and 1-dodecaethiol (C₁₂H₂₆S) were used.

2.1. Synthesis of CdTe nanoparticles

CdTe nanoparticles were synthesized with the following procedure. Cadmium chloride (CdCl₂) was dissolved in water and with this thioglycolic acid was added to it with constant stirring. The resultant turbidity of the solution indicates the formation of cadmium–thiolate (Cd–TGA) complex. Trisodium citrate dihydrate was added with this complex and stirred well and then the solution was adjusted to pH 10.5 and allowed constant stirring under N₂ flow in the three necked flask. About 0.5 mM of potassium tellurite was taken in another three necked flask in 50 ml water and with it excessive sodium borohydride was added. This mixture was allowed to heating to about 50 °C for half an hour. The solution was changed from pink colour to colourless. The resultant colourless solution was injected into the Cd–TGA flask. The entire mixture was subjected to heating. The appearance of the yellow in colour indicates the formation of the CdTe nanoparticles in the solution. The solution was further refluxed into an hour and kept to normal atmosphere. The overall reaction can be expressed as,



2.2. Phase transfer of the CdTe nanoparticles

The synthesized nanoparticles in aqueous medium were successfully transferred into organic medium by the method proposed by Gaponik et al. (2002). In briefly, the above synthesized CdTe nanoparticles were added into the equal amount of 1-dodecanethiol (1-DDT). With this, a measured amount of acetone was added and allowed to mild heating with constant stirring. After sometime, the CdTe nanoparticles present in the aqueous medium were completely transferred into the 1-DDT phase. This organically soluble CdTe nanoparticles (hereafter, OS-CdTe) were precipitated by the addition of methanol. The resultant powdered nanoparticles were dried in vacuum and redispersed in chloroform. The entire partial ligand exchange process was depicted as shown in Fig 1. The dispersed nanoparticles were found stable in organic phase. The prepared OS-CdTe nanoparticles were mixed with chloroform and P3HT polymer in 50:50 volume ratio and the entire solution was allowed stirring for overnight. Then, ITO coated glass substrate was pre-treated with

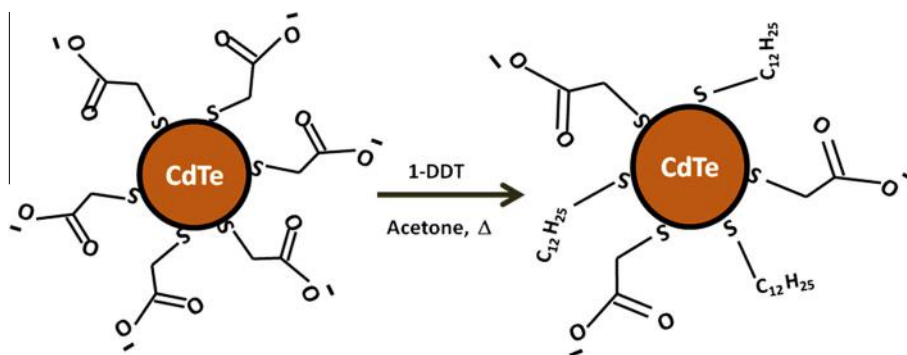


Fig. 1. Schematic diagram of the phase transfer process of CdTe nanoparticles.

various solvents including acetone, iso-propanol, methanol and dried in vacuum. The prepared OS-CdTe/P3HT blend was then coated on the substrate at 1500 rpm. The substrate was annealed at 100 °C for 10 min to eliminate the solvent from the substrate. The finally obtained layer was used for further characterisation.

3. Results and discussion

Absorption spectra of the particles were analysed through the ELICO SL-159 UV–Visible conventional spectrophotometer in the range of 200–800 nm. Photoluminescence spectrum was recorded using JASCO FP-6300 spectrofluorometer at the excitation wavelength of 400 nm. HRTEM images were obtained using the electron microscope (Tecnai G2 model T-30 s-twin) with an accelerating voltage of 300 kV. SEM images were analysed using the Carl Zeiss MA15/EVO 18 Scanning Electron Microscope. AFM analysis of the samples was done using Park XE-100 Atomic Force Microscope through non-contact mode. For SEM analysis, the blend was prepared using chloroform solvent and coated on the ITO/PEDOT:PSS layer using spin coating method (2000 rpm). For UV–Visible and Photoluminescence analysis, the samples were taken in liquid form. For XRD analysis the powder samples were prepared after the addition of iso-propanol with the as synthesized an phase transferred nanoparticles. For TEM analysis the particles were dispersed in acetonitrile and allowed to ultrasonification. Finally it was dispersed on a carbon grid.

The powder XRD patterns of as synthesized TGA capped CdTe nanoparticles and phase transferred CdTe nanoparticles are as shown in Fig 2. In both the cases, the particles possess the same characteristic peaks. The broad XRD patterns reveal the nanodimension of the particles in both the cases. There was no difference in the diffraction pattern of the particles in aqueous or organic medium. The diffraction peaks corresponding to different planes confirm the formation of zinc blende structure of the particles (JCPDS No: 65-8367). The TEM image of the synthesized nanoparticles is shown in Fig 3. The particles possess very good monodispersability of size distribution. The size histogram of the

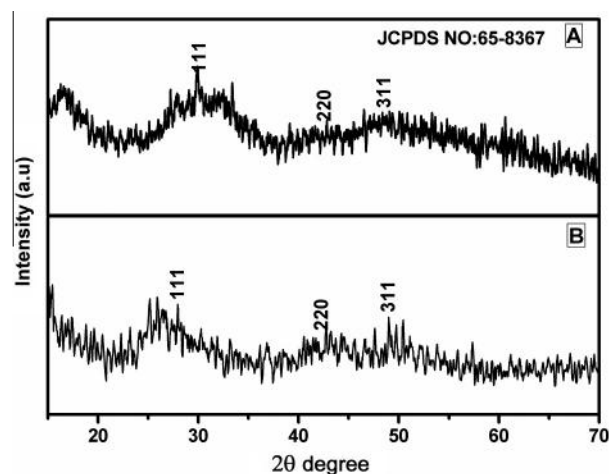


Fig. 2. XRD pattern of (a) TGA capped CdTe and (b) OS-CdTe nanoparticles.

prepared CdTe nanoparticles is given in Fig 3(b). The average size of the particles in the solution was found to be 5.8 nm. The Energy dispersion Analysis (EDX) of the prepared particles clearly indicates the existence of Cd, Te, and S. The presence of sulphur in the spectra may be due to the attachment of the ligand on the surface of the nanoparticles. Thioglycolic acid, an organic thiol ligand, is an effective capping ligand for metal nanoparticles due to its short chain and hence it was more preferred than TOPO (a bulky group ligand) in the present work. Moreover, the complexity associated with the later can be avoided when we go through thiol ligand. The phase transfer process lead to quenching in absorption and photoluminescence of the particles compared with parent medium. The morphology of the CdTe nanoparticles was modified with phase transfer process using 1-DDT. The comparative absorption spectra of the cadmium telluride nanoparticles synthesized in water and the transferred into chloroform is as shown in Fig 4. The absorption edge was observed at 450 nm of the particles in both the mediums. The slight difference in the absorption spectra may be due to the change of medium from water to chloroform. During the phase transformation process, it was observed that the addition of acetone plays an important role, which makes the particles diffuse from the aqueous

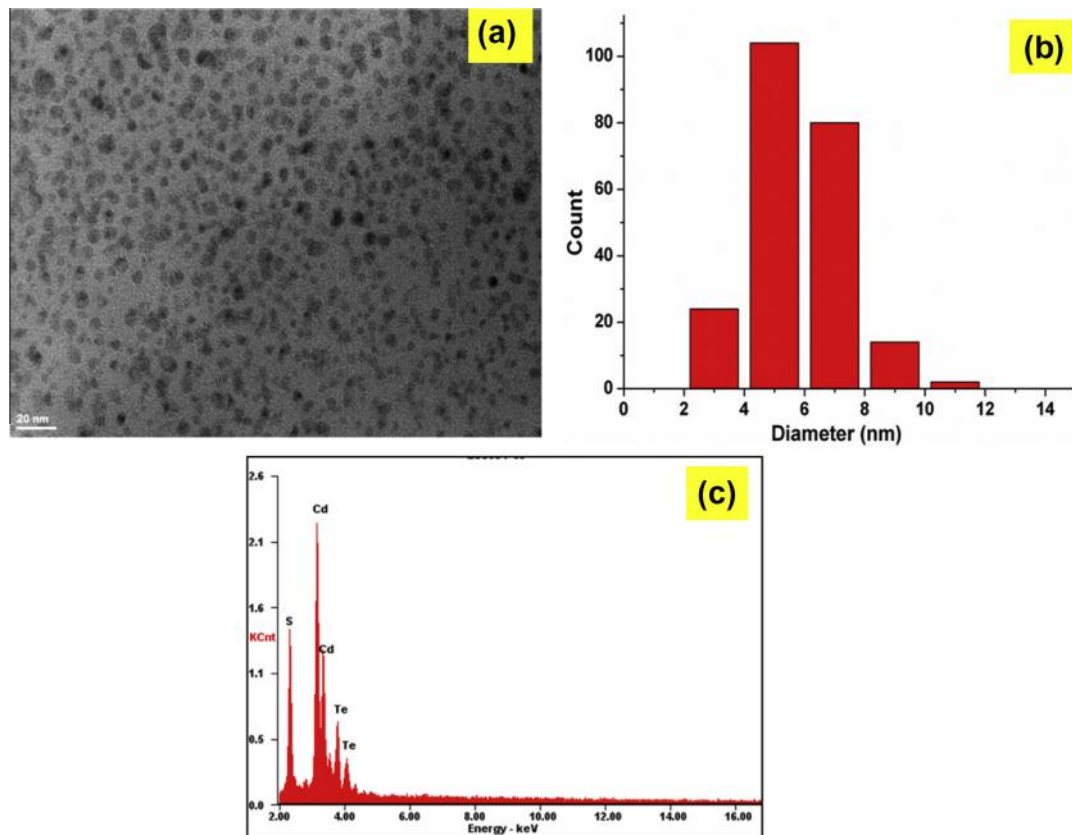


Fig. 3. (a) TEM image of the synthesized CdTe nanoparticles (b) histogram of particle size distribution of the CdTe nanoparticles (c) EDX spectrum of the CdTe nanoparticles.

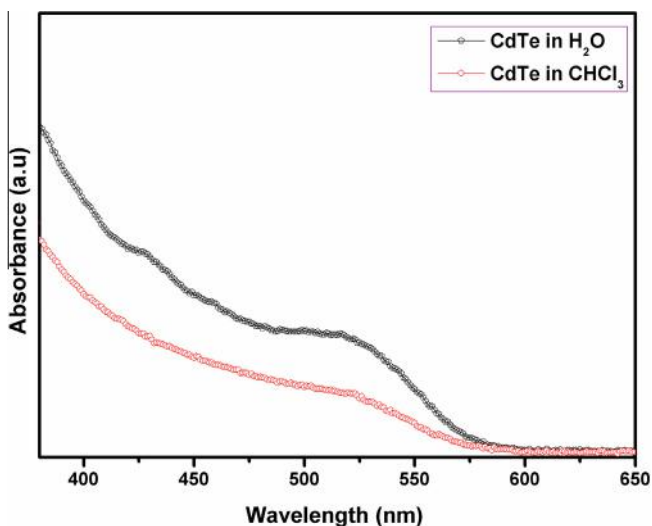


Fig. 4. Absorption spectra of CdTe nanoparticles in water and in chloroform.

medium into the organic phase. Excess amount of acetone lead to aggregation/precipitation of the particles and completely deteriorate the phase transfer process. There was a dimensional change of the particles when the particles were surface modified with 1-DDT (Ding et al., 2009). In the present case, no such changes were observed. Acetone acts as the

interfacial agent in this process and facilitates the efficient transfer, which depends on the volume level of the acetone. When excess of acetone was used, the flocculation of the particles was observed which resulted into precipitation. The partial ligand exchange of nanoparticles was also motivated by the temperature. In the present case the temperature of around 50–60 °C was used (i.e.) closer to the boiling point range of acetone. The presence of CdTe nanoparticles before and after the phase transfer in aqueous and organic medium is given in Fig 5. The blended OS-CdTe–P3HT nanocomposites were analysed through absorption and fluorescence emission spectroscopy. Fig. 6 represents the combined absorption spectra of the OS-CdTe nanoparticles, P3HT and OS-CdTe/P3HT blends. It was observed from the OS-CdTe/P3HT nanocomposites that the absorption spectrum of nanocomposites lies in between the absorption spectrum of the OS-CdTe nanoparticles and P3HT polymer which confirms that the nanocomposites were blended together. The addition of CdTe nanoparticles with the polymer makes the increase of the absorption in the spectrum relative to the individual P3HT polymer signal ($\lambda_{\text{max}} = 450 \text{ nm}$). Photoluminescence spectroscopy studies could be the best tool to confirm the efficient charge transfer process which takes place in the polymer nanoparticles hybrid blends. The quenching can also be pointed out as the indirect measurement of the effectiveness of the ligand exchange. When there is a decreasing intensity of the PL emission of the polymer

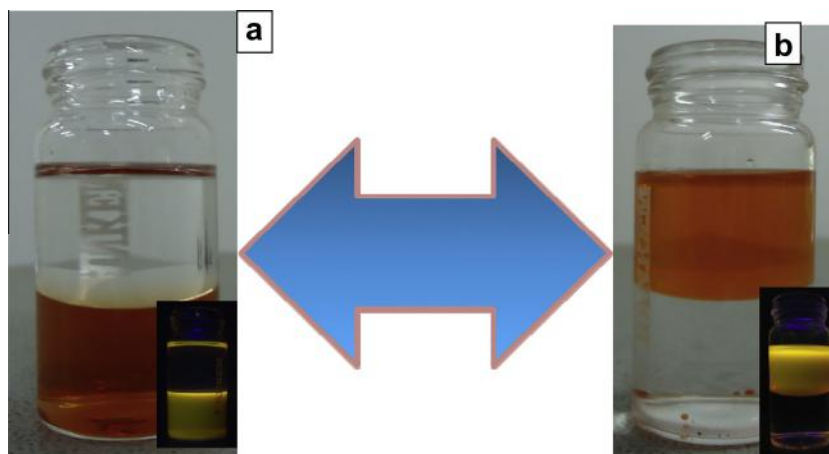


Fig. 5. Presence of CdTe nanoparticles in water (a) and in 1-dodecanethiol (b) inset shows the fluorescence images of the particles under UV light (365 nm).

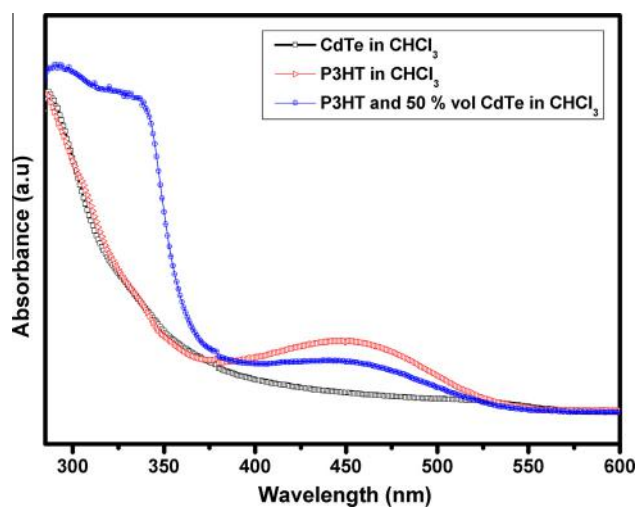


Fig. 6. UV–Visible spectra of pure P3HT, OS-CdTeNP and OS-CdTeNP/P3HT blend in CHCl_3 .

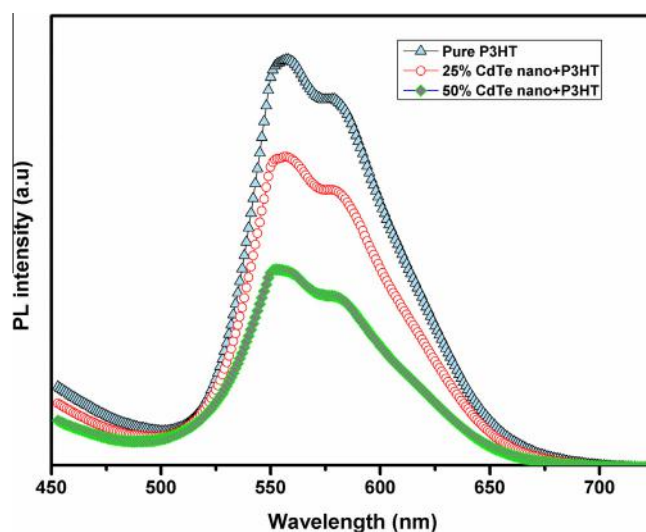


Fig. 7. Photoluminescence spectra of OS-CdTe/P3HT blends under various volume ratios in CHCl_3 (excitation wavelength 400 nm).

with respect to nanoparticles, it clearly reveals that there is an efficient charge separation at the interface of the blend. In the present case, there is a formation of hole in the polymer and the arrival of electron in the CdTe nanoparticles. This characteristic excitonic separation of the blends can be addressed through PL quenching. Fig 7 represents the emission spectra of the P3HT and CdTe nanoparticles blended P3HT composites. The spectra clearly reveal that the PL quenching of the P3HT is observed on the different volume addition of the CdTe nanoparticles. The decrease in emission intensity of the nanoparticles blended with polymer which clearly indicates that the efficient charge transfer process exhibits between the nanoparticles and polymer at the interface. The decreasing of the intensity also indicates that the nanoparticles are effectively bonded with the P3HT polymer and acts as very good electron acceptors. The 50% volume addition of the CdTe nanoparticles with polymer has the least level of quenching compared with 25% volume addition of nanoparticles. The optimum level of

nanoparticles content in the blend is the essential one for the efficient solar cell performance. The SEM image of the blended films of the OS-CdTe nanoparticle and P3HT polymer in the volume level of the 50:50 ratio is shown in Fig 8. It clearly indicates that the particles are well distributed in the polymer matrix. And, the particles get agglomerated in some places and appeared as large size. The formation of the macro size phase separation is the major problem in the blend based hybrid and organic solar cell devices. In the present case, since, chloroform was used as the solvent to blend the polymer and nanoparticles, choosing the aromatic solvent system make the blend to reduce the surface roughness of the film. The increasing level of the nanoparticles in the polymer may render the efficient charge collection due to the decrease of the percentage of the polymer content in the blend, hence the appropriate percentage level of the nanoparticles are required to blend with the polymer to improve the performance of the solar cell in the hybrid based

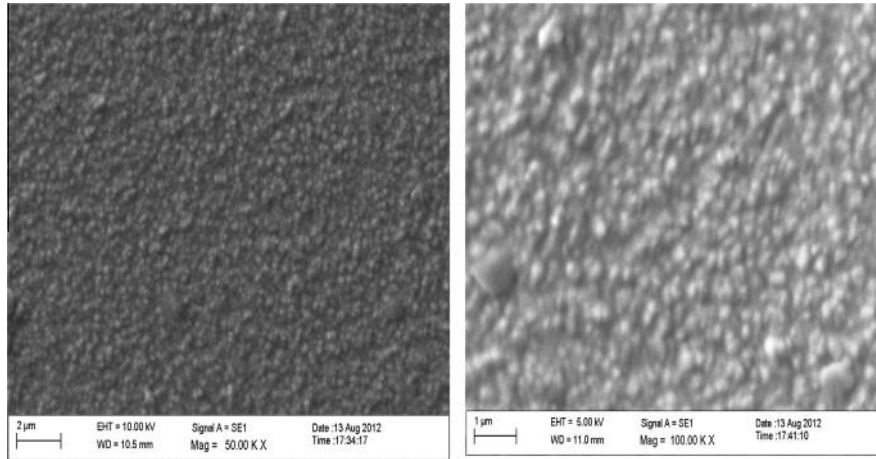


Fig. 8. SEM images of the OS-CdTe/P3HT blends processed from Chloroform (ratio 50:50 in volume).

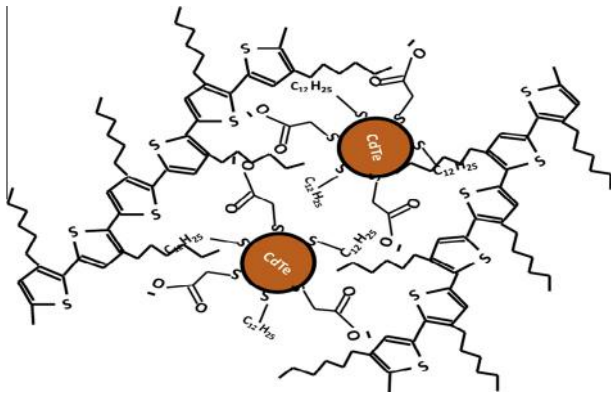


Fig. 9. Schematic diagram of interpenetrating network formation of CdTe nanoparticles/P3HT blend.

devices. Further studies may explore the optimum level of the nanoparticles which is required for the high efficiency

performance. The interpenetrating network formation of polymer and nanoparticles in Fig. 9 predicts the ideal formation of the blend. The RMS value which is obtained from AFM analysis of the nanoparticle–polymer blend film provides the information about the roughness. The tapping mode AFM image of the CdTe-P3HT blends for the 50:50 volume ratio is given in Fig. 10. The picture clearly shows that the particles are well distributed in the polymer. The roughness of the formed film indicates that the formation of nano level phase separation which is the essential one for the enhancement of the interfacial area for efficient exciton dissociation. The agglomeration of the particles on the surface was also observed in some places which may be due to the annealing process which was done after coating the active layer. The RMS value of the resultant hybrid film was found to be 9 nm which clearly shows that the surface smoothness has to be improved further. This could be achieved through the organic solvents based approach

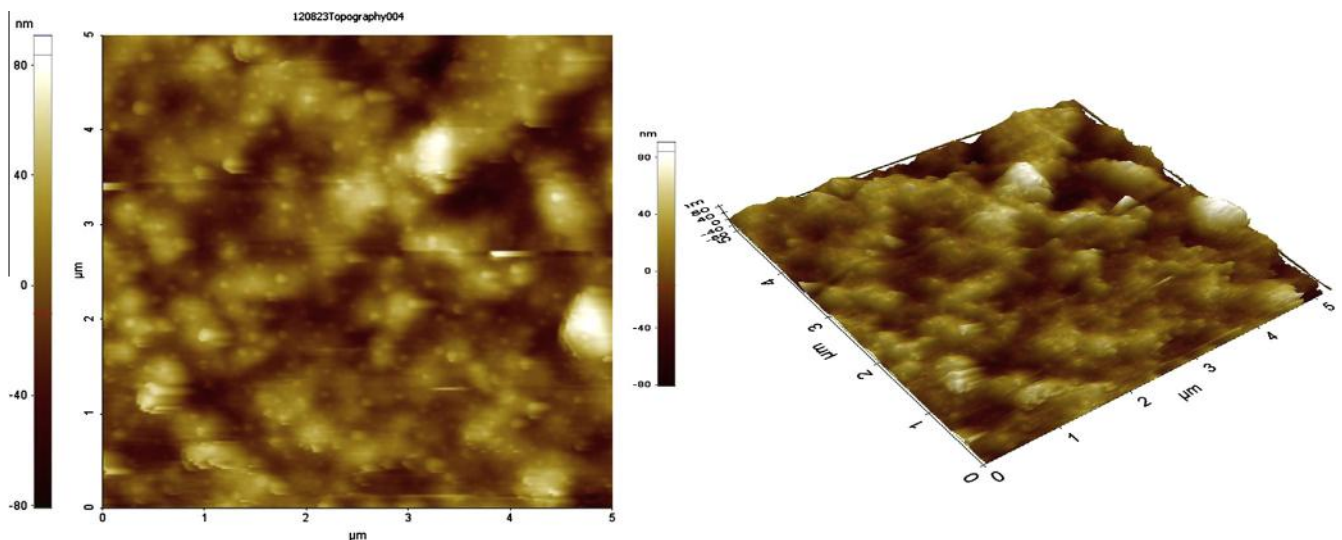


Fig. 10. AFM images of the OS-CdTe/P3HT blends in CHCl_3 , volume ratio 50:50 RMS = 9 nm.

4. Conclusion

The CdTe nanoparticles were prepared through aqueous medium via thioglycolic acid as the capping ligand and the synthesized nanoparticles were transformed into organic phase through partial ligand exchange process using 1-dodecanethiol. Structural studies confirm the cubic nature of the particles. The synthesized particles were successfully blended with P3HT polymer in chloroform. The blends were characterised and the electronic interaction was confirmed through photoluminescence quenching. The blended particles were spin coated on hole transporting layer which was coated on the ITO coated glass substrate and the uniformity of the dispersion of the particles in the polymer matrix was studied through its morphological analysis. This method would definitely provide a new pathway to utilize the aqueous medium synthesized semiconducting nanoparticles for photovoltaic applications.

Acknowledgements

The authors sincerely thank UGC, Govt of India (F.No. 42-885/2013 (SR)) for funding the research. S. Ananthakumar and J. Ramkumar sincerely thank Ministry of New and Renewable Energy (MNRE), Govt. of India for providing fellowship under the National Renewable Energy Fellowship (NREF) Scheme.

References

- Abd El-Sadek, M.S., Babu, S.M., 2010. Growth and optical characterization of colloidal CdTe nanoparticles capped by a bifunctional molecule. *Physica B* 405, 3279–3283.
- Biju, V., Itoh, T., Anas, A., Sujith, A., Ishikawa, M., 2008. Semiconductor quantum dots and metal nanoparticles; syntheses, optical properties and biological applications. *Anal. Bioanal. Chem.* 391, 2469–2495.
- Celik, D., Krueger, M., Veit, C., Schleiermacher, H.F., Zimmermann, B., Allard, S., Dumsch, I., Scherf, U., Rauscher, F., Niyamakom, P., 2012. Performance enhancement of CdSe nanorod-polymer based solar cells utilizing a novel combination of post-synthetic surface treatment. *Sol. Energy Mater. Sol. Cells* 98, 433–440.
- Chen, H.C., Lai, C.W., Wu, I.C., Pan, H.R., Chen, I.W.P., Peng, Y.K., Liu, C.L., Chen, C.H., Chou, P.T., 2011. Enhanced performance and air stability of 3.2% hybrid solar cells: how the functional polymer and CdTe nanostructure boost the solar cell efficiency. *Adv. Mater.* 23, 5451–5455.
- Chen, J., Zhao, D.W., Song, J.L., Sun, X.W., Deng, W.Q., Liu, X.W., Lei, W., 2009. Directly assembled CdSe quantum dots on TiO₂ in aqueous solution by adjusting pH value for quantum dot sensitized solar cells. *Electrochem. Commun.* 11, 2265–2267.
- Cheng, K.H., Ajimo, J., Chen, W., 2008. Exploration of functionalized CdTe nanoparticles for latent fingerprint detection. *J. Nanosci. Nanotechnol.* 3, 1170–1173.
- Ding, J., Wang, X., Zhuo, L.H., Tang, B., 2009. Hierarchical assembly of CdTe nanotubes and nanowires at water–oil interface. *J. Mater. Chem.* 19, 3027–3032.
- Fan, Z., Zhang, H., Yu, W., Xing, Z., Wei, H., Dong, Q., Tian, W., Yang, B., 2011. Aqueous-solution processed hybrid solar cells from poly(1,4-naphthalene vinylene) and CdTe nanocrystals. *Appl. Mater. Interfaces* 3, 2919–2923.
- Fu, W., Shi, Y., Qiu, W., Wang, L., Nan, Y., Shi, M., Li, H., Chen, H., 2012. High efficiency hybrid solar cells using post deposition ligand exchange by monothiol. *Phys. Chem. Chem. Phys.* 14, 12094–12098.
- Gallardo, D., Dunn, S., Gaponik, N., Eychmuller, A., 2007. Fabrication and characterization of red-emitting electroluminescent devices based on thiol-stabilized semiconductor nanocrystals. *Appl. Phys. Lett.* 90, 034107.
- Gao, M., Kristein, S., Mohwald, H., Rogach, A.L., Kornowski, A., Eychmuller, A., Weller, H., 1998. Strongly photoluminescent CdTe nanocrystals by proper surface modification. *J. Phys. Chem. B* 102, 8360–8363.
- Gaponik, N.P., Talapin, D.V., Rogach, A.L., 1999. A large emitting device based on a CdTe nanocrystal/polyaniline composite. *Phys. Chem. Chem. Phys.* 1, 1787–1789.
- Gaponik, N., Talapin, D.V., Rogach, A.L., Eychmuller, A., Weller, H., 2002. Efficient phase transfer of luminescent thiol-capped nanocrystals: from water to nonpolar organic solvents. *Nano Lett.* 2, 803–806.
- Green, M., Harwood, H., Barrowman, C., Rahman, P., Eggeman, A., Frestry, F., Dobson, P., Ng, T., 2007. A facile route to CdTe nanoparticles and their use in bio-labelling. *J. Mater. Chem.* 17, 1989–1994.
- Gunes, S., Neugebauer, H., Sariciftci, N.S., Roither, J., Kovalenko, M., Pillewein, G., Heiss, W., 2006. Hybrid solar cells using HgTe nanocrystals and nanoporous TiO₂ electrodes. *Adv. Funct. Mater.* 16, 1095–1099.
- Guijarro, N., Villarreal, T.L., Sero, I.M., Bisquert, J., Gomez, R., 2009. CdSe quantum dot-sensitized TiO₂ electrodes: effect of quantum dot coverage and mode of attachment. *J. Phys. Chem. C* 113, 4208–4214.
- Jiang, H., Jia, J., 2007. Complete, reversible phase transfer of luminescent CdTe nanocrystals mediated by hexadecylamine. *J. Mater. Chem.* 18, 344–349.
- Kumar, S., Nann, T., 2004. First solar cells based on CdTe nanoparticles/MEH-PPV composite. *J. Mater. Res.* 19, 1990–1994.
- Kovalenko, M.V., Kaufmann, E., Pachinger, D., Roither, J., Huber, M., Stangl, J., Hesser, G., Schaffler, F., Heiss, W., 2006. Colloidal HgTe nanocrystals with widely tunable narrow band gap energies: from telecommunications to molecular vibrations. *J. Am. Chem. Soc.* 128, 3516–3517.
- Li, L., Qian, H., Fang, N., Ren, J., 2006. Significant enhancement of the quantum yield of CdTe nanocrystals synthesized in aqueous phase by controlling the pH and concentrations of precursor solutions. *J. Lumin.* 116, 59–66.
- Lokteva, I., Radychev, N., Witt, F., Borchert, H., Parisi, J., Olesiak, J.K., 2010. Surface treatment of CdSe nanoparticles for application in hybrid solar cells: the effect of multiple ligand exchange with pyridine. *J. Phys. Chem. C* 114, 12784–12791.
- Moule, A.J., Chang, L., Thambidurai, C., Vidu, R., Stroeve, P., 2012. Hybrid solar cells: basic principles and the role of ligands. *J. Mater. Chem.* 22, 2351–2368.
- Murray, C.B., Norris, D.J., Bawendi, M.G., 1996. Synthesis and characterization of nearly monodisperse CdE (E = sulphur, selenium, tellurium) semiconductor nanocrystallites. *J. Am. Chem. Soc.* 115, 8706–8715.
- Olson, J.D., Rodriguez, Y.W., Yang, L.D., Alers, G.B., Carter, S.A., 2010. CdTe Schottky diodes from colloidal nanocrystals. *Appl. Phys. Lett.* 96, 242103.
- Qin, B., Zhao, Z., Song, R., Shanbhag, S., Tang, Z., 2008. A temperature-driven reversible phase transfer of 1-(diethylamino)ethanethiol-stabilized CdTe nanoparticles. *Angew. Chem.* 120, 10023–10026.
- Rogach, A.L., Gaponik, N., Lupton, J.M., Bertoni, C.D., Gallardo, E., Dunn, S., Pira, N.L., Paderi, M.P., Repetto, Romanov, S.G., Dwyer, C.O., Torres, C.M.S., Eychmuller, A., 2008. Light-emitting diodes with semiconductor nanocrystals. *Angew. Chem. Int. Ed.* 47, 6538–6549.
- Wang, L., Liu, Y., Jiang, X., Qin, D.H., Cao, Y., 2007. Enhancement of photovoltaic characteristics using a suitable solvent in hybrid polymer/multiarmed CdS nanorods solar cells. *J. Phys. Chem. C* 111, 9538–9542.

- Wuister, S.F., Swart, L., Driel, F.V., Hickey, S.G., Donega, C.D.M., 2003. Highly luminescent water-soluble CdTe quantum dots. *Nano Lett.* 3, 503–507.
- Yu, W.W., Wang, Y.A., Peng, X., 2003. Formation and stability of size, shape, and structure-controlled CdTe nanocrystals: ligand effects on monomers and nanocrystals. *Chem. Mater.* 15, 4300–4308.
- Zhao, K., Dai, J., Zhuang, J., Li, J., Yang, W., 2007. Highly efficient transfer of water soluble ZnS:Mn²⁺ nanocrystal into organic phase by 1-dodecanethiol. *Colloids Surf. A: Physicochem. Eng. Aspects* 296, 154–157.



Hydrothermal synthesis and characterization of CuInSe₂ nanoparticles using ethylenediamine as capping agent

J. Ramkumar, S. Ananthakumar, S. Moorthy Babu*

Crystal Growth Centre, Anna University, Chennai 600 025, India

Received 31 July 2013; received in revised form 8 April 2014; accepted 12 April 2014

Available online 9 May 2014

Communicated by: Associate Editor Smagul Zh. Karazhanov

Abstract

Ethylenediamine capped CuInSe₂ nanoparticles were synthesized by wet chemical method at room temperature and hydrothermal method at 150 °C for 2 h at two different mole ratio of the capping agent. The effect of the synthesis method and ratio of the capping agent on the optical, structural, and morphology of the synthesized nanoparticles were analyzed. The optical property of the synthesized nanoparticles was estimated from the UV–Vis spectra and also from the emission spectra. The surface capping was confirmed through the FT-IR. Powder XRD analysis reveals that the nanoparticles exhibit wurtzite phase and the crystallinity increases while increasing the capping ratio and hydrothermally synthesized nanoparticles show higher crystallinity. Raman analysis shows that the hydrothermally synthesized samples exhibit B₂ (LO) mode. The surface morphology was modified depending on the synthesis method and capping agent ratio (i.e.) rod like and cube like morphology were obtained for the hydrothermally synthesized nanoparticles with 5 and 10 mol ratio of the capping agents respectively.

© 2014 Elsevier Ltd. All rights reserved.

Keywords: Hydrothermal; Band gap; Wurtzite; Morphology

1. Introduction

Third generation photovoltaics aspire to unite high efficiency with low cost. Solution-processed colloidal nanocrystals in solar cells offer considerable promise as a third-generation photovoltaic candidates (Debnath et al., 2011). Significant advancement in the last two decades has led to exponential growth in the synthesis and assembly of semiconductor nanocrystals (NCs). These NCs provide unique opportunities for the development of next generation organic/inorganic hybrid solar cells as one of the most promising alternatives to Si solar cells to deliver efficient

energy conversion with inexpensive fabrication (Zhao et al., 2011). Semiconductor NCs can be well dispersed in many solvent and deposited as films via low cost process such as spin-casting, dip-coating and printing, and easily mixed with polymers to form hybrid light-absorbing layers with enhanced performance. An important parameter in their use is the band gap energy of NCs, which can be tuned by their size, shape and composition. The electronic properties of the semiconductor nanoparticles were influenced by their stoichiometric composition, morphology, and impurities, which are dependent on the method and conditions of preparation (Grisaru et al., 2003). Nanoparticle based coating techniques are inexpensive since they do not require high temperature and high vacuum processing (Juhaiman et al., 2010). The exploration of NC applications has mainly focused on cadmium- and lead-based

* Corresponding author. Tel.: +91 44 22358333.

E-mail addresses: smoorthybabu@gmail.com, babu@annauniv.edu (S. Moorthy Babu).

NCs, which have a doubtful future because of their high toxicity. A current challenge is to move away from these toxic materials and turn to more environmental friendly semiconductor NCs. In this direction, I–III–VI₂ semiconductors, such as CuInS₂, CuInSe₂, and AgInS₂, have been identified as candidates for low toxicity light-emitters and solar-harvesters. CuInSe₂ has the lowest direct band gap of ~1.04 eV and large calculated exciton Bohr radius of ~10.6 nm, and the bulk material has excellent photovoltaic performance (Zhong et al., 2011). CuInSe₂ has received considerable interest as an important photovoltaic material due to its very high optical absorption coefficient. The band gap of CuInSe₂ could be varied from 1.04 to 1.68 eV via adding gallium ions, can be obtained with both p/n-type conductivity depending upon the preparation conditions. This permits the formation of homo and hetero junctions from CuInSe₂ with selective dopants. Also, these junctions have electrical properties that are compatible for photovoltaic device fabrication. There are many non-vacuum solution based techniques available to prepare CuInSe₂ nanoparticles such as colloidal, hydrothermal, sonochemical, microwave assisted wet chemical, and sol–gel synthesis. These preparation processes for CIS nanoparticles are comparatively simple and inexpensive. Among the various non-vacuum processes wet chemical and hydrothermal synthesis have become very attractive nowadays (Lin and Yaw-Shyan 2012., and Chung-Hsien et al., 2011).

Li et al. (1999) has synthesized nanowhiskers and nanoparticles of CuInSe₂ using ethylenediamine as solvent using solvothermal method at a temperature of 180 °C for 15 h. CuInSe₂ and CuInGaSe₂ nanoparticles were synthesized by solvothermal method in an autoclave with alkylamine as a solvent at 180–250 °C for 36 h resulting in nanoparticles and nanorods (Kim et al., 2004). Similarly, single-crystalline CuInSe₂ nanorods have been successfully synthesized in a soft solvothermal reaction with ethylenediamine as the reaction solvent (Yang and Chen, 2006). CuInSe₂ microspheres were synthesized by a solvothermal method with a mixed solvent of ethylenediamine and ethanol (1:1, v/v). Different morphologies of CuInSe₂ such as platelets and rods were obtained by selecting different solvothermal conditions (Zhang et al., 2007). Chen et al. (2010) have concluded that high pure CuInSe₂ nanoparticles can be obtained using ethylenediamine as solvent in the temperature range of 180–220 °C. The micro emulsion-derived CuInSe₂ powders exhibited spherical shape and were much smaller than the powders prepared via the conventional solvothermal process (Lu et al., 2010). Well-controlled wurtzite CuInS₂ hexagonal plates were obtained when triethanolamine is added as an agent while ethylene glycol as solvent (Sheng et al., 2011). In general, the magnitude of nanoparticles prepared via solution method can be controlled by the parameters such as reaction time, temperature, pH value, concentrations of precursors, solvent, and so on.

In the present work, efforts were made to synthesize CuInSe₂ nanocrystals by simple in-expensive wet chemical

and hydrothermal process using ethylenediamine as capping agent. Synthesis was carried out at relatively low temperature in two different mole ratio's of ethylenediamine. Ethylenediamine was used as solvent so far, rather than a surfactant or as a capping agent. The nitrogen atom present in the amine group acts as a chelating agent and provides the one dimensional growth while it is used as capping agent. Hence, attempts were made to synthesis CuInSe₂ nanoparticles using water as solvent by wet chemical method at room temperature. Hydrothermal method was used with ethylenediamine as capping agent at relatively lower temperature of 150 °C and a short duration time of 2 h. Previous reports on hydrothermal indicate synthesis at the temperature range of 180–220 °C and time duration of more than 15 h. CuInSe₂ nanoparticles were synthesized by two different mole ratio of capping agent. The effect of the synthesis method and ratio of the capping agent with the precursors on the structural and morphology of the synthesized nanoparticles were analyzed through X-ray Diffraction, Raman analysis, Scanning Electron Microscope and Transmission Electron Microscope.

2. Experimental details

All the chemicals used were of analytical grade and used without further purification (i.e.) cupric chloride (Alfa Aesar), indium chloride (Alfa Aesar), sodium selenite (SRL) and ethylenediamine (CDH). Deionised water was used as solvent. For the synthesis, separate stock solutions (A, B, C) were prepared. For the wet chemical synthesis, solution A contains 1 mM of cupric chloride dissolved in 50 ml of Millipore water in the presence of 5 mM of ethylenediamine. Solution B contains 1 mM of indium chloride dissolved in 50 ml of Millipore water in the presence of 5 mM of ethylenediamine. Solution C contains 2 mM of sodium selenite dissolved in 50 ml Millipore water in the presence of 10 mM of ethylenediamine. An equal volume of these solutions A, B and C were mixed together and stirred continuously for 2 h at room temperature. Similarly for the hydrothermal method the reaction mixer was taken in a Teflon lined autoclave of 200 ml capacity. The autoclave was sealed and maintained at 150 °C for 2 h in a resistive heating box furnace and then allowed to cool to room temperature. The formation of black color precipitate confirms the formation of the material and fine powders of ethylenediamine stabilized CuInSe₂ nanoparticles were filtered off. The powders were washed with distilled water and ethanol for about three to four times in order to remove the residual impurities. Then it was dried at 45 °C for 1 h. The mole ratio of Cu, In, Se and ethylenediamine in the reaction was 1:1:2:5 (5 EW) for the wet chemically synthesized sample and 5 EA for the hydrothermally synthesized sample respectively. Similarly another reaction was carried out with 10 mol ratio of the capping agent i.e. the mole ratio of Cu, In, Se and ethylenediamine was kept as 1:1:2:10 (10 EW) for the wet chemically synthesized and 10 EA for the hydrothermally synthesized samples.

The optical properties were analyzed through the UV–Vis absorption spectra recorded on a double beam ultraviolet–visible spectrophotometer with a photomultiplier tube (PMT) detector. (V650, Jasco Analytical Instruments, Japan). The emission spectra were recorded using Jobin Yvon FLUOROLOG – FL3-11 Fluorescence Spectrometer. The phase and the crystallographic structure of the products were identified by X-ray diffraction (XRD; Rigaku Ultima III Japan, Cu K α : 1.541). Raman analysis was carried out using Renishaw inVia Raman microscope operating with 785 nm laser with spatial resolution of one micrometer. The morphology and particle size of the products were investigated by the field emission scanning electron microscopy (FESEM; SU6600-Hitachi Japan at 15 kV) and high resolution transmission electron microscopy (HRTEM; TECNAI G²-FEI company at 300 kV).

3. Results and discussion

The optical absorption of the synthesized samples is shown in Fig. 1. In the optical absorption spectra, a broad absorption onset and shoulder were observed; the shoulder was attributed to the optical band gap. The spectra indicate that maximum absorption was observed for the samples synthesized by hydrothermal method with high mole ratio of capping agent i.e. 10 EA. The absorption decreases in the order for 10 EW, 5 EA and 5 EW. The sample 5 EW has minimum absorption among the four samples. The existence of a band tail was confirmed from the absorption measurements which clearly show the strong band tail absorption below the energy gap.

Fig. 2 shows the emission spectra of the CuInSe₂ nanoparticles. Emission spectra were recorded at room temperature with an excitation wavelength of 460 nm for all the samples. A sharp emission was observed at 630 nm which corresponds to the band edge emission for the samples. This peak is stable and does not shift with variation in intensity of power as well as small variation in wavelength. There is another defective emission at about 758 nm. This

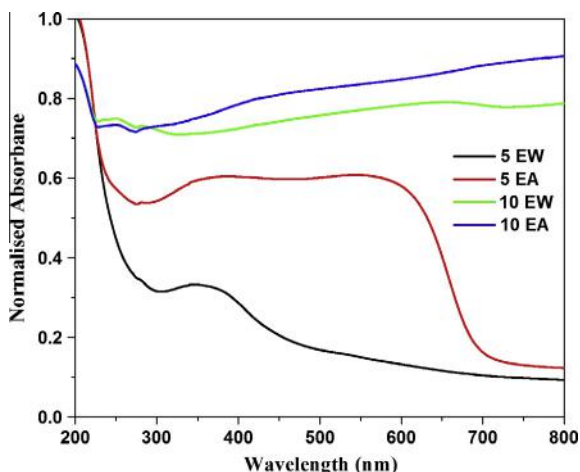


Fig. 1. UV–Vis spectra of CuInSe₂ nanoparticles.

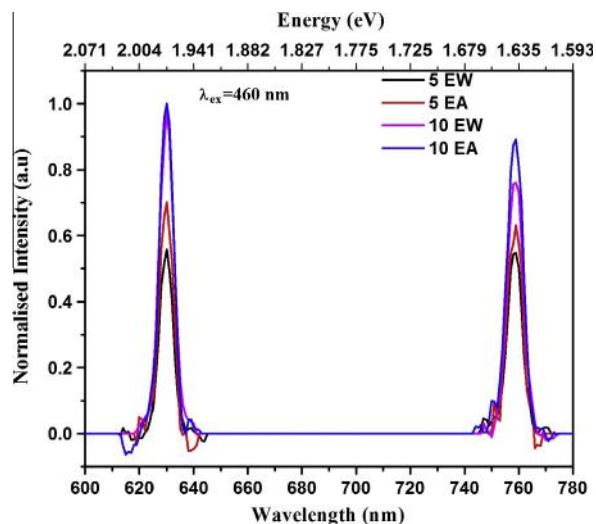


Fig. 2. Emission spectra of CuInSe₂ nanoparticles.

emission peak is blue shifted from the optical absorption peak. This emission is related to the intermediate optical band gap states that appear in defective CuInSe₂ and, therefore, emissions related with these excitons have wavelengths smaller than the optical band gap of CuInSe₂ (Liborio et al., 2011). This defect emission at 758 nm is sharp and does not shift with variation of intensity of power of the excitation wavelength. The possible origins of defect levels in CuInSe₂ are due to the atomic vacancies, atoms on wrong lattice site (antisite) and interstitial atoms (Sites and Hollingsworth, 1987). While considering the formation energy of defects and the composition of CuInSe₂, the defect peaks has been attributed to transitions from the conduction band to various acceptor levels in the material (Wasim, 1986). The narrow emission peak at 758 nm clearly indicates the level of high density trap states associated with the synthesized nanoparticles. The defect states may be due to Cu on an In site (acceptor site) (Lange et al., 1985; Schon et al., 1997). The transition from the conduction band to the Cu_{In} antisites (acceptor sites) might have led to the strong emission at 758 nm. Usually, the broad luminescence results in chalcopyrite system due to the donor–acceptor pair mechanism (Shen et al., 1996). But in the present case, the obtained narrow emission peak can be correlated with the stoichiometric ratio of Cu/In in the system. It has been observed that the narrow emission is a common one for the nearly stoichiometric CuInSe₂ (Siebentritt et al., 2004). Besides, this observation can also be related with the absence of potential fluctuations in the CuInSe₂ nanocrystals which results this narrow emission (Krustok et al., 2006).

The FT-IR spectra of ethylenediamine capped CuInSe₂ synthesized by wet chemical as well as hydrothermal method is shown in Fig. 3. The intense broad band between 2500 cm⁻¹ and 3750 cm⁻¹ was due to –OH stretching vibration of water molecule. The bending vibration of water yielded a peak at 1635 cm⁻¹ for both the samples. As the –OH stretching vibration of water was very much

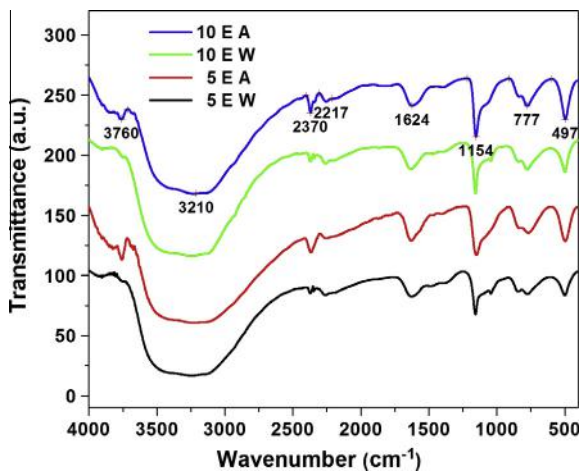


Fig. 3. FT-IR spectra of ethylenediamine capped CuInSe₂ nanoparticles.

broad, the N–H stretching vibration were not clearly resolved. Eventhough, the peaks due to the –NH₂ asymmetric and symmetric vibration of –NH₂ group showed maxima at about 3400 and 3250 cm⁻¹. The –CH₂ bending vibration of EDA were clearly seen just below 1500 cm⁻¹. More importantly the C–N stretching vibration that occurred at 1157 cm⁻¹ appeared broad covering the region 1100–1200 cm⁻¹. It establishes that the nanoparticles were capped with EDA. The peak at 772 and 499 cm⁻¹ in the spectra were tentatively assigned to metal–selenide vibrations.

XRD pattern of the synthesized nanoparticles is shown in Fig. 4. The major peaks which are common to both sphalerite and chalcopyrite structure are at 26.65°, 44.22°, 52.39°, 64.36° and 70.90°. Similarly, the minor peaks for the chalcopyrite structure are at 17.14°, 27.74° and 35.55° (Guo et al., 2008). The binary phase Cu_{2-x}Se has its own characteristic peaks at 26.90°, 44.78° and 53.02° (Choi et al., 2010). The absence of peaks in these region shows that the synthesized nanoparticles does not belong to either sphalerite or chalcopyrite and moreover it does

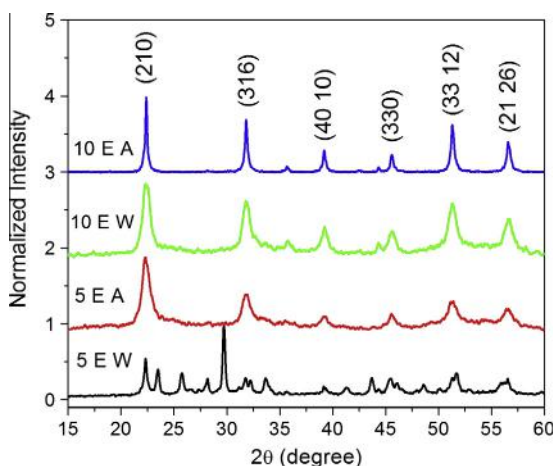


Fig. 4. XRD patterns of CuInSe₂.

not have any secondary binary phases also. The determined diffraction peaks match well with the JCPDS No. 38-0956. The peaks were assigned at 22.32°, 31.82°, 39.2°, 45.56°, 51.28°, 56.58° corresponding to (210), (316), (4010), (330), (3312), (2126) planes. The diffraction peaks of sample 5 EA are very much broadened as compared to those of sample 10 EW, indicating the poor crystallinity of CuInSe₂ with low molar ratio of the capping agent. At the same time the hydrothermally synthesized sample 10 EA has better crystallinity among all the samples. The XRD patterns confirm the wurtzite phase of CuInSe₂.

Raman spectra of CuInSe₂ nanoparticles prepared at various mole ratio of ethylenediamine is presented in Fig. 5. Raman spectra contain valuable information concerning secondary phases, lattice strains and chemical composition. The Raman spectra of CuInSe₂ show A₁ mode at approximately 175 cm⁻¹, generally observed in the I–III–VI₂ chalcopyrite compounds. The intensity of Raman peaks strongly depends on the surface morphology and the phase composition in CuInSe₂. A₁ band is the most intense band in the spectra of chalcopyrite type compounds. The absence of peak at 258 cm⁻¹ indicates the absence of Cu_xSe secondary phase, with symmetry of lattice vibrations different from chalcopyrite (Zaretskaya et al., 2003). The spectral position of Cu–Au (CA) related bands lays at higher frequencies than the totally symmetric band of the respective chalcopyrite structure. The CA ordered phase exhibits three distinct fundamental lattice modes at 175, 185 and 232 cm⁻¹ (Park et al., 1994). In the present case the peaks observed at 236 cm⁻¹ was attributed to highest B₂ LO mode. The intensity of B₂ mode increases with increasing ratio of the capping agent. Raman analysis reveals that the B₂ (LO) mode has higher intensity in the hydrothermally synthesized samples while compared to the wet chemically synthesized samples.

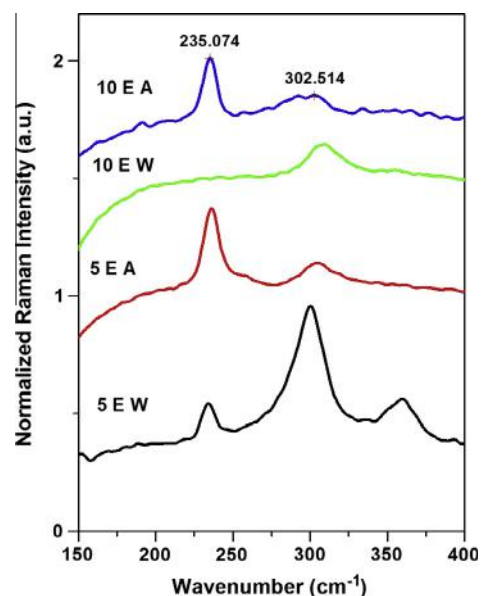


Fig. 5. Raman spectra of CuInSe₂ nanoparticles.

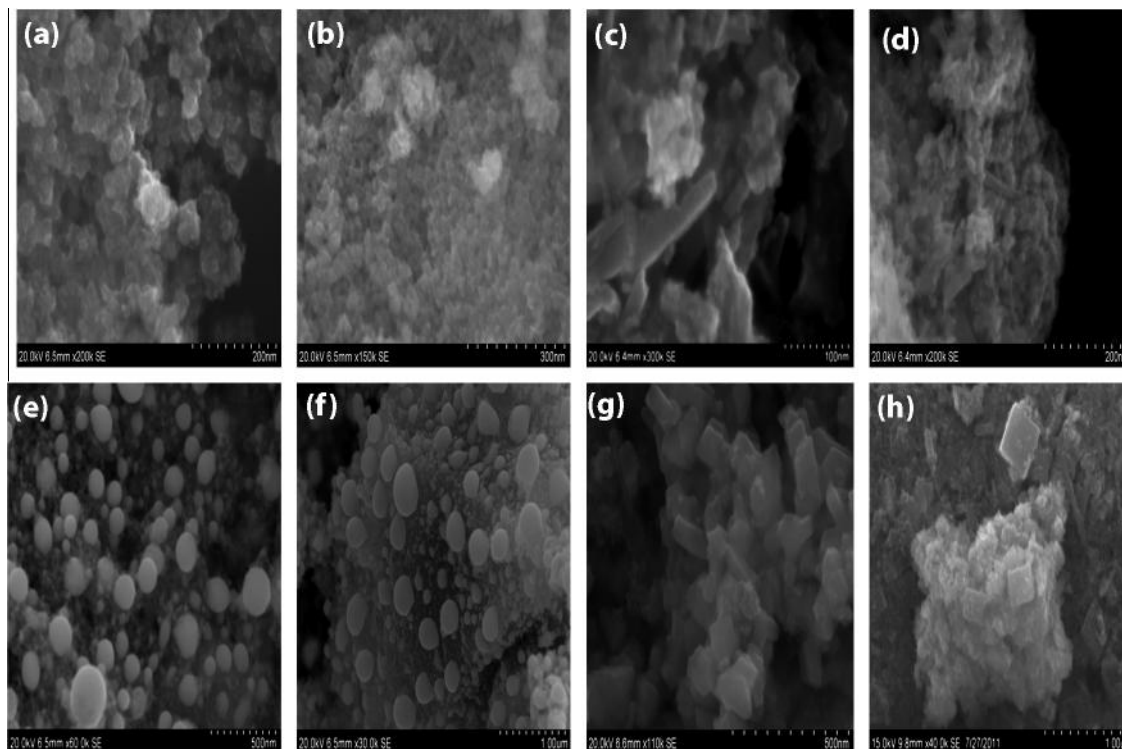


Fig. 6. SEM images 5 EW (a and b), 5 EA (c and d), 10 EW (e and f) and 10 EA (g and h).

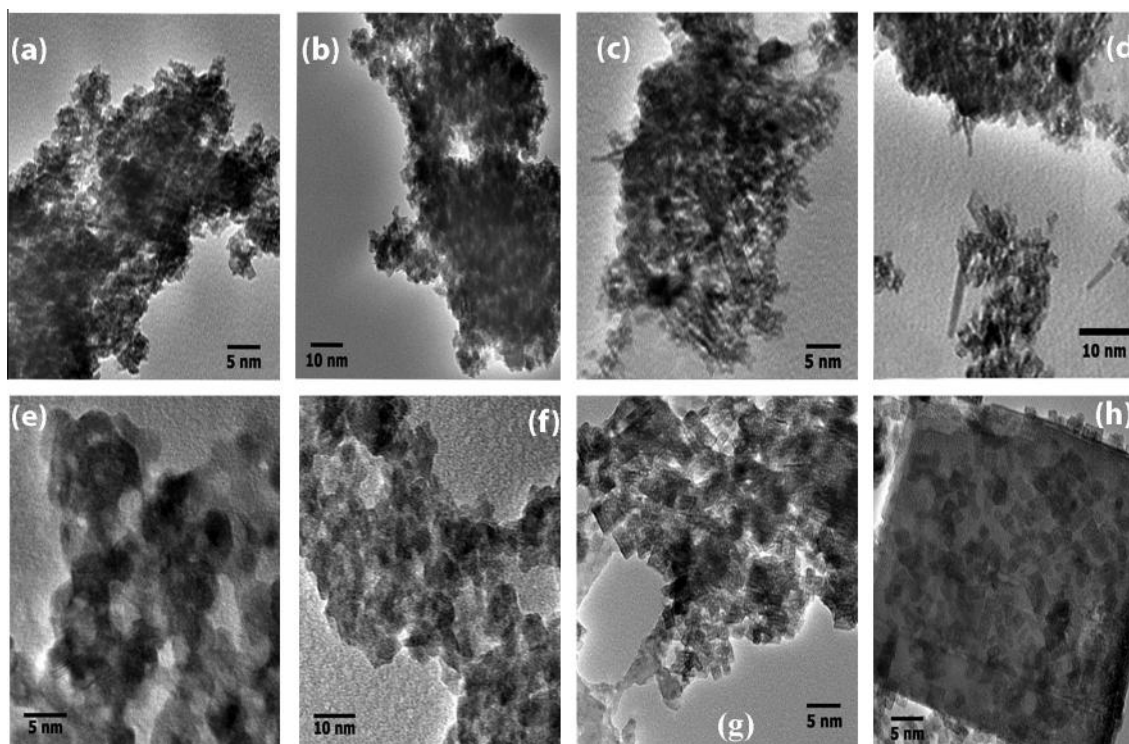


Fig. 7. TEM images 5 EW (a and b), 5 EA (c and d), 10 EW (e and f) and 10 EA (g and h).

Figs. 6(a–d) and 7(a–d) shows the SEM & TEM images of CuInSe₂ nanoparticles obtained for 5 mol ratio of the capping agent by wet chemical and hydrothermal method respectively. Figs. 6(a) and 7(a) illustrate that the

morphology of the nanoparticles are sponge one. Figs. 6(c) and 7(c) indicates that the synthesized product is mainly composed of nanorods with diameters of about 6–10 nm. As seen in Figs. 6(c) and 7(d), at higher

magnification the data reveals that the nanorods are randomly oriented. Figs. 6(e–h) and 7(e–h) illustrate the SEM & TEM images of CuInSe₂ obtained by wet chemical and hydrothermal method for 10 mol ratio of the ethylenediamine. Figs. 6(e) and 7(e) clearly indicates that the synthesized product has spherical morphology for the wet chemical synthesis. Hydrothermally synthesized samples have nanocubes like morphology revealed from Figs. 6(g) and 7(g). At higher magnification, Figs. 6(h) and 7(h) it reveals that the nanospheres and nanocubes are monodispersed uniformly. The influence of the capping agent on the morphology of the CuInSe₂ was clearly observed from the SEM and TEM analysis. Moreover, Arici et al. (2004) has reported that this morphology of the CuInSe₂ nanoparticles plays an important role in the hybrid solar cell systems.

4. Conclusion

A convenient simple wet chemical and hydrothermal synthesis method was used for the synthesis of CuInSe₂ nanoparticles using ethylenediamine as capping agent. The synthesis method and ratio of capping agent influences the structural, optical and morphological properties of the synthesized CuInSe₂ nanoparticles. The evolution of crystalline phase and morphology of the products were tuned by varying the synthesis method and capping agent ratio. Wurtzite phase CuInSe₂ nanoparticles were synthesized by wet chemical synthesis at room temperature and also by hydrothermal method at 150 °C for 2 h. The crystallinity was found to be higher for the hydrothermally synthesized samples with 10 mol ratio of the capping agent. While the optical absorption and emission is concerned the 10 EA has higher absorption and emission intensity followed by the 10 EW. In the wet chemical synthesis the morphology was tuned from sponge to sphere when we increase the mole ratio of the capping agent. The 10 mol ratio of the capping agent leads to cube like morphology while 5 mol ratio leads to the formation of rod like morphology in the hydrothermal synthesis. The optical, structural and morphology of the CuInSe₂ was varied by changing the synthesis method as well as capping agent ratio and the synthesized nanoparticles can be used for further application as absorber materials for photovoltaic devices.

Acknowledgments

The authors sincerely thank UGC, Govt of India (F. No 42-855/2013(SR)) for providing financial support. J. Ramkumar and S. Ananthakumar sincerely thanks Ministry of New and Renewable Energy (MNRE), Govt of India for providing fellowship under the National Renewable Energy Fellowship (NREF) scheme.

References

- Arici, E., Hoppe, H., Schaffler, F., Meissner, D., Malik, M.A., Sariciftci, N.S., 2004. Morphology effects in nanocrystalline CuInSe₂-conjugated polymer hybrid systems. *Appl. Phys. A* 79, 59–64.
- Chen, Huiyu, Yu, Seong-Man, Shin, Dong-Wook, Yoo, Ji-Beom, 2010. Solvothermal synthesis and characterization of chalcopyrite CuInSe₂ nanoparticles. *Nanoscale Res. Lett.* 5, 217–223.
- Choi, Jaewon, Kang, Narae, Yang, Hye Yun, Kim, Hae Jin, Son, Seung Uk, 2010. Colloidal synthesis of cubic-phase copper selenide nanodisks and their optoelectronic properties. *Chem. Mater.* 22, 3586–3588.
- Wu, Chung-Hsien, Chen, Fu-Shan, Lin, Shin-Hom, Chung-Hsin, Lu, 2011. Preparation and characterization of CuInSe₂ particles via the hydrothermal route for thin-film solar cells. *J. Alloys Compd.* 509, 5783–5788.
- Debnath, Ratan, Bakr, Osman, Sargent, Edward H., 2011. Solution-processed colloidal quantum dot photovoltaics: a perspective. *Energy Environ. Sci.* 4, 4870.
- Grisaru, Haviv, Palchik, Oleg, Gedanken, Aharon, 2003. Microwave-assisted polyol synthesis of CuInTe₂ and CuInSe₂ nanoparticles. *Inorg. Chem.* 42 (22), 7148–7155.
- Guo, Qijie, Kim, Suk Jun, Kar, Mahaprasad, Shafarman, William N., Birkmire, Robert W., Stach, Eric A., Agrawal, Rakesh, Hillhouse, Hugh W., 2008. Development of CuInSe₂ nanocrystal and nanoring inks for low-cost solar cells. *Nano Lett.* 8, 2982–2987.
- Juhaiman, Layla Al, Scoles, Ludmila, Kingston, David, Patarachao, Bussaraporn, Wang, Dashan, Bensebaa, Farid, 2010. Green synthesis of tunable Cu(In_{1-x}Ga_x)Se₂ nanoparticles using non-organic solvents. *Green Chem.* 12, 1248–1252.
- Kim, Ki-Hyun, Chun, Young-Gab, Park, Byung-Ok, Yoon, Kyung-Hoon, 2004. Synthesis of CuInSe₂ and CuInGaSe₂ nanoparticles by solvothermal route. *Mater. Sci. Forum* 449–452, 273–276.
- Krustok, J., Jagomagi, A., Grossberg, M., Raudoja, J., Danilson, M., 2006. Photoluminescence properties of polycrystalline AgGaTe₂. *Sol. Energy Mater. Sol. Cells* 90, 1973–1982.
- Lange, P., Neff, H., Fearheiley, M., Bachmann, K.J., 1985. Photoluminescence and photoconductivity of CuInSe₂. *Phys. Rev. B* 31, 4074–4076.
- Li, Bin, Xie, Yi, Huang, Jiaying., Qian, Yitai., 1999. Synthesis by a solvothermal route and characterization of CuInSe₂ nanowhiskers and nanoparticles. *Adv. Mater.* 11, 1456–1459.
- Liborio, Leandro M., Bailey, Christine L., Mallia, Giuseppe, Tomić, Stanko, Harrison, Nicholas M., 2011. Chemistry of defect induced photoluminescence in chalcopyrites: the case of CuAlS₂. *J. Appl. Phys.* 109, 023519.
- Lin, Pei-Ying, Yaw-Shyan, Fu, 2012. Fabrication of CuInSe₂ light absorption materials from binary precursors via wet chemical process. *Mater. Lett.* 75, 65–67.
- Lu, Chung-Hsin, Lee, Chung-Han, Wu, Chung-Hsien, 2010. Microemulsion-mediated solvothermal synthesis of copper indium diselenide powders. *Sol. Energy Mater. Sol. Cells* 94, 1622–1626.
- Park, J.H., Yang, I.S., Cho, H.Y., 1994. Micro-Raman spectroscopy on polycrystalline CuInSe₂ formation. *Appl. Phys. A* 58, 125–128.
- Schon, J.H., Alberts, V., Bucher, E., 1997. Structural and optical characterization of polycrystalline CuInSe₂. *Thin Solid Films* 301, 115–121.
- Shen, W.Z., Shen, S.C., Chang, Y., Tang, W.G., Yip, L.S., Lam, W.W., Shih, I., 1996. Photoluminescence studies of CuInSe₂. *Infrared Phys. Technol.* 37, 509–512.
- Sheng, Xia, Wang, Lei, Luo, Yeping, Yang, Deren, 2011. Synthesis of hexagonal structured wurtzite and chalcopyrite CuInS₂ via a simple solution route. *Nanoscale Res. Lett.* 6, 562–567.
- Siebentritt, Susanne, Rega, Niklas, Zajogin, Alexander, Lux-Steiner, Martha Ch, 2004. Do we really need another PL study of CuInSe₂? *Phys Status Solidi (c)* 1, 2304–2310.
- Sites, J.R., Hollingsworth, R.E., 1987. Photoluminescence in polycrystalline CuInSe₂ solar cells. *Solar Cells.* 21, 379–386.

- Wasim, S.M., 1986. Transport properties of CuInSe₂. *Solar Cells* 16, 289–316.
- Yang, Yi-Han, Chen, Yit-Tsong, 2006. Solvothermal preparation and spectroscopic characterization of copper indium diselenide nanorods. *J. Phys. Chem. B* 110, 17370–17374.
- Zaretskaya, E.P., Gremenok, V.F., Riede, V., Schmitz, W., Bente, K., Zaleski, V.B., Ermakov, O.V., 2003. Raman spectroscopy of CuInSe₂ thin films prepared by selenization. *J. Phys. Chem. Solids* 64, 1989–1993.
- Zhang, Li, Liang, Jing, Peng, Shengjie, Shi, Yunhui, Chen, Jun, 2007. Solvothermal synthesis and optical characterization of chalcopyrite CuInSe₂ microspheres. *Mater. Chem. Phys.* 106, 296–300.
- Zhao, Lei, Pang, Xinchang, Adhikar, Ramkrishna, Petrich, Jacob W., Jeffries-EL, Malika, Lin, Zhiqun, 2011. Organic – inorganic nanocomposites by placing conjugated polymers in intimate contact with quantum rods. *Adv. Mater.* 23, 2844–2849.
- Zhong, Haizheng, Wang, Zhibin, Bovero, Enrico, Lu, Zhengong, van Veggel, Frank C.J.M., Scholes, Gregory D., 2011. Colloidal CuInSe₂ Nanocrystals in the quantum confinement regime: synthesis, optical properties, and electroluminescence. *J. Phys. Chem. C* 115, 12396–12402.

Conference Paper

Synthesis and Efficient Phase Transfer of CdSe Nanoparticles for Hybrid Solar Cell Applications

S. Ananthakumar, J. Ramkumar, and S. Moorthy Babu

Crystal Growth Centre, Anna University, Chennai 25, India

Correspondence should be addressed to S. Moorthy Babu; babu@annauniv.edu

Received 6 January 2013; Accepted 30 April 2013

Academic Editors: B. Bhattacharya and U. P. Singh

This Conference Paper is based on a presentation given by S. Ananthakumar at “International Conference on Solar Energy Photovoltaics” held from 19 December 2012 to 21 December 2012 in Bhubaneswar, India.

Copyright © 2013 S. Ananthakumar et al. This is an open access article distributed under the Creative Commons Attribution License, which permits unrestricted use, distribution, and reproduction in any medium, provided the original work is properly cited.

Colloidal cadmium selenide (CdSe) nanoparticles capped by a short chain thiol ligand thioglycolic acid (TGA) were prepared in aqueous medium at 100°C using sodium selenite as the selenium source. The prepared particles were efficiently transferred into organic phases through the partial ligand exchange process using 1-dodecanethiol (1-DDT). The FT-IR spectrum analysis shows the existence of the ligands on the surface of the nanoparticles in aqueous and organic phase through their characteristic modes. TEM analysis of the prepared samples reveals the size and crystalline nature of the particles. EDX analysis indicates the presence of respective elements in the resultant powdered sample. The possible mechanism of the phase transfer process was analysed. The resultant phase-transferred particles can efficiently be blended with a low band gap semiconducting polymer in a common solvent for active layer in hybrid solar cell fabrication. The results are discussed in detail.

1. Introduction

II–VI group semiconductor nanoparticles have attracted much attention in recent years for solar cells due to their size tunable optical properties, absorption of light in the visible region, and so forth [1]. Among them, CdSe nanoparticles have shown potential applications due to their high quantum yield, the tunable emission spectrum wavelength, and so forth. So far, organometallic precursors-based syntheses are widely reported which need high temperature, pyrophoric nature and extremely toxic one [2]. The aqueous-based synthesis of CdSe nanoparticles is, hence, much attracted. But in application purpose, the major hindrance of aqueous synthesized particles is the setback in terms of solubility in organic solvents. This makes them keeping away from their usage in solar cells. But, by applying phase transfer chemistry, it is possible to replace the ligands on the surface of the nanoparticles thereby making them into photovoltaics and other applications. Phase transfer of semiconductor nanoparticles was reported using various types of ligands [3]. Here, in the present work, aqueous synthesis of CdSe

nanoparticles is reported using air stable selenium source, sodium selenite. The synthesized particles were transferred into organic phase using 1-dodecanethiol through partial ligand exchange strategy. The synthesized and phase-transferred nanoparticles were studied using various characterization techniques.

2. Experiment

2.1. Chemicals. Cadmium chloride (CdCl_2), sodium selenite (Na_2SeO_3), trisodium citrate dihydrate ($\text{Na}_3\text{C}_6\text{H}_5\text{O}_7$), sodium borohydride (NaBH_4), sodium hydroxide (NaOH), thioglycolic acid (TGA), 1-dodecanethiol (1-DDT), and acetone ($\text{C}_7\text{H}_6\text{O}$) are used.

2.2. Synthesis of CdSe Nanoparticles. Cadmium chloride was dissolved in water and with this thioglycolic acid (TGA) added in dropwise under vigorous stirring. Trisodium citrate dihydrate, sodium selenite, and sodium borohydride were added with this mixture successively. The entire mixture was

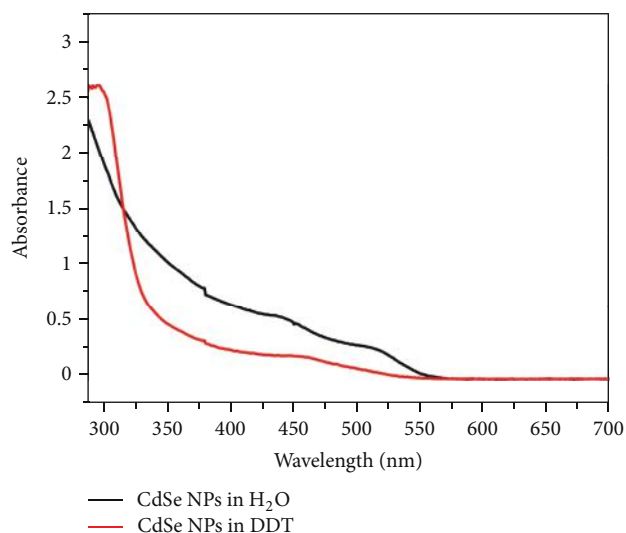
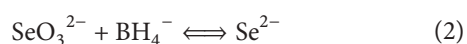
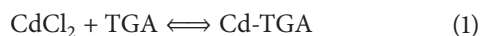


FIGURE 1: Absorption spectra of the CdSe nanoparticles in water and in chloroform with 1-DDT.

taken in the three-necked flask and allowed into heat under the nitrogen atmosphere. The temperature was followed as 100°C. The appearance of yellow color of the solution represents the formation of the CdSe nanoparticles in the solution. The solution was strongly refluxed to get different sizes at different time intervals. The overall reaction of the formation of CdSe nanoparticles can be summarized as



The synthesized particles were precipitated by adding isopropanol by strong stirring. The particles were separated through centrifugation and dried in vacuum.

2.3. Phase Transfer of CdSe Nanoparticles. Aqueous synthesized cadmium selenide nanoparticles were transferred into organic medium through the method proposed by Gaponik et al. [4]. In brief, about 50 ml of the synthesized particles were taken in the beaker and equal volume of the 1-dodecanethiol was added and with this about 70 ml of acetone was added. This mixture was allowed into mild heating with constant stirring. After about 10 minutes, the transfer of CdSe nanoparticles from aqueous to 1-DDT medium was achieved. This organic phase was carefully separated out and mixed with chloroform. Then methanol was added dropwise under stirring which made the particles as powder form settled under bottom of the vessel. The particles were finally separated out and redispersed in chloroform. These particles are described as organically soluble CdSe nanoparticles (OS-CdSe).

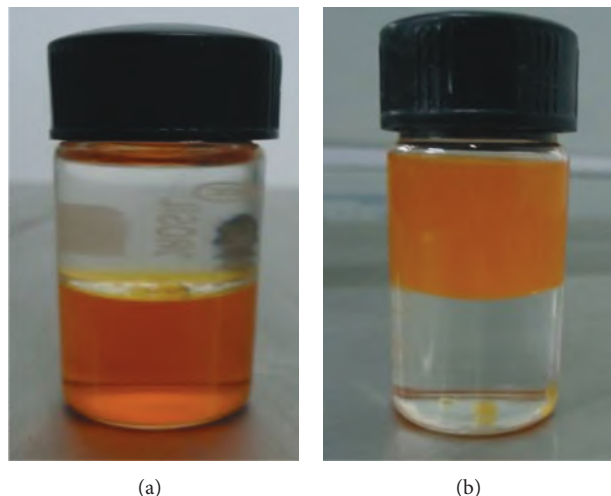


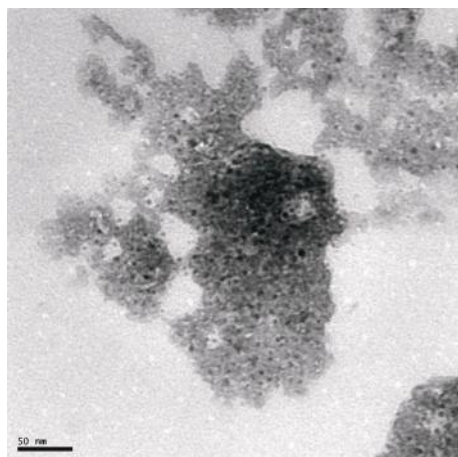
FIGURE 2: Existence of CdSe nanoparticles in water (a) and in 1-dodecanethiol (b).

3. Results and Discussion

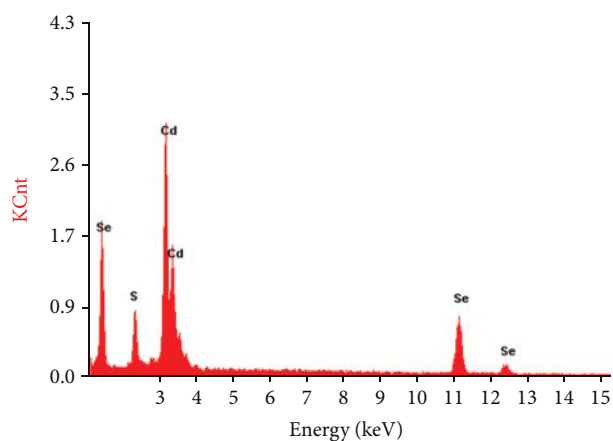
UV-visible spectrum of the synthesized particles and phase-transferred nanoparticles is given in Figure 1. The spectrum clearly shows that the particles have the approximately similar absorption edge in two phases. The slight variation in their spectra may be due to their change of medium. The photographical representation of the synthesized and phase-transferred particles is shown in Figure 2.

It was observed that when 1-dodecanethiol was added into the aqueous synthesized particles, a clear distinct boundary between the two phases appeared due to the hydrophobic nature of 1-DDT. The change of the particles from aqueous to organic phase may be due to the bulky nature of 1-DDT which replaces the short chain thioglycolic acid on the surface of the CdSe nanoparticles. Even though the replacement of TGA was done effectively, it was observed that only partial exchange of the ligand TGA was done by the long chain ligand 1-DDT [4].

The particles were more stable in 1-DDT phase as like in aqueous phase. The transfer of the nanoparticles from aqueous to organic phase depends upon volume of the 1-DDT, amount of acetone, and the temperature used for the transformation process. The HRTEM image of the phase transferred particles has very good size distribution as shown in Figure 3. The particles have the size around 5 nm. Since the particles were synthesized in aqueous medium, most of the particles were found in agglomerated form. The EDX analysis of the prepared phase-transferred powdered sample was also given in Figure 3. It is shown clearly that the particle contains their respective elements. The presence of sulphur in the spectrum is attributed from the attachment of the ligand thiol on the surface of the nanoparticles. The FTIR spectrum of TGA-capped CdSe nanoparticles, OS-CdSe, is shown in Figure 4. It is clear that the ligands are attached with the particles on its surface. The variation of the stretching frequencies in the phase-transferred CdSe nanoparticles from TGA-capped nanoparticles shows that



(a)



(b)

FIGURE 3: HRTEM image and EDX spectrum of CdSe nanoparticles.

TABLE 1: IR frequencies of TGA-CdSe and OS-CdSe.

TGA-CdSe		OS-CdSe	
Wave number (cm ⁻¹)	Type of vibration	Wave number (cm ⁻¹)	Type of vibration
3426	(-OH)	2923	(ν _{as} -CH ₂ -)
1560	(ν _{as} COO-)	2854	(ν _s -CH ₂ -)
1046	(νC-O)	1450	(δ _{as} -CH ₃)
683	(νC-S)	718	(νC-S)

the confirmation of the attachment of the 1-DDT ligand on the surface [5, 6].

The various stretching frequencies associated with the TGA-capped CdSe and OS-CdSe are given in Table 1.

4. Conclusion

Colloidal cadmium selenide (CdSe) nanoparticles were synthesized in aqueous medium and transferred into organic medium through efficient phase transfer process. The transferred particles can be used as the good electron acceptors in

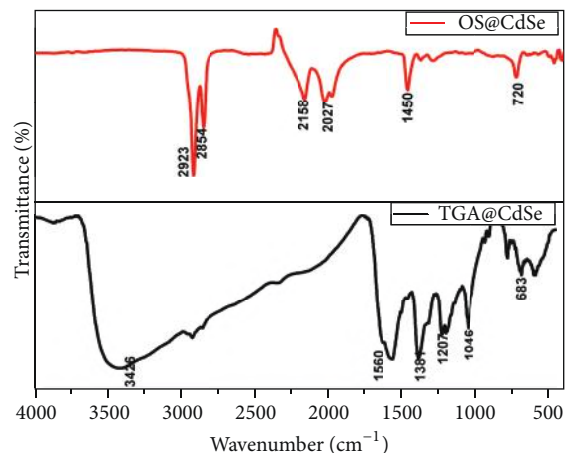


FIGURE 4: FT-IR spectrum of TGA@CdSe and OS-CdSe.

active layer with organic polymer in the presence of suitable organic solvent to fabricate hybrid solar cell.

Acknowledgments

The authors sincerely thank DST, Government of India (DST/TSG/PT/2008/15) and UGC (F. no. 42-855/2013(SR)) for funding the research. S. Ananthakumar and J. Ramkumar sincerely thank the Ministry of New and Renewable Energy (MNRE), Government of India, for providing fellowship under the National Renewable Energy Fellowship (NREF) Scheme.

References

- [1] G. Zhang, S. Finefrock, D. Liang et al., "Semiconductor nanostructure-based photovoltaic solar cells," *Nanoscale*, vol. 3, no. 6, pp. 2430–2443, 2011.
- [2] N. Gopanik and A. L. Rogach, "Aqueous synthesis of semiconductor nanocrystals," in *Semiconductor Nanocrystal Quantumdots-Synthesis, Assembly, Spectroscopy and Applications*, pp. 73–99, Springer, New York, NY, USA, 2008.
- [3] J. Yang, J. Y. Lee, and J. Y. Ying, "Phase transfer and its applications in nanotechnology," *Chemical Society Reviews*, vol. 40, no. 3, pp. 1672–1696, 2011.
- [4] N. Gaponik, D. V. Talapin, A. L. Rogach, A. Eychmüller, and H. Weller, "Efficient phase transfer of luminescent thiol-capped nanocrystals: from water to nonpolar organic solvents," *Nano Letters*, vol. 2, no. 8, pp. 803–806, 2002.
- [5] M. S. Abd El-Sadek and S. Moorthy Babu, "Growth and optical characterization of colloidal CdTe nanoparticles capped by a bifunctional molecule," *Physica B*, vol. 405, no. 16, pp. 3279–3283, 2010.
- [6] R. Seoudi, A. Shabaka, Z. A. El Sayed, and B. Anis, "Effect of stabilizing agent on the morphology and optical properties of silver nanoparticles," *Physica E*, vol. 44, pp. 440–447, 2011.